UNIVERSITÀ DEGLI STUDI DI MILANO

FACOLTÀ di MEDICINA E CHIRURGIA
Scuola di dottorato in Scienze Biomediche, Cliniche e Sperimentali
Dipartimento di Medicina Traslazionale

CORSO di DOTTORATO DI RICERCA in
PATOLOGIA E NEUROPATOLOGIA SPERIMENTALI
XXIV ciclo
Settori scientifico-disciplinari MED/03 MED/04MED/05

FUNCTIONAL STUDY OF *MARK4,* A GENE ENCODING FOR TWO PROTEIN ISOFORMS, IN GLIOMA AND NORMAL CELLS

TESI di DOTTORATO DI RICERCA di
LAURA MONTI
Matricola R08024

Tutor e Docente Guida: Prof.ssa LIDIA LARIZZA
Dott.ssa IVANA MAGNANI
Coordinatore: Prof. ALBERTO MANTOVANI

Anno Accademico 2010/2011

Table of Abbreviations Used in this Thesis			
AD	Alzheimer Disesase	**MAPs**	Microtubule Associated Proteins
ADCs	Analog to Digital convertors	**MARK4**	MAP/Microtubule Affinity-Regulating Kinase 4
AID	Auto-Inhibitory Domain	**MARKK**	MARK-Kinase
AMPK	AMP-activated protein Kinases	**MGMT**	06-Methyl-Guanine-MeThyltransferase
aPKC	Atypical Protein Kinase C	**MRCK**	Miotonyc distrofy Related kinase Cdc42 binding kinase
BTSC	Brain Tumour Stem Cell	**MTOC**	MicroTubule Organizing Center
CAMK	Ca2+-Calmodulin dependent protein Kinases	**MTs**	Microtubules
CCV	Clathrin-Coated Vesicles	**NC - axis**	Nucleus - Centrosome axis
CD site	Common Docking site	**NF1**	Neurofibromin 1
CGH	Comparative Genomic Hybridization	**NOR**	Nucleolus Organizing Regions
CHO	Chinese Hamster Ovary	**NS**	Non-Specific
CHX	Cycloheximide	**NSCs**	Neural Stem Cells
CIN	Chromosomal Instability	**NT**	Non-Treated
CMV	Cytomegalovirus	**PAK5**	p21-Activated Kinase
CNS	Central Nervous System	**PDGFR**	Platelet Derived Growth Factor Receptor
DAPI	4',6-Di Amidino-2-Phenyl Indole.	**Pen-Strept**	Penicillin-Streptomycin
dsRNA	double strand RNA	**PKCλ**	Protein Kinase C lambda
EGFR	Epidermal Growth Factor Receptor	**PKP2**	Plakophilin 2
EtOH	Ethanol	**PMTs**	Photomultiplier Tubes
FBS	Fetal Bovine Serum	**PNC**	Perinucleolar Compartment
FITC	Fluorescein IsoThioCyanate	**PTB**	Polypirimidine Tract Binding
FSC	Forward Scatter Channel	**PTEN**	Phosphatase and Tensin homolog
GBM	Glioblastoma	**RISC**	RNA Induced Silencing Complex
GBM CSCs	Glioblastoma-derived cancer stem cells	**RNAi**	RNA interference
GBMO	Glioblastomas oligodendroglioma-derived	**RTEL1**	Regulator of Telomere Elongation Helicase
GFAP	Glial Fibrillary Acidic Protein	**SHH**	Sonic HedgeHog
GFP	Green Fluorescent Protein	**siRNAs**	small interference RNA
GSK3β	Glycogen Synthase Kinase 3β	**SSC**	Side Scatter Channel
HDACs	Histone Deacetylases	**SVZ**	Sub-Ventricular Zone
IDH2	Isocitrate DeHydrogenase	**TERT**	Telomerase Reverse Transcriptase
IF	Immunofluorescence	**TGFβIAF**	Transforming Growth Factor β-Inducing Anti-apoptotic Factor
KA Domain	Kinase-Associated domain	**TRITC**	TetramethylRhodamine IsoThioCyanate
KSR1	Kinase Suppressor of Raf-1	**UBA domain**	Ubiquitin-associated domain
LKB1	Liver Kinase B1	**WB**	Western Blot
LOH	Loss of Heterozigosity	**WHO**	World Health Organization

Abstract

MARK4 (MAP/Microtubule Affinity-Regulating Kinase 4) belongs to a family of serine-threonine kinases phosphorylating Microtubule Associated Proteins, causing their detachment from the microtubules (MTs) and thus increasing MTs dynamics. MARK proteins show high homology with PAR complex proteins family, involved in assessing cell polarity during embryogenesis, epithelial morphogenesis, neural differentiation, and cell migration. MARK proteins are thus implied in several processes involving MT network: cytoskeleton dynamics, cell polarity, centrosomes formation, chromosomal segregation, cytokinesis.

The *MARK4* gene (19q13.2) encodes at least two alternatively spliced isoforms, L and S, differentially expressed in human tissues. MARK4S is the predominant isoform in normal brain and post-mitotic neurons. MARK4L has been found up-regulated in glioma cell lines and neural progenitors, as well as in hepatocarcinoma cell lines, suggesting a role in cell proliferation. The dual nature of MARK4 isoforms has been pinpointed by their expression profile in glioblastoma-derived cell lines and neural stem cells (NSCs), other than glioma, and the balance of the two isoforms, favouring the L splicing variant in glial tumors, is being investigated as a potential target of dysregulation in gliomagenesis. A linked view is whether the predominant expression of MARK4L, isoform of a gene involved in the microtubule dynamics, may concur to mitotic errors during gliomagenesis.

Both isoforms of MARK4 have been found associated to centrosomes and midbody, in glioma as well as in normal cells, suggesting that the kinase might have a role in all phases of the cell cycle. Moreover, MARK4L showed an additional nucleolar localization in glioma, raising the idea that, in tumors, the L variant has isoform specific functions and interactions with nucleolar components.

To verify the functional impact of MARK4 gene in glioma and in normal cells and to define the role of MARK4S and L isoforms with respect to their subcellular localization, we set up a functional study by RNA interference in glioblastoma (GBM) cell lines and normal fibroblasts, with specific silencing of both MARK4S and MARK4S+L.

We showed that MARK4 depletion determines heavy alterations in the cell shape of both G-32 GBM cell line and fibroblasts, corroborating MARK4 implication in cytoskeleton organization, and in accordance with the known role of MARK proteins in MTs dynamics.

MARK4 silencing particularly affected the centrosome cycle. Silenced G-32 GBM cell line and fibroblasts presented most of cells with the duplicated centrosome, apical to the nucleus, as typical of G_1/S transition, while differently, control cells displayed centrosomes in all phases of the centrosome cycle. Accordingly, after MARK4 silencing, cell cycle analysis showed in both tumor

cells and fibroblasts, an increase of G_1 cells fraction and a strong reduction of mitoses, most of which displayed aberrations of spindle poles. These findings indicate that MARK4 depletion targets the G_1/S transition checkpoint, probably knocking down a positive regulator.

It is worth noticing that the observed alterations of cell morphology, centrosome and cell cycle progression, and of mitosis were more pronounced when silencing MARK4S+L, as if the depletion of the sole MARK4S might be partially compensated by MARK4L, being both isoforms localized at centrosomes and midbody.

MARK4 silencing on nucleoli revealed that the L isoform of MARK4 is not a specific marker of tumor (glioma) cell lines, in fact it was also detectable in fibroblasts. However, MARK4 depletion showed a nucleolar pattern different in G-32 GBM cells from that of fibroblasts: G-32 showed, after both anti-MARK4S and MARK4S+L siRNA, a pronounced intensity of MARK4L signal in several nucleoli, while some others appeared silenced. In contrast, silenced fibroblasts showed, particularly after anti-MARK4S+L siRNA, several nucleoli unlabelled with MARK4L. It's currently unknown the molecular basis for this difference which may be more than a quantitative one due to the higher levels of MARK4L in the nucleolar compartment of tumor cells where it's generally upregulated.

The concomitant alterations of both centrosomal and nucleolar compartments highlighted by MARK4 silencing raise the hypothesis of a MARK4 role in the regulation of the Nucleus - (Nucleolus) - Centrosome (NC) axis. NC - axis is oriented and paired with the polarization and migration axis of many cell types, including fibroblasts and neural cells. Microtubules act as major actors in organizing a dynamic structure along NC - axis, regulating nuclear movement during cell migration and polarization. Since MARK4 cooperates with the microtubule network, its depletion may interfere with the correct orientation of the NC – axis.

Background

1. MARKs (MAP/Microtubule Affinity-Regulating Kinases)

MAP/Microtubule affinity-regulating kinases (MARKs) are a serine-threonine kinases family responsible for phosphorylation of Microtubule Associated Proteins (MAPs) including Tau, MAP2, MAP4 and doublecortin. MARKs-mediated phosporylation causes MAPs detachment from microtubules, resulting in increased MTs dynamics and favouring MTs instability and disassembly [Drewes 1997, Matenia 2009].

MARK kinases are members of AMPK (AMP-activated protein kinases) family, subfamily of the Ca^{2+}-calmodulin dependent protein kinases (CAMK) [Bright 2009].

Orthologs of MARK kinases are described in lower eukaryotes, such as Par-1 (partition-defective) in *Caenorhabditis elegans* and KIN1/KIN2 in *S. pombe* [Elbert 2005]. PAR proteins are known to cooperate in cellular polarization, interacting with microtubule dynamics and several other cellular processes [Pellettieri & Seydoux 2002].

The human genome contains four functional MARK4 genes: MARK1, MARK2 (EMK1), MARK3 (C-TAK1) and MARK4 (MARKL-1), mapping on human chromosomes 1, 11, 14 and 19 respectively [Espinosa 1998], plus 30 pseudogenes (www.itb.cnr.it/kinweb/pseudogene.php).

1.1 MARKs STRUCTURE

MARKs have a highly conserved structure consisting of six sequence segments, as other AMPK kinases [Marx 2010] (Figure 1).

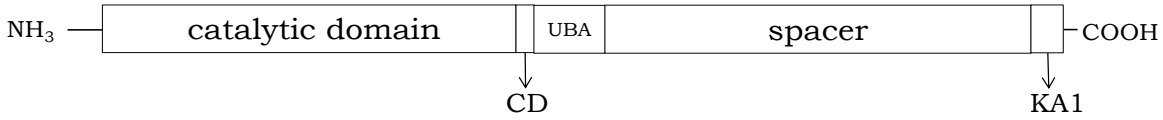

Figure 1: schematic representation of MARK protein structure. Boxes are not drawn to scale.

N-terminal header

The N-terminal sequence is usually different for each protein of the family: its role is still unknown.

Catalytic domain

MARKs catalytic domain has the typical bi-lobate structure of protein kinases. The larger carboxy-terminal lobe (~ 170 residues) is mostly α-helical, while the smaller amino-terminal lobe (~ 80 residues) consists mainly of β-strands with a single α-helix. The two lobes define the cleft of the active site, for substrate and ATP, consisting of a P-loop (phosphate-binding loop), a catalytic loop,

and a T-loop (activation loop, containing a conserved consensus sequence, LDTFCGSPP, where threonine and serine residues work as phosphorylation targets). This structure is very flexible, allowing conformational changes responsible for activation/inactivation. The catalytic loop contains a RD motif consisting of a highly conserved, catalytically active aspartate, preceded by an arginine residue, assumed to interact with the primary phosphorylation site of the T-loop.

The T-loop is anchored to the base of the active site: in the inactive state, the T-loop is partially disordered and folded into the cleft, blocking the access of substrates and ATP. When MARK proteins are activated by T-loop phosphorylation, the catalytic site becomes accessible, leading the protein to exert its kinase activity.

The P-loop assists the γ-phosphate transfer to the substrate phosphorylation site [Timm 2008].

Linker

The linker is a negatively charged motif, resembling the Common Docking (CD) site of MAP kinases and possibly binding interactors or co-factors.

UBA domain

This small and globular domain is homologous to Ubiquitin-Associated proteins but differently and peculiarly folded: probably the MARK UBA domain, instead of binding ubiquitin, interacts with MARK catalytic domain (in its N-terminal lobe) locking it in an open (inactive) conformation. Two different functions were proposed for MARK UBA domain:

- autoinhibition: locking the kinase in an open conformation, the UBA domain prevents substrate and ATP binding [Panneerselvam 2006];
- positive regulation: the open conformation favours the access of activating/deactivating kinases to the activation loop [Murphy 2007].

Based on these hypotheses, depending on both the phosphorylation state of the kinase domain and cofactors interactions, the UBA domain may play functions of inhibition, activation and stabilization[Marx 2010].

Spacer

This is the most variable region among the MARK members, likely with a regulatory role, since it holds phosphorylation sites targeted by aPKC[1].

[1] Atypical Protein Kinase C

The C-terminal tail (KA1 domain)

The Kinase-Associated (KA1) domain (~ 100 aminoacids) is characterized by a N-terminal hydrophobic and concave surface, surrounded by conserved and positively charged residues: this motif may be the binding site for negatively charged regions of cytoskeletal proteins, MARK catalytic domain, or MARK CD domain, probably with an autoinhibitory function [Tochio 2006].

This view is sustained by evidences reported for yeast KIN1 and KIN2 and for Snf1-pKD (an AMPK protein from *Schizosaccharomyces pombe*): Snf1 C-terminal region is an autoinhibitory domain (AID) binding both the N-terminal and C-terminal lobes of the kinase domain, reducing its mobility [Chen L. 2009]. Also in yeast, the C-terminal tail physically interacts with the N-terminal kinase domain (presumably in its open conformation) with an autoinhibitory effect [Elbert 2005].

The KA1 domain has been also reported to be involved in protein localization [Tochio 2006].

1.2 MARKs REGULATION

MARK kinases are regulated through multiple pathways, as summarized in Figure 2 [Matenia, 2009]. In general, as above mentioned, MARK activation increases microtubule dynamics, while its inhibition stabilizes microtubules.

Phosphorylation events in the catalytic domain of MARK can enhance or reduce kinase activity. Additionally, MARK activity can be positively or negatively modulated by interaction with other proteins.

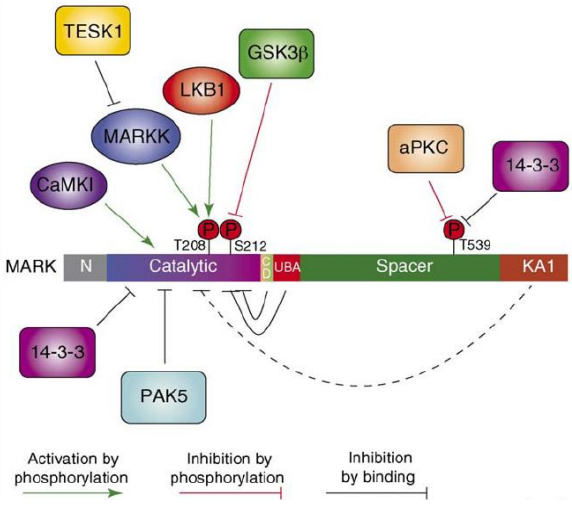

Figure 2 schematic representation of MARK interactions/regulation (from Matenia 2009)

ACTIVATION BY PHOSPHORYLATION

Liver Kinase B1 (**LKB1**) and MARK-Kinase (**MARKK**) activates MARK proteins by phosphorylation on the threonine residue in the T-loop (MARK1 T215; MARK2 T208; MARK3 T211; MARK4 T214). Similarly, the activated Calcium/calmodulin-dependent protein kinase I (**CaMKI**) binds and phosphorylates MARK2 within its kinase domain, but at different sites [Matenia 2009].

INHIBITION BY PHOSPHORYLATION

Glycogen Synthase Kinase 3β (**GSK3β**) negatively regulates MARKs proteins by phosphorylating a serine residue located near the threonine activation site in the T-loop (MARK1 S219; MARK2 S212; MARK3 S215; MARK4 S218). The inhibitory effect occurs independently from the phosphorylation status of the threonine, since the phosphorylated serine is no longer able to stabilize, by interactions with other aminoacids, the activating loop. The inhibitory phosphorylation by GSK3β even overrides previous activation by MARKK or LKB1 at T208 [Timm 2008].

Mammalian **aPKC** (required for cell polarity together with MARK2) down-regulates MARK2 by phosphorylation in its spacer domain (T595), enhancing MARK capability to bind 14-3-3[2] protein, and thus promoting the dissociation of MARK2 from the lateral membrane in polarized cells.

The human **PIM1** kinase, a downstream effector of many cytokine-signalling pathways, associates with and phosphorylates MARK3, leading to a substantial decrease in kinase activity [Suzuki 2004, Hurov 2004, Matenia 2009].

INHIBITION BY INTERACTION

14-3-3 proteins (Par-5 homologues) bind MARK kinases in their catalytic domain [Benton 2003] or in the spacer (after MARK phosphorylation by aPKC), downregulating MARKs activity and modifying their localization, probably by stabilizing the inhibitory interaction between KA1 domain and the aminoterminal or the catalytic domain.

PAK5 (p21-activated kinase) inhibits MARK2 by interaction with its catalytic domain [Matenia 2005].

Also **ubiquitin** and MARK **UBA and KA1 domains** are able to interact with MARK kinasic domain with inhibitory effects.

[2] phospho-serine/phospho-threonine binding proteins that interact with many partners and regulating different biological processes.

Very recently, 4 synthetic compounds (sharing a 9-oxo-9H-acridine-10-yl as functional group) have been designed to inhibit MARK activity [Timm 2011]: these compounds are capable to overcome the toxicity due to MARK2 overexpression in neurons (causing microtubule breakdown, with alteration of cells shape, which look rounded and reduced in size).

INHIBITION BY DIMERIZATION

Dimerization, a common event for kinases, is a candidate mechanism for MARK autoinhibition: MARK proteins are able to crystallize as dimers, linked by covalent disulfide bridges between T-loops. This conformation (open state) ends in MARK inhibition which is marked by the activation loop folded into the cleft to lock it. Currently no direct *in vivo* evidences of this interaction are available [Marx 2010].

1.3 MARKs LOCALIZATION AND FUNCTION

MARK1, MARK2 and MARK3 are known to localize in the cytoplasm, where they associate with the intracellular microtubule network [Drewes 1997]. Differently, MARK4 associates to centrosomes and the midbody [Trinczek 2004, Magnani 2009].

According with their localization and role as regulators of MAPs/microtubule affinity, MARK kinases are implicated in several cellular processes involving the microtubule network as depicted in Figure 3: cytoskeleton dynamics [Schneider 2004], centrosome formation, chromosomes segregation in mitosis and cytokinesis [Fukasawa 2002]. Interestingly some of the cellular processes involving MARK activity are characteristic of neurons physiology and some pathologies, such as Alzheimer's disease and tumours.

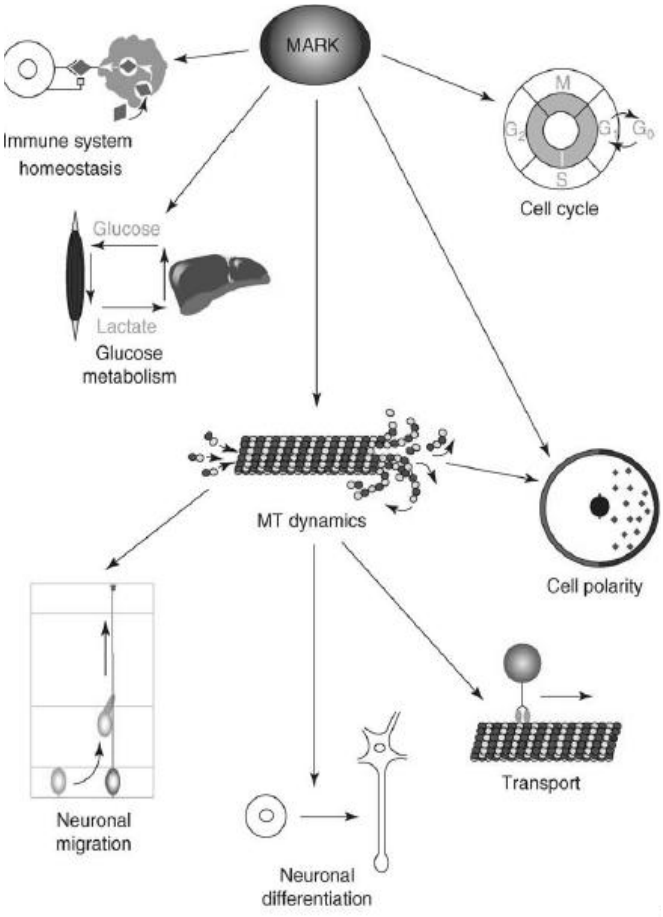

Figure 3 Overview of the role of MARK family kinases in cellular processes (from Matenia 2009)

MICROTUBULE-DEPENDENT TRANSPORT AND ENDOCYTOSIS

MARK proteins are involved in regulation of microtubule-dependent transport, (i.e. in axons): more specifically, MARK2 regulates this process by phosphorylating MAPs, which are known to interfere with motor proteins responsible for organelle, vesicle and protein transport [Mandelkow 2004].

A similar role in endocytosis has been demonstrated: MARKs co-localize with clathrin, and act as regulators of microtubule-dependent transport of clathrin-coated vesicles (CCV) [Schmitt-Ulms 2009].

EMBRYONIC DEVELOPMENT AND CELL POLARIZATION

Par-1 homologues in *C. Elegans* and *Drosophila* play a role in establishing polarity: they accumulate asymmetrically in the embryo, inducing asymmetric division and axis polarization, which are essential for a correct embryonic development [Tomankak 2000]. KIN1 and KIN2 homologues in *Schizosaccharomyces pombe* show a similar role in cell polarization, since they are responsible for the bipolar growth leading to the typical yeasts rod-shape [Drewes 2003].

Accordingly, an asymmetric localization of MARK proteins, together with aPKC and Par-5 (14-3-3), characterizes epithelial and neuronal cells polarization in mammals [Bohm 1997; Matenia 2009].

MARK2, in particular, has a role in polarized neurite outgrowth and maintenance of neuronal polarity in mammalian cells, which requires dynamic instability of microtubules. Indeed, overexpression of MARK2 in CHO[3] cells leads to microtubule disruption and consequently to cell shrinking and death: the effect can be counteracted by using microtubule stabilizers (such as taxol) or by synthetic compounds specifically inhibiting MARK activity [Drewes 1997, Timm 2011]. In accordance, the overexpression of inactive MARK2 disturbs the polarity in mammalian epithelial cells and inhibits axon formation. Conversely, reduction of MARK2 expression by RNA interference (RNAi) induces multiple axons in hippocampal neurons [Biernat 2003, Chen 2006, Terabayashim 2007]. Similarly, MARK2 is involved in the reorganization of the microtubule network during epithelial differentiation of liver and kidney cells [Cohen 2004].

Interestingly, *Helicobacter pylori* CagA protein mimics MARK substrate, thus interacting with MARK/Par-1: binding the catalytic loop of the kinase, CagA inhibits kinase activity [Nesic 2010], leading, in gastric carcinomas, to the disorganization of the gastric epithelial structure [Saadat 2007] and spindle misorientation with mitotic delay [Umeda 2009].

[3] Chinese hamster ovary

NEURONAL MIGRATION

Microtubules dynamics is essential for proper neuronal migration. Phosphorylation by MARK proteins of doublecortin (a MAP highly enriched in leading processes of migrating neurons) modifies its affinity for microtubules, affecting the motility of neurons [Schaar 2004] and, in the developing mouse cortex, MARK2 knockdown determines failure of neurons migration beyond the intermediate zone [Sapir 2008].

Interestingly, knockdown of MARK2 in mice influences other physiological processes, such as fertility, homeostasis of the immune system, memory, growth and metabolism [Bessone 1999; Hurov 2001; Hurov 2007; Segu 2008].

CELL CYCLE, CELL SIGNALLING AND SUBCELLULAR LOCALIZATION CONTROL

MARK3 phosphorylation of Cdc25 phosphatase induces its binding to 14-3-3, inhibiting Cdc25-mediated activation of Cdc2/cyclinB complex, and thus blocking mitosis initiation [Peng 1998]. In addition, Pim-1 phosphorylation and inhibition of MARK3 promote cell cycle progression at the G_2/M phase [Bachmann 2004].

MARK3 also regulates Ras-MAPK pathway, by phosphorylation of KSR1[4] and induction of 14-3-3 binding [Muller 2001].

Finally, MARK3 regulates class IIa Histone Deacetylases (HDACs) subcellular localization: phosphorylation of 14-3-3 binding sites on HDACs prevents the interaction with 14-3-3 proteins, responsible for HDACs nuclear exclusion (following MARK3 phosphorylation, HDACs are instead retained in the nucleus) [Dequiedt 2006]. Similarly, phosporylation by MARK3 mediates PKP2[5] nuclear retention, by activating its 14-3-3 binding site [Muller 2003].

MARK4 specific expression and localization in glioma, a group of tumors that have been extensively charaterized in our laboratory, is discussed further on in detail.

[4] Kinase Suppressor of Raf-1
[5] Plakophilin 2

1.4 MARKs IN HUMAN PATHOLOGIES

Hyperphosphorylation of Tau (a MAP highly expressed in the Central Nervous System) is a key hallmark of **Alzheimer disesase (AD)**: it can be induced by MARKs, CDK5 and GSK3 kinases, with consequent alteration of Tau localization and proteolytic cleavage [Drewes 2004].

Cleaved hyperphosphorylated Tau is thought to accumulate in neuron somatodendritic compartments: by aggregating into paired helical filaments, hyper-P-Tau forms insoluble neurofibrillary tangles, characteristic of **Alzheimer's disease** (together with loss of synapses and neurons) [Chin 2000; Gamblin 2003]. A role for MARK proteins in this neurodegenerative pathology has been suggested by MARKs co-localization with neurofibrillary tangles [Chin 2000] Furthermore hyperphosphorylated Tau, enhanced kinases activity (including MARKs) and breakdown of microtubules are commonly found in the missorted dendritic regions with Alzheimer disease progression [Zempel 2010]. The location of *MARK4* gene close to the locus of susceptibility (ApoE) to AD (Trinczek 2004) is an additional hint.

Considering a different aetiological model, Tau phosphorylation is not the initiating event but a consequence of β-amyloid aggregation [Chatterjee 2009], which causes transport defects (due to increase and bundling of microtubules) and improper distribution of Tau into the somatodendritic compartments [Zempel 2010].

Further support for a possible role of MARKs/MAPs in Alzheimer's disease is provided by the finding that MARK2 activation in the early steps of pathogenesis can rescue transport mechanisms and synapses [Thies 2007].

The *MARK1* gene, overexpressed in the prefrontal cortex of post-mortem brain tissues from autistic patients, is a candidate **autism** susceptibility gene as appointed by the significant association of several SNPs within the gene with the disease.

MARK1 involvement in the regulation of synaptic plasticity [Jeon 2005] and in cognition has been suggested to be responsible for subtle changes in dendritic functioning [Maussion 2008]. Interestingly, *MARK1* gene is localized within a fragile site (FRA1H) and its expression levels are significantly altered in tumour-derived cell lines [Pelliccia 2007]. This datum together with MARK1 silencing by methylation in primary gastric cancers [Yamashita 2006] and its up-regulation in lung carcinoma [Sun 2004] makes plausible a role of MARK1 in **neoplastic transformation** .

2. MARK4 (MAP/MICROTUBULE AFFINITY-REGULATING KINASE 4)

MARK4 gene (19q13.2) consists of 18 exons. At least two MARK4 isoforms are known (Figure 4):

- MARK4S (Short) mRNA (3609 bp) consists of 18 exons and encodes a 688 aa[6]-protein whose predicted MW[7] is 75.3 kDa;
- MARK4L (Long) mRNA (3529 bp) derives from exon 16 skipping and the consequent shift of the reading frame, leading to the production of a 752 aa-protein with a predicted MW of 82.5 kDa.

MARK4 sequence shares 55% homology with other MARKs (90% in the catalytic domain). Both MARK4 isoforms maintain the characteristic protein structure of MARK family previously described, with a N-terminal catalytic domain, a CD domain, the UBA domain, a wide spacer region and the C-terminal tail. The main phosporylation sites in the the T-loop of the catalytic domain are T214 and S218.

As a consequence of the alternative splicing, the two isoforms differ in the C-terminal tail: MARK4L includes, as other MARK proteins, the KA1 domain, whereas MARK4S contains a domain with no homology to any known structure [Espinosa 1998], suggesting different functions for the two isoforms. MARK4 C-tail domain folds in a conformation similar to those of MARK1, 2 and 3, suggesting a similar autoinhibitory and interactive function [Marx 2010].

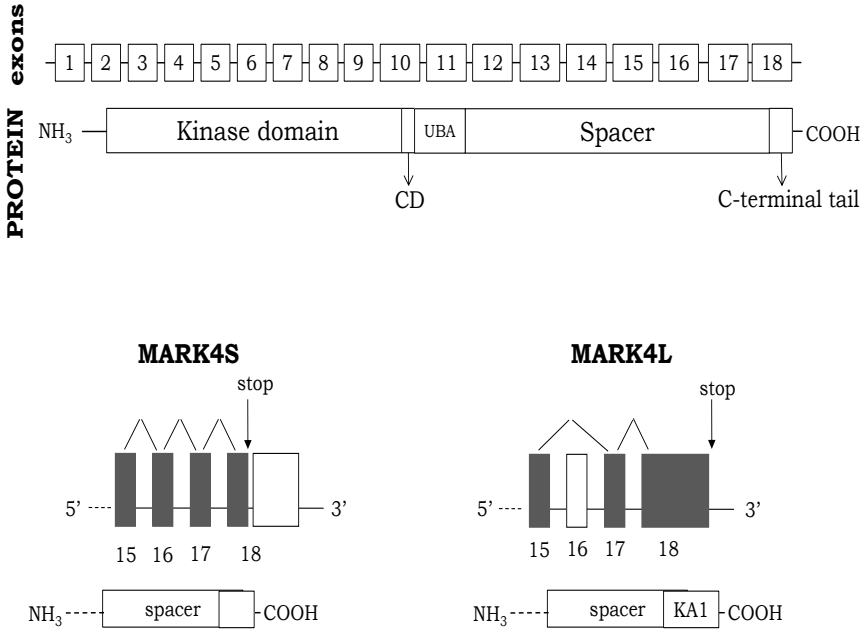

Figure 4 [top] schematic representation of *MARK4* exons and respective protein domains; **[bottom]** alternative splicing of exon 16 gives origin to MARK4 isoforms. MARK4S RNA includes exon 16 (right): the STOP codon is inside exon 18 and MARK4S protein lacks the KA1 domain. With exon 16 skipping, the stop codon is shifted forward: MARK4L protein is longer and has the classical KA1 domain (right). Boxes are not drawn to scale.

[6] Aminoacids.
[7] Molecular Weight

2.1 MARK4 REGULATION and INTERACTION

MARK4 is regulated similarly to other MARK members.

LKB1 phosphorylates T214 in the T-loop, activating MARK4 [Lizcano 2004; Brajenovic 2004].

It has been demonstrated that MARK4 is polyubiquitinated and interacts with the deubiquitinating enzyme USP9X [Al-hakim 2008]. As non-USP9X-binding mutants of MARK4 are hyperubiquitinated and not phosphorylated at T214, it is likely that polyubiquitination inhibits LKB1 activation of MARK4. This model implicates that, in the steady state, MARK4 UBA domain is ubiquitinilated and does not interact with the catalytic domain, making the T-loop less accessible to LKB1. Alternatively, ubiquitin may mask T214 site or induce conformational modifications favouring the activity of phosphatases [Al-hakim 2008].

It has also been established that MARK4 interacts with aPKC [Brajenovic 2004] and could therefore be phosphorylated and inactivated by this kinase, as reported for MARK2 and MARK3 [Hurov 2004].

Tandem Affinity Purification and Immunoprecipitation experiments led to the identification of at least twenty putative MARK4 interactors, of which PKCλ[8] and Cdc42 are implicated in cell polarity control and TGFβIAF[9] is thought to be hortolog of Miranda, a protein involved in the asymmetric division of neuroblasts in *Drosophila*. MARK4 interacts with 14-3-3 protein (14-3-3η isoform) known to control many cellular processes by binding phosphorylated proteins (possibly direct regulators of MARK4 itself) and also interconnecting different pathways. ARHGEF2, a cytoskeleton binding protein, and Phosphatase 2A, associated with microtubules and Tau regulator, are indicated as putative MARK4 interactors [Brajenovic 2004; Angrand 2006].

Exogeneous MARK4 protein was also found to co-purify in a protein complex containing α, β, and γ tubulin, non-muscle myosin and actin [Trinczek 2004; Brajenovic 2004].

As previously mentioned, MARK4 interacts with LKB1 and aPKC kinases and with the deubiquitinating enzyme USP9X.

2.2 MARK4 EXPRESSION

MARK4L was initially identified as one of the overexpressed transcripts in hepatocarcinoma cells, characterized by inactivation of the Wnt/β-catenin pathway and β-catenin accumulation in the

[8] Protein Kinase C lambda

[9] Transforming Growth Factor β-Inducing Anti-apoptotic Factor

nucleus, suggesting it might be a downstream component of the Wnt-signalling pathway, potentially involved in hepatocellular carcinogenesis [Kato 2001].

Northern Blot and semi-quantitative competitive PCR on different organisms (human, rat and mouse tissues) showed that *MARK4* gene is ubiquitously expressed, with particularly elevated levels in brain and testis. In detail, MARK4L was found highly expressed in testis, brain and also in kidney, liver and lung [Trinczek 2004; Schneider 2004; Moroni 2006], while MARK4S levels were found elevated in testis, heart and brain [Kato 2001; Moroni 2006].

MARK4S was instead found rapidly and transiently up-regulated after an ischemic event in brain, mainly at the hippocampus, together with many other genes overexpressed in the injured brain (if compared to the healthy counterpart), including LKB1. Induced overexpression of MARK4S in hepatocytes leads to a reduced cell vitality, suggesting that MARK4S up-regulation in the early stages of an ischemic event might increase the probability of neuron death [Schneider 2004].

MARK4 IN HUMAN GLIOMA

CYTOGENOMICS AND EXPRESSION DATA

MARK4 gene maps at 19q13.2 locus, centromeric to the Loss of Heterozigosity (LOH) area in gliomas the most common and malignant tumours in the Central Nervous System (CNS), [Hartmann 2002]. By characterizing the chromosomal rearrangements affecting the 19q13 region in gliomas and by array-CGH analysis, we found that MARK4 was never deleted in these tumours. Conversely it was duplicated in one glioblastoma cell line (MI-4) and a BAC clone of the gene was found included in a “gain” region in a few tested glioma cell lines [Roversi 2006, Magnani 2009].

In an attempt to describe in detail these findings, MARK4 expression has been widely investigated in glioma by different approaches. By semi-quantitative PCR, MARK4L splicing variant resulted up-regulated in 58 samples including cell lines and tissue gliomas, and in human neural progenitor cells, and down-regulated during glial differentiation into astrocytes, suggesting a role for the kinase in proliferating and undifferentiated cells. Conversely, MARK4S was found highly expressed in normal brain and hardly detectable in glioma and neural progenitors [Beghini 2003]. Since MARK4S expression level was observed to increase during neuronal differentiation this isoform was delineated as a neuron-specific marker in the CNS.

Immunohistochemistry revealed nonetheless that both MARK4L and S proteins were expressed in neurons of the grey matter (whereas the white matter was unlabeled) suggesting that both forms play a general role in neural tissues [Moroni 2006].

Recently, by sequencing analysis we ruled out mutations (see below) as the cause of the sustained expression of the MARK4L variant in glioma and demonstrated by real-time PCR, immunoblotting and immunohistochemistry that both MARK4 isoforms are co-expressed in 21 glioma cell lines and 36 tissue samples of different malignancy grades. MARK4L is confirmed as the predominant isoform, whereas MARK4S transcript levels are significantly decreased in comparison and have an inverse correlation with malignancy grade. The switch towards MARK4L was also observed in glioblastoma-derived cancer stem cells (GBM CSCs) and neural stem cells (NSCs) suggesting that the balance between the MARK4 isoforms is carefully guarded during the normal neural differentiation program, but may be subverted during gliomagenesis. We hyphotesized that MARK4 alternative splicing may be the most likely mechanism regulating MARK4L and S balance. By immunohistochemistry MARK4L, but not MARK4S, was detected in cells of the subventricular zone in human and mice [Magnani, *In press*].

2.3 MUTATION ANALYSIS

Mutations in protein kinase genes are often implicated in cancer initiation and development, since most kinases are involved in cell proliferation. Most of the activating alterations occur inside the catalytic domain, including the ATP-binding site.

Only a few *MARK4* sequence changes are reported in the literature:

- A splice-site mutation (exon 13 +1 G>A; spacer region) identified in one glioblastoma sample (among 91 GBM samples analyzed) [The Cancer Genome Atlas Research Network 2008].
- 5 *MARK4* alterations identified in a panel of 210 different human cancers investigating 518 protein kinase genes [Greenman 2007]:
  - two missense mutations in two colorectal adenocarcinomas:
    exon 12 (R377Q and R418C; spacer region);
  - two silent mutations in multiple tumour samples
    exon 5 (Y137Y)
    exon 9 (I286I) (kinase domain);
  - one intronic mutation in a lung cancer specimen
    exon 8 +5 C>T; (kinase domain);

In patients affected by Peutz-Jeghers Syndrome, typically characterized by LKB1 mutations, no MARK4 mutations have been found [de Leng 2007].

Mutation analysis of *MARK4* has been performed in our laboratory, by screening *MARK4* exons pointed out by the literature as possible targets of mutation (exons 5, 8, 9, 12, 13) and functionally relevant regions, such as the kinase domain (exons 2-10), the ubiquitin-associated (UBA) domain (exons 10-12) and exon 13.

Direct sequencing of the coding regions and flanking regulatory sequences on a panel of glioma cell lines and tissue samples of different malignancy only revealed a synonymous substitution in a GBM cell line (c1101G>C variation in exon 11) which does not affect the splicing process, as confirmed by cDNA analysis.

Also intron retention between exons 3-4, 5-6 and 11-12 was tested, but no splicing errors were detected.

Since MARK4 mRNA undergoes alternative splicing (exon 16 is skipped in MARK4L) the entire fragment between exons 15 and 17 has been analyzed, showing a yet unreported single nucleotide alteration, c1878-61G>A, in several samples (both cell lines and tissues): this change however does not affect the splicing process [Magnani, *In press*].

2.4 SUBCELLULAR LOCALIZATION

Recently, MARK4L localization in glioma cell lines, assessed by Immunofluorescence (IF), showed multiple localization sites of the endogenous protein. MARK4 kinase, under microtubule-stabilizing conditions, associated to normal and aberrant centrosomes, observed particularly in glioblastoma cell lines, and in the midbody as demonstrated by γ-tubulin co-localization [Magnani 2009].

This result confirms previous data referring to MARK4 protein conjugated to GFP (green fluorescent protein) showing co-localization with microtubules and interphase centrosome of CHO and neuroblastoma cell lines [Trinczek 2004].

Furthermore, we could establish that the centrosome association was not abolished by nocodazole-induced depolymerization of microtubules, suggesting that MARK4L is a core component of centrosomes. Moreover, under standard IF conditions, MARK4L associated with the nucleolus, as confirmed by nucleolin counterstaining. These IF results have been validated by immunoblotting in centrosomes, nucleoli and midbody fractions [Magnani 2009].

Recently, by IF, we provided evidence that also the MARK4S isoform, like MARK4L, associates with the centrosome and midbody, but it is not detectable in the nucleolus of glioma cell lines. In normal cells, including human neural progenitors, adult fibroblasts and myoblasts, we found that

both MARK4 isoforms are undetectable in the nucleoli, but associate to the centrosome and midbody as previously observed in glioma cell lines [Magnani 2009]. Furthermore, MARK4L showed a nucleolar localisation in glioblastoma (GBM) derived cancer stem cells (CSCs), but not in neural stem cells (NSCs). Thus the nucleolar association appears to be a specific feature of the L isoform, and a definite feature of glioma cells. An association of MARK4L with nucleolar RNAs or ribonucleoprotein has been suggested since RNAse treatment of GBM cells disrupts the nucleolar localisation of MARK4L and nucleophosmin, one of the major structural component of nucleoli [Magnani, *In press*].

The relevant features of Centrosome, Midbody and Nucleolus are summarized further on.

BOX 1 – MARK4 POSITIVE SUBCELLULAR COMPARTMENTS

Centrosome

Centrosome is a primary MTOC (MicroTubule Organizing Center), thus capable to nucleate and organize microtubules, localized in the cytoplasm, adiacent to the nucleus without any delimitating membrane [Fukasawa 2002]. Two distinct domains are distinguishable in the centrosomal structure:

- the centriolar domain including centrioles, cylindrical organelles responsible for centrosome organization and replication. Each centriole consists of 9 triple microtubules;
- the pericentriolar domain an accumulation of many fibers and proteins surrounding the centriole, responsible for microtubules nucleation, mediated by association of α and β-tubulin dimers on a γ-tubulin ring [Doxsey 2001].

The centrosome has important functions in both interphase and mitosis, devoted to the organization of the cytoskeleton (and thus regulating cell polarity, adhesion and motility) and the mitotic spindle [Kramer 2002]. Centrosome is also involved in many different cellular processes, such as cell cycle progression, cytokinesis, cellular response to stress and signal transduction [Doxsey 2005, Martinez-Garay 2006]. Centrosome replication is strictly regulated during cell cycle, specifically occurring during G_1/S transition and in S phase, to ensure the formation a bipolar spindle at mitosis (Figure 5).

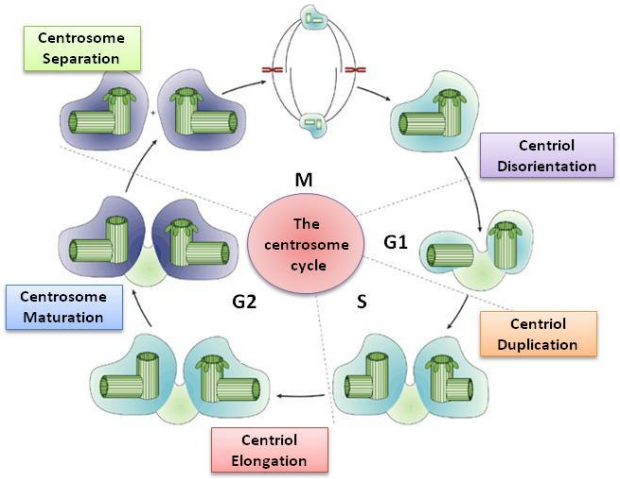

Figure 5 Centrosome duplication cycle, modified from Nigg 2002

Alterations in centrosome number, structure and function (typically observed in tumours) can lead to the formation of aberrant multipolar spindles, and consequently to errors in chromosome segregation, thus causing chromosomal instability (CIN), a hallmark of many tumours.

Midbody

At the end of the mytotic process, with cytokinesis, in correspondence of the midzone, a contractile ring of actin and myosin determines the approaching of the two opposite surfaces of the membrane and their merging and closing, causing the separation of the two daughter cells [Bringmann 2005].

The two daughter cells are initially connected by a narrow intercellular bridge, whose core is the midbody, consisting of microtubules and a dense matrix [Mullins 1982]. The diameter of the intercellular bridge progressively decreases until vanishing, so that the two daughter cells are effectively separated. The midbody, finally discarded, undergoes degradation [Mullins 1977].

The midbody is thought to have an important role in maintaining a bipolar spindle and in correctly separating the cytoplasm between the two daughter cells.

Nucleolus

The nucleolus is a subnuclear structure not delimited by membranes mainly functioning as the “ribosome factory of the cell”. In mammalian cells the nucleolus is disorganized in prophase and reassembled at the end of mitosis concomitantly with restoration of rDNA transcription at the level of competent Nucleolus Organizing Regions (NOR), clusters of genes (rDNA), coding for ribosomal RNA (rRNA), located on the short arm of acrocentric chromosomes 13, 14, 15, 21 and 22. In immunofluorescence, the nucleolus is visible as a DAPI-poor rounded region.

The nucleolus consists of three main components, identified by electronic microscopy:

- the fibrillar center (FC) of clustered rDNA (NOR);
- the dense fibrillar component, consisting of pre-rRNA;
- the granular component, consisting of nucleolar proteins and pre-ribosomes, derived from rDNA transcription in pre-rRNAs, properly rearranged and assembled with ribosomal proteins to move into the cytoplasm [Carmo-Fonseca 2000; Schwarzacher 1983].

According to the so-called "plurifunctional nucleolus hypothesis", this compartment plays an important role not only in ribosome biogenesis, but also in cellular stress response, cell cycle regulation [Visintin 2000] and cell growth [Zhang 2010], cell aging, post-translational modifications (phosphorylation and sumoylation) of proteins and retention/sequestration of molecules normally active outside the nucleolus.
Moreover, nucleolar activity is linked with several pathologies. As an example, B23[10] nucleolar protein and nucleolin, two major nucleolar components, are implicated in cancer pathogenesis and cell proliferation, as indicated by the findings of: i) high nucelolin levels in tumours and actively dividing cells and ii) nucleolin need for chromosome congression and maintenance of mitotic spindle integrity [Ugrinova 2007]. Furthermore, nucleostemin is able to interact with p53/Mdm2 pathway, with a potential role in cell transformation, and some viruses interact with the nucleolus with recruitment of nucelolar proteins facilitating virus replication [Pederson 2011; Sirri 2008; Amin 2008]

Perinucleolar Compartment (PNC)

PNC is a discoid structure, situated on the nucleolus, covering a portion of its surface as a "cap". PNC is not detectable in all cell types, but it is specific for mammalian transformed cell lines and tumour derived cell lines or tumour biopsy, suggesting a role in tumour initiation or progression. The perinuclear compartment was originally described during the characterization of hnRNP I /PTB[11] protein, which localizes in the perinuclear area: the PNC is physically associated with the nucleolus but constitutes a distinct and dynamic structure, moving discretely along the nucleolar periphery. As it happens with nucleoli, PNC is disassembled during mitosis and reconstituted during late telophase. PNC is characterized by enrichment in specific proteins (mainly involved in processing pol II-derived RNAs) and RNAs, especially small non coding RNAs transcribed by pol III (which though are not transcribed in PNC). Among perinucleolar proteins, PTB is involved in pre-mRNA splicing, alternative splicing and regulation of RNA polyadenilation and translation: in general, the enrichment of RNA processing proteins in the PNC suggests a role in RNA metabolism. Some of PNC-associated proteins are known to interact with one another [Pollock and Huang 2010].

[10] Also known as nucleophosmin (NPM)
[11] Polypirimidine Tract Binding

The integrity and stability of PNC is strictly dependent on RNAs: RNAse, but not DNAse, treatment on permeabilized cells, disrupts perinucleolar compartment. Similarly specific inhibition of RNA pol II activity can determine PNC disassembly.

BOX 2 - CENTROSOME, NUCLEUS AND NUCELOLUS: THE TRICKY TRIO

Immediately after centriole discovery, the existence of a nucleus-centrosome axis has been postulated. NC-axis is oriented and paired with the polarization and migration axis of many cells types (such as neurons and fibroblasts), raising the hypothesis of a role for centrosome and nucleus positioning in the regulation of cell polarity and migration [Wakida 2010; Gant Luxton 2011]. Indeed centrosome ablation has been demonstrated to inhibit cell polarization. MTs act as major actors in this process, organizing a dynamic structure along NC-axis and regulating vesicular trafficking and nuclear movement during cellular migration and polarization (fig.6)

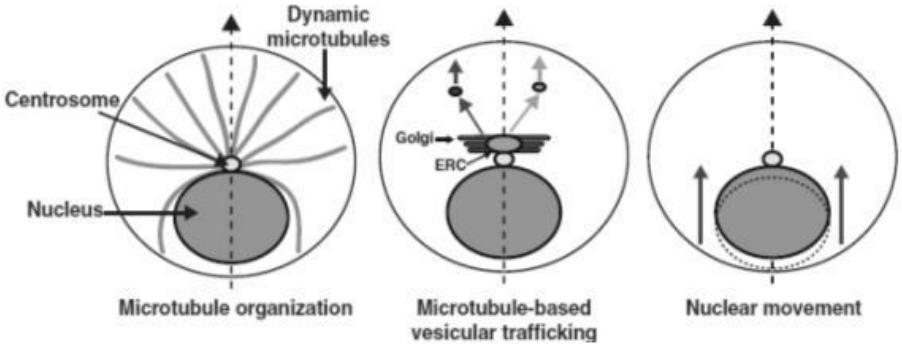

Figure 6 Effector functions of the NC-axis (ERC is the perinuclear endocyitic recycling compartment).

From Gant Luxton 2011

Typically, MTs minus-ends are anchored to the centrosome, and the plus end can extend freely in the cytoplasm, but because of nucleus proximity, MTs spreading from centrosome is not symmetrical, and it is strictly regulated by nucleus and centrosome position (that means by NC axis). NC axis ensures polarization of vesicular compartments (Golgi and exocytic apparata) thanks to interactions with the MTs network and with the motor protein dynein: in migrating cells, where nuclear movement is functional to migration, dynein plays a key role in keeping closed nucleus and centrosome, as well as myosin II. Very interestingly, Par6α localizes to the centrosome and is essential for centrosome positioning during glial-guided neuronal migration.

Cdc42, already identified as MARK4 potential interactor (see before), is implied in controlling NC-axis formation during fibroblasts migration, thanks to its effect on Par6 and MRCK[12].

Also actin and myosin II are implied in defining the NC axis, together with cell-cell junctions mediated by cadherin. Similarly, these effectors and processes can be crucial during cell division [Gant Luxton 2011].

[12] Miotonyc distrofy Related kinase Cdc42 binding kinase

Very interestingly, nucleus-centrosome interactions extend also to the nucleolus. Representing the most active and dynamic nuclear domain, the nucleolus plays a prominent role in various cellular processes, such as cell proliferation, cell-cycle regulation and various aspects of ribosome biogenesis. It has been demonstrated that depletion by siRNA of nucleolar major components, such as B23 and nucleolin, results in cell growth arrest, delays in mitotic entry and increase in apoptosis, together with accumulation of micronuclei and multiple nuclei or, more generally, aberrant nuclear morphology, and rearrangements at severe nucleolar components. In addition, after nucleolin silencing, a significant number of mitotic cells showed defects in centrosome duplication, with multiple centrosomes and multipolar spindles, sustaining the importance of nucleolar proteins for centrosome duplication [Ugrinova 2007, Amin 2008].

2.5 CONCLUSION

MARK4, by phosphorylating MAP proteins, regulates microtubule dynamics and influences the multiple cellular processes implying microtubules [Brajenovic 2004, Matenia 2009].

Additional hints about MARK4 regulation in microtubules dynamics, particularly those affecting the centrosome and the midbody, stemmed from the evidence that both MARK4 isoforms localize in these cellular compartments, taking part in all phases of cell cycle [Magnani 2009].

MARK4L association with the nucleolus in glial tumours [Magnani 2009], like others protein kinases sequestered in this compartment, could underlie a spatial regulation of the kinase by alternate translocation in and out of the nucleolus, according to cell cycle phases [Visintin and Amon, 2000].

MARK4 implication in cell proliferation, pinpointed by cytogenomics and by molecular and expression profiles, features in the dual nature of the two different isoforms (MARK4L and S) the potential target of dysregulation in glial tumours.

Interestingly, MARK4L, the alternative splicing variant, has been found up-regulated in glioma. Alternative mRNA splicing has been considered a mechanism not only increasing proteomic complexity but also implied in cancer, through its involvement in the activation/inactivation of oncogenes and tumour suppressor genes and through the generation of chromosomal instability (CIN) [Lòpes-Saavedra & Herrera, 2010]. CIN is a common feature of aneuploid cancer cells and defects in the regulation of centrosome numbers are considered an intriguing mechanism underlying aneuploidy [Duesberg 2006; Weaver 2007]. Defects in centrosomal number and structure have been well documented in gliomas [D'Assoro 2002; Katsetos 2006; Magnani 2009], raising the issue whether the increased levels of MARK4L, isoform of a gene involved in the microtubule dynamics, may concur to errors in chromosomal segregation driving gliomagenesis.

3. GLIOMA

Glioma, the most common type of primary brain tumour in adults, accounts for more than 70% of all the tumours in the Central Nervous System (CNS) [Ohgaki 2009], with high incidence in children between 0-8 years and in adults between 50-70 years and a slight male predominance [Gladson 2010].

3.1 HISTOLOGICAL CLASSIFICATION

Classification of gliomas is based on histological features, that resemble astrocytes, oligodendrocytes or ependymal cells.

The two main cell types identifiable in the human brain are in fact neurons (2-10% of the cells in the CNS) and glia, for which three different sub-populations can be distinguished:

- Astrocytes, the most abundant glial cells, are responsible of neuron nourishing and protection, regulation of synapse formation and activation of the immune response
- Oligodendrocytes release neuronal growth factors and cover neuronal axons with their cytoplasmatic processes to form myelin
- Microglia, mainly located in proximity of blood capillaries cells, act as phagocytes, with a protective role.

According to World Health Organization (WHO) classification, gliomas are classified as follows (drafted in 1993 and updated in 2008) [Rousseau 2008]

ASTROCYTIC TUMOURS:

- Pilocytic astrocytoma
- Diffuse astrocytoma (fibrillary, protoplasmic and gemistocytic astrocytomas)
- Anaplastic astrocytoma
- Pilomyxoid astrocytoma
- Glioblastoma
- Giant cell glioblastoma
- Gliosarcoma
- Pleomorphic xantoastrocytoma
- Subependymal giant cell astrocytoma

– OLIGODENDROGLIAL TUMOURS:

- Oligodendroglioma
- Anaplastic oligodendroglioma

- MIXED GLIOMAS:
    - Oligoastrocytoma
    - Anaplastic oligoastrocytoma
- EPENDYMOMAS
- OTHER NEURONAL, NEURO-GLIAL AND NEUROEPITHELIAL TUMOURS

3.2 WHO MALIGNANCY CLASSIFICATION

Gliomas can be classified in four malignancy grades, depending on the presence/absence of nuclear atypia, mitosis, microvascular proliferation and necrosis:

- WHO grade I: lesions with low proliferative potential and with a good prognosis (treatment with surgical resection is usually sufficient for the complete recovery).
- WHO grade II: generally infiltrating lesions with low mitotic activity and possible recurrences. Some of these tumours can progress to higher malignancy grade lesions.
- WHO grade III: lesions with histological evidence of malignancy, generally characterized by high mitotic activity, pronounced anaplasia and infiltrative capacity.
- WHO grade IV: lesions with high mitotic activity, prone to necrosis and generally associated with a rapid pre- and post-operation evolution of the disease.

The WHO classification, however, is not sufficient for a correct diagnosis or prediction of survival and therapy response: gliomas show in fact considerable heterogeneity and variability among tumours of the same type and grade, and within individual tumours, so that biopsies can often not be really representative of the whole tumour mass. In addition, genetic alterations can differ in tumours of the same histotype: classification on the basis of tumour genetics could thus lead to a more accurate prognosis prediction.

3.3 CLINICS

Symptoms: Depending on the anatomical site, as characteristic of brain tumours, symptoms are typically due to increased intracranial pressure:

- partial or generalized seizures (epilepsy);
- nausea, vomiting, drowsiness, headache, visual abnormalities, changes in speech, hearing or balance.

- focal and progressive neurological deficits. The type of deficit (motor or sensory) is generally indicative of the tumour site;
- cognitive dysfunctions, in most cases symptomatic of meningeal involvement or diffuse tumour infiltration.

Diagnosis:

- Magnetic resonance imaging or computed tomography (although less sensitive) to confirm a suspect of brain tumour;
- Surgical biopsy with histological examination to diagnose tumour type and grade.

Therapy: Glial tumours are treated by surgery, radiation and chemotherapy. Complete resection is difficult because of tumour location and its typical extensive infiltration into surrounding normal tissue. However, even though not curative, surgery can establish the diagnosis and relieve symptoms by decompressing the brain. To increase survival, surgery is usually combined with adjuvant post-operation radiotherapy and chemotherapy (temozolomide, nitrosurea or by the combination of procarbazine, lomustine and vincristine – PCV), however, disease recurrence is virtually inevitable and very common. Both the invasive nature of the tumour and its heterogeneity probably contribute to the poor response to currently available treatment regimens [Park 2009].

Thanks to advances in understanding the molecular mechanisms of gliomagenesis, new therapies are being developed, in order to inhibit transduction pathways often constitutively altered and driving uncontrolled proliferation in glial tumours [Sathornsumetee 2007]. Monoclonal antibodies and kinase inhibitors unfortunately showed little efficacy, probably because of their low specificity and reduced ability to cross the blood brain barrier [Chi 2007].

Recent therapeutic advances include immunotherapy and anti-angiogenic drugs, such as anti-VEGF drugs (the Vascular Endothelial Growth Factor is responsible for the high vascularization commonly found in gliomas and is involved in a pathway frequently altered in these tumours) [Jain 2007].

Prognosis: The median survival depends on tumour grade and is estimated around 5-8 years for grade II tumours, 3 years for grade III anaplastic astrocytomas and 12-18 months for glioblastomas (with typically a shorter survival for patients > 60 years old) [Gladson 2010].

3.4 AETIOLOGY

Glioma risk factors:

Specific risk factors for glioma have not yet been identified. In general, occupational exposure to organic solvents or pesticides [Gladson 2010], and exposure to ionizing radiations [Fisher 2007] can be predisposing. There are hints of association between immunological factors and gliomas, with a lower risk for atopic people [Linos 2007] and a correlation between high IgE and a longer survival [Wrensch 2006]. Since Cytomegalovirus (CMV) RNA can be detected in glioblastomas, CMV infection has also been suggested to play a role in the etiology and progression of some gliomas [Mitchell 2008].

Genetics:

Even though most brain tumours are sporadic, some familiar syndromes, such as Li-Fraumeni syndrome (involving *p53* gene on chromosome 17p13), neurofibromatosis I (*NF1* 17q11) and the Cowden syndrome (*PTEN* 10q22-q23), are known to be associated with an increased incidence of brain tumours: in these context gliomas occur in combination with other clinical signs, usually tumours in other locations.

Various cytogenetic abnormalities have been identified in sporadic gliomas: deletions and duplications of entire chromosomal segments, Loss Of Heterozigosity and gene amplification, genetic alterations in oncogenes and tumour suppressor genes. These anomalies cause deregulation of pathways involved in cell cycle control, proliferation and cell differentiation. Even though the genes found altered in gliomas are not specific of this class of tumours, their combination and their particular accumulation inside glial cell are typical of gliomas and correlate with neoplastic transformation and tumour progression [Zhu 2002].

It has recently been shown that microRNA (miRNA) play a role in gliomagenesis, since they may repress control genes or, when down-regulated, do not target oncogenes anymore [Huse 2010].

Oligodendroglioma (WHO **grade II**) and **Anaplastic oligodendroglioma** (WHO **grade III**)

- 1p (1p36.22-p36.31) and 19q13.3 LOH [Smith 2000] are positive prognostic predictors, correlating with a favorable response to therapy and a longer survival [Collins 2004]. However, the genes of these loci specifically involved in glioma initiation and/or growth promotion are not known [Gladson 2010].
- Promoter methylation or 10q chromosome loss cause downregulation of *PTEN* [13] tumour suppressor gene (10q22-q23).
- *PDGFRα* [14]can be amplified (4q12), leading to uncontrolled cell proliferation.
- EGF receptor signaling, together with cell-adhesion receptors and proteases, play an important role in promoting both a highly proliferative phenotype and an invasive phenotype. Anaplastic oligodendrogliomas (grade III) show genetic and epigenetic aberrations of *INK4A-ARF* and *INK4B,* involved in regulating the G1/S phase transition.

Astrocytomas (WHO **grade II**)

- Frequently exhibit amplification of the PDGFRα and/or PDGFRβ and their ligands (PDGF-A, -B, -C and –D), suggesting an autocrine or paracrine loop amplifying this signaling pathway [Shapiro 2002].
- Loss of *p53*by LOH or missense mutations is common and early in neoplastic transformation [Reifenberger 1996].

Anaplastic astrocytomas (WHO **grade III**)

originating from II grade astrocytomas, usually are characterized by the same genetic alterations, but also genes for cell-cycle progression control are involved:

- loss of the *Rb* gene,
- *CDK4* amplification,
- *p16/CDKN2A* deletion or promoter hypermethylation
- *MDM2* amplification (p53 inhibitor).

Glioblastomas (WHO **grade IV**)

are the most aggressive glial tumours, arising *de novo* (**primary GBM**, showing mainly an astrocytic component) or from pre-existing low-malignancy lesions (**secondary glioblastomas**) (Fig. 7). A small subgroup of grade IV GBM contains areas of oligodendrocytes and is thus indentified as oligodendroglioma-derived (**GBMO**). Primary and secondary GBM are histologically indistinguishable

[13] Phosphatase and Tensin homolog
[14] Platelet Derived Growth Factor Receptor

but develop through distinct genetic pathways, showing different expression profile and epigenetic aberrations and consequently a diverse response to therapy [Ohgaki 2009].

- In **primary glioblastoma** proliferation and invasion can be promoted by amplification and/or mutation of the *EGFR*[15] gene, which alterations are mutually exclusive with *MDM2* overexpression. No *p53* mutations or deletion are known, while LOH of chromosome 10q causes deletion of *PTEN* gene. Mutations and/or deletions in *NF1*[16] can be also present in sporadic glioblastomas [Huse 2010].
- Hypermethylation of *MGMT*[17] promoter occurs in both primary and secondary GBM, representing a positive prognostic factor, since associating with a better response to temozolomide therapy [Ney 2009].
- Genome-wide studies identified *RTEL1*[18] and *TERT*[19] SNPs associated with increased glioma incidence [Shete 2009; Wrensch 2009].
- Missense mutations in *IDH1* and *IDH2*[20] , found in a significant number of astrocytomas and oligodendrogliomas, are largely absent in primary glioblastomas, suggesting that primary and secondary GBM may originate from different progenitor cells [Ohgaki 2009]; multivariate analysis also suggests that they are favorable prognostic markers [Huse 2010].

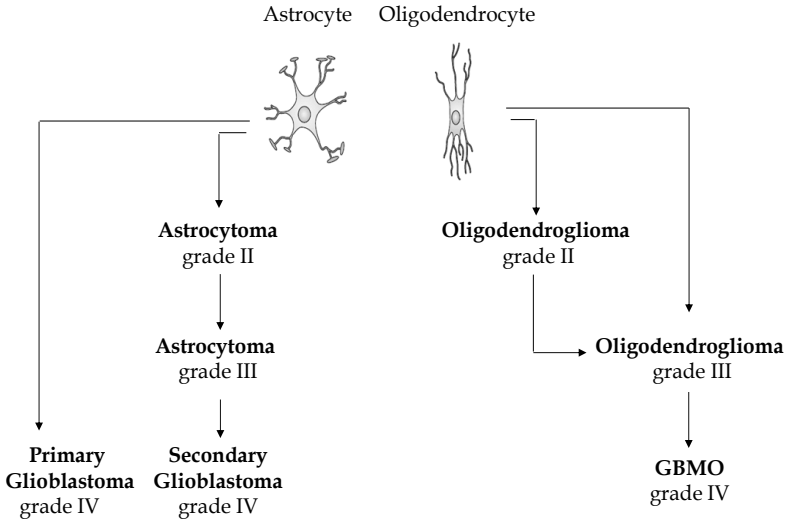

Figure 7: schematic representation of different grade gliomas.

[15] Epidermal Growth Factor Receptor
[16] Neurofibromin 1
[17] 06-Methyl-Guanine-MeThyltransferase
[18] Regulator of Telomere Elongation Helicase
[19] Telomerase Reverse Transcriptase
[20] Isocitrate DeHydrogenase

3.5 GLIOMAGENESIS

The cell of origin of glioblastoma was traditionally thought to be the astrocyte, due to some staining/morphologic similarities, and the fact that the astrocyte is one of the few cell types capable of proliferation in the mature brain. However, the presence of pluripotential neural progenitor cells in the subventricular zone of mature brain, and in glioblastoma tumours, prompted to raise the hypothesis of a staminal origin of gliomas [Quigley 2007]. The stem cell origin could account for the existence of mixed glial tumours, with both astrocytic and oligodendrocytic component, together with the high heterogeneity characterizing brain tumours. Moreover, the presence of a progenitor compartment in glioma could offer an explanation for the resistance to treatment typical of these tumours, as the neoplastic progenitor may continue to seed the brain, despite local treatment to the tumour mass [Quigley 2007].
Glioma arising from a tumour initiating stem-like cell (named brain tumour stem cell, BTSC) is now universally accepted, but the origin of the BTSC cell itself is strongly debated.

The presence of Cancer Stem Cells (CSCs) with various genetic and epigenetic features in glioma could indeed explain the cellular heterogeneity and resistance to therapy characteristic of malignant glioblastomas [Reya 2001].
Cancer stem cells were isolated from glioblastoma biopsies for the first time in 2002 [Ignatova 2002] and were identified as stem-like cells, growing in neurospheres and being able to differentiate in neuronal and astroglial cells. More specifically, the term “Brain Tumour Stem Cell” refers to multipotent cells, which thus can differentiate into the three neural cell lineages (astrocytes, oligodendrocytes and microglia). BTSC can long-term proliferate and self-renew, and are capable of giving rise to tumours *in vivo* [Vescovi 2006].
Typically, cancer stem cells account for less than 5% of the cells within the tumour mass [Gladson 2010] and reside in the perivascular area of the tumour (vascular niche), offering a specialized microenvironment which allows the maintenance of CSCs features [Huse 2010]. Changes in this local microenvironment (niche; growth factors levels; interactions with immune cells) may thus play a role in glioma formation [Germano 2010; Park 2009].
Different surface markers (CD133, BMI1, nestin, Sox2, Notch) have been tested to identify and isolate CSCs from GBMs but this sole approach was proven to be insufficient: in fact the genetic deregulation that occurs in cancer may lead to ectopic protein expression [Park 2009].

Literature data suggest that tumorigenesis can be achieved by two different mechanism:

- Hierarchical model: one specific CSC population, among the different stem subpopulations of the tumour mass is responsible for repopulating the tumour.
- Stochastic mechanism: different types of cancer stem cells, with different tumorigenic ability, are involved in tumour formation, accordingly with the heterogeneity typical of glioblastomas.

Brain tumour Stem Cell may thus derive from oncogenic transformation of different cell types:

- ***Neural stem cells (NSCs):*** even though self-renewing and with long life-time, stem cells are usually quiescent, thus less prone to acquire genomic errors [Park 2009]. However, survival of neural stem cells and maintenance of the undifferentiated state are mediated by pathways reported to be constitutively activated in gliomas (Notch, EGFR, SHH[21], PTEN, BMI1) [Purow 2005; Vescovi 2006; Stiles 2008].

  In the adult central nervous system, NSCs are located in the Sub-Ventricular Zone (SVZ) of the forebrain and the dentate gyrus of the hippocampus, where genesis of new neurons is strongly documented.

  SVZ represent the NSCs niche with the highest neurogenic rate, characterized by the presence of three undifferentiated and highly proliferative cell types: type A, B and C cells (Fig. 8). Type B cells express markers of both mature astrocytes (GFAP[22]) and immature and radial glial cells (vimentin and nestin) and are supposed to be relatively quiescent stem cells with low proliferation rate, but generating fast-proliferating, transit-amplifying progenitor cells (C cells). Type C cells are multipotent and generate neuronal precursors (type A cells or neuroblasts), which leave the SVZ and migrate to several brain areas where they terminally differentiate [Galli 2003]. Some C cells express oligodendroglial markers (Oligo2, NG2) and originate oligodendrocytes [Stiles 2008].

  While *in vivo* endogenous NSC seem able to produce almost exclusively neurons, *in vitro* they are able to generate mainly astrocytes but also oligodendrocytes and neurons. This evidence highlights the importance of epigenetic signals in the neurogenic niches, where glial cells and neurons exert mutual influences [Gritti 2007].

[21] Sonic HedgeHog.
[22] Glial Fibrillary Acidic Protein.

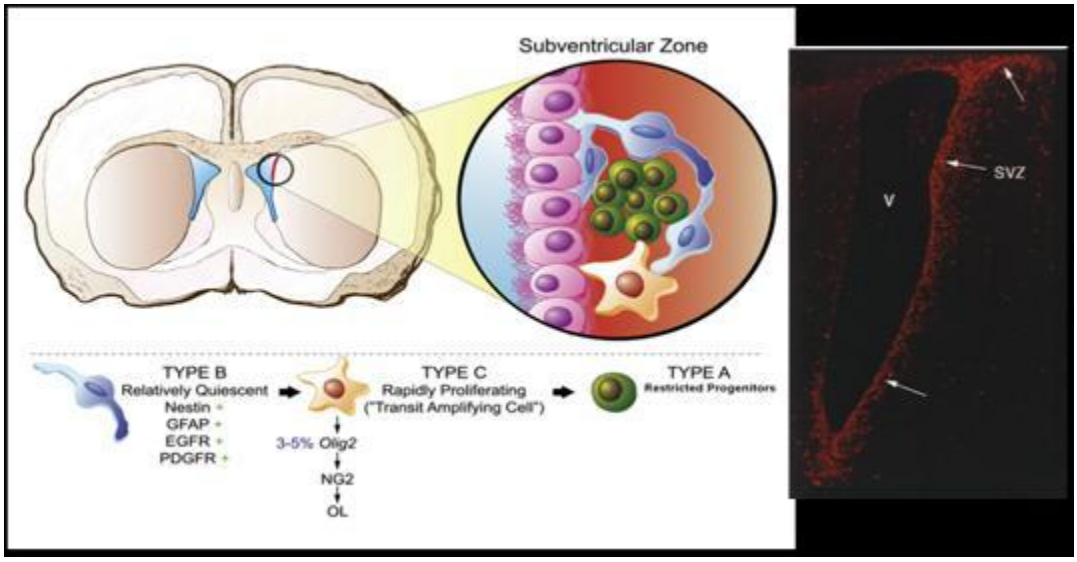

Figure 8 [Left]: stem cells (B cells; blue), neural progenitors (C cells; amber) and neuroblasts (A cells; green) in the sub-ventricular zone [Stiles 2008]. **[Right]:** adult rodent brain ventricle (V) and sub-ventricular zone (SVZ). Arrows point to some of the proliferating cells in the SVZ that were labeled after intraperitoneal injection of the thymidine analogue, 5-bromodeoxyuridine [modified from Galli 2003].

- ***Neural progenitors:*** being more proliferative than stem cells and differentiated cells, these cells can easily undergo oncogenic mutations that are fixed during replication. Many of the pathways found abnormally activated in gliomas are also sustained in neural progenitor cells, since they are necessary for progenitor proliferation and migration. Progenitors can migrate as well as tumour cells, even if glioma cells can proliferate and migrate at the same time, whereas progenitor cells have limited migration capacities and enter mitosis only after they have reached the final destination [Canoll 2008].

  Neural progenitors are characterized by a high plasticity, and can modify their differentiation state in response to specific stimuli [Vescovi 2006].

- ***De-differentiated mature glial cells:*** these cells, after mutation accumulation could acquire a stem-like phenotype, originating multipotent malignant cells able to sustain glioma proliferation. In fact glioma cells express both undifferentiated and differentiated markers: a high number of de-differentiation markers, paired with a decrease of differentiation markers, correlates with glioma progression [Germano 2010]. However, there is no knowledge of a de-differentiation process in these cells capable to originate multipotent malignant cells.

A new classification of primary glioblastoma has been proposed, on the basis of spatial relationship with SVZ (known to be enriched in stem cells) and cortex [Lim 2007]:

- **group I**: GBM contacting SVZ and infiltrating cortex; characterized by multifocality and tumour recurrences noncontiguous with the initial lesion (so with a more invasive and migratory phenotype);
- **group II**: GBM contacting SVZ but not involving cortex;
- **group III**: GBM not contacting SVZ but involving cortex;
- **group IV**: GBM neither contacting SVZ nor infiltrating cortex, never multifocal with recurrent lesions always bordering the primary site

It has been suggested that group I GBMs originate from transformed NSC, maintaining expression of matrix metalloproteinases (as typical of highly aggressive and infiltrating tumours); the contact with the SVZ niche, may also be permissive for tumour growth and migration. In contrast, group IV GBMs may arise from white matter glial progenitors, which have very limited migration potential.

Worth to be noted, oncogenic transformation and gliomagenesis can be obtained by induction of PDGFB expression, in nestin^{+} progenitor cells, committed oligodendroglial precursors or mature GFAP^{+} astrocytes [Huse 2010] and stimulation of PDGFR signaling can induce tumour-like proliferation of NSC. In addition, combinations of oncogenes/ tumour suppressor genes deregulation trigger tumorigenesis from differentiated astrocytes [Zhu 2009; Park 2009]. The discrepancies in these studies indicate that several different cell types probably harbor tumorigenic potential and that their ability to initiate neoplasia may depend on the precise mechanisms governing the underlying oncogenic stimulus and/or the molecular subclass of the tumour in question [Huse 2010].
Experimental models indicate that gliomas can arise from both undifferentiated multipotent cells and well differentiated astrocytes: it may be possible that the differences between the primary/de novo and secondary/progressive GBM reflect a different cell of origin.
Certainly, various evidences underline that gliomas could be maintained by a population of malignant cells that exhibit stem-like properties of self-renewal and multipotency, irrespective of the cell of origin: a stem cell, a progenitor, or a differentiated somatic cell that has reacquired the stem-like properties, as summarized in figure 9 [Park 2009, Huse 2010].

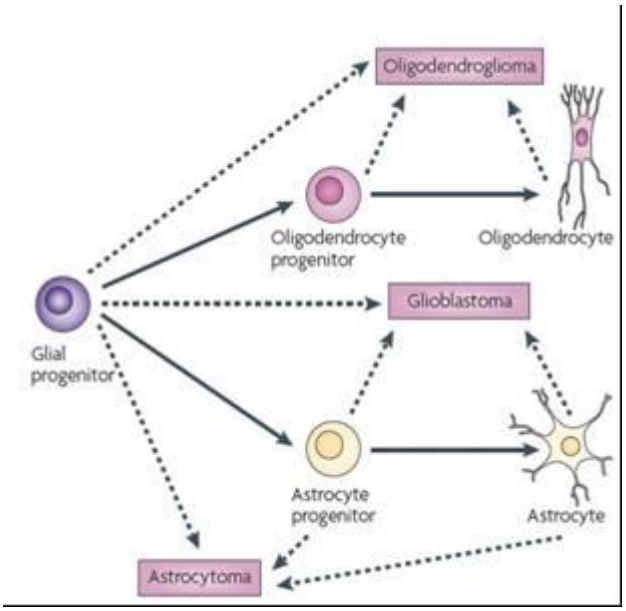

Figure 9 Although the precise cells of origin for diffuse glioma variants remain largely unknown, a selection of likely candidates for each (dashed arrows) is indicated. (Modified from Huse 2010)

4. RNAi

RNA interference process (RNAi), identified in *C. Elegans* [Fire, 1998], consists in the degradation of specific mRNA mediated by a homologous double strand: it is a conserved biologic mechanism in various eukaryotic organisms, responsible for viral RNA degradation and transposon suppression and implicated in regulatory process during embryogenesis [Bernstein 2001].

A common mechanism has been identified [Elbashir 2001; Dykxhoorn 2003; Bantounas 2004]:

1. RNAi is triggered by a dsRNA (exogen or viral RNA, transposons, endogenous dsRNA): dsRNA is processed by Dicer enzyme and becomes a small interfering RNA (siRNA) 21-22 bp long. siRNAs are characterized by a protruding 3' –OH, as typical of degradation mediated by RNAsi III, and a phosphate group at 5'.
2. The mRNA is silenced by a sequence specific target mechanism: Dicer efficiency is proportional to dsRNA length: the longest the dsRNA is, the most are the derived siRNAs and the silencing effect. siRNAs derived from Dicer processing are recruited by RISC endonuclease (*RNA induced silencing complex*).

3. Target degradation requires evolutionary conserved enzymatic complexes: RISC, by its ATP dependent - helicase activity, separates the 2 strands of siRNAs, retaining the anti-sense strand [Martinez 2002; Hammond 2000]. The target mRNA is recognized thanks to base-pairing and digested by RISC [Elbashir 2001]. (Figure 9)

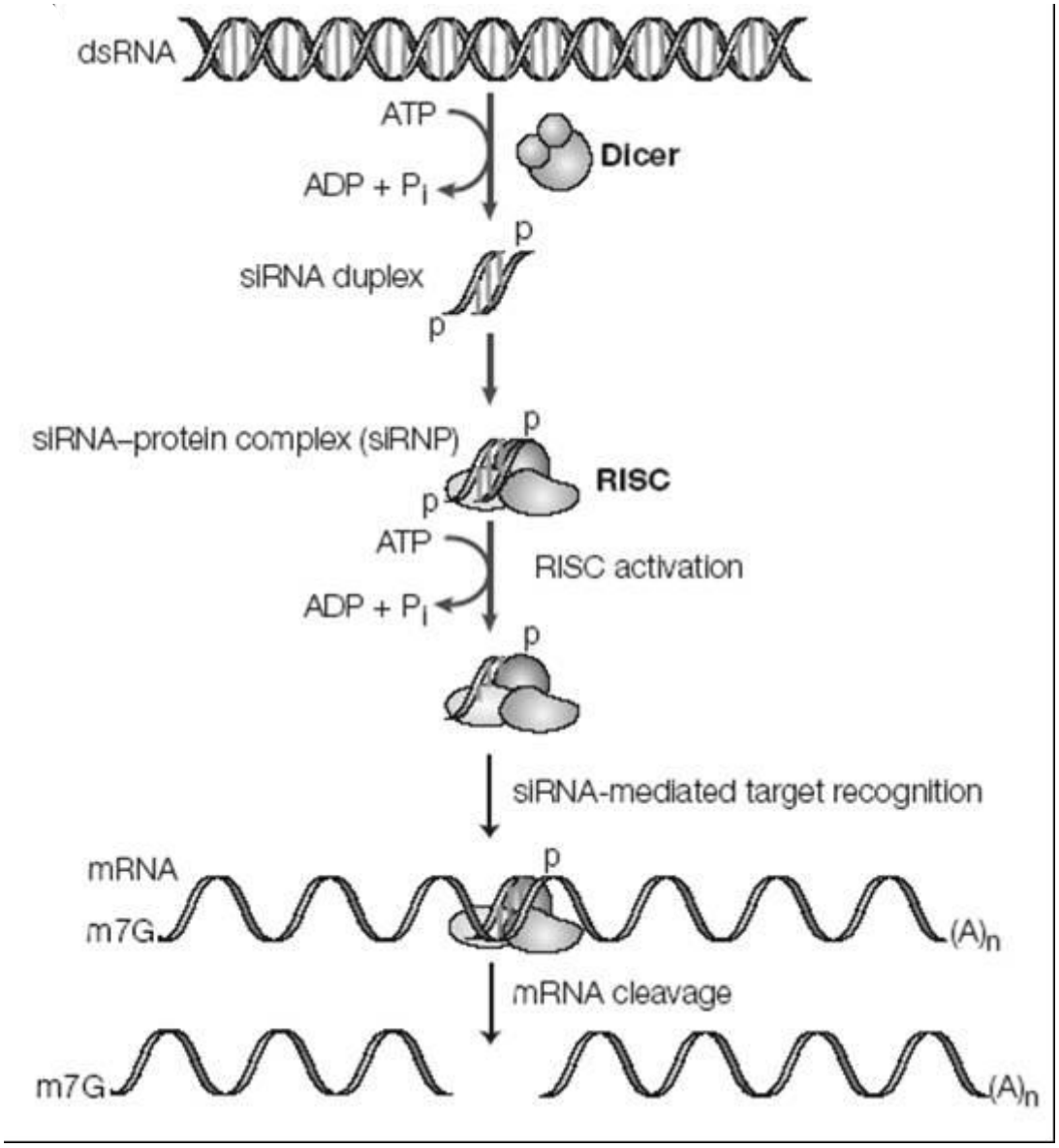

Figure 9: RNA interference**:** long dsRNA are processed by Dicer in siRNAs, which are incroporated by RISC (*Nature reviews Mol Cell Biol 2003, 4: 457-467)*

RNAi by long dsRNA has been demonstrated to be a very useful tool in functional studies in *Drosophila* and other eukaryotic organisms: unfortunately, in mammals, this approach can only generate an unspecific response, mediated by interferon, with inhibition of protein synthesis and a global RNA degradation [Bass 2001]. However, RNAi can be induced in mammalian cell lines by transfection with chemically syntethized dsRNA 21-22 bp long, that are presumed to directly interact with RISC [Elbashir 2001].

To obtain a specific silencing, the siRNA molecule has to be designed using specific algorithms which identify the best region for silencing in the mRNA target: usually more than one siRNA is tested to verify the silencing efficiency [Holen 2002].

Secondary structures of siRNA and of the target mRNA can also influence the silencing efficiency, together with the transfection method (electroporation, lipid-based transfection).

Even though siRNAs represent a very useful tool in functional studies, the main bias is represented by their transient activity: cellular duplication causes a progressive dilution of the siRNA molecules, until a level under the threshold necessary to maintain the silencing: thus in actively replicating cells, silencing duration is strongly correlated with the number of cell divisions. [Elbashir 2001]. Usually, the effect on the cell phenotype persists for a maximum of 7 days, sometimes not sufficient to obtain the silencing of a gene codifying for long half-life proteins [Paddison 2002].

Literature reports depletion of centrosomal proteins (such as Tastin, Cep55, Centriolin and 4.1R) by siRNA [Yang, 2008; Fabbro 2005; Gromley 2003; Krauss 2008], resulting in severe alteration of cell cycle progression and apoptosis induction, multi-nucleated cells, mitotic arrest and alterations in spindle formation, compatible with the disruption of centrosome functions.

Materials & Methods

1. CELL CULTURES

1.1 Human primary glioma cell lines

Glioblastoma (GBM) cell lines used for functional studies have been selected from a panel of 21 human primary glioma cell lines obtained from post-surgery specimens and characterized as described elsewhere [Perego 1994; Beghini 2003; Magnani 2004; Roversi 2006]. Features of cell lines are reported in table 1.

SEX/ AGE at surgery	CELL LINE	HISTOLOGICAL DIAGNOSIS	WHO GRADE	KARYOTYPE
M / 63	G-32	GBM	IV	64, XXY, +1, +7, , +8, +9, +10, +11, -12, +13, +14, +15, -18, +19, +21, +22, +3mar
F / 36	MI-60	GBM	IV	45-46, XX, add(1)(q12), der(19)t(19;19)(pter;q12), del(19)(q12)/ 92, XXXX, add(1)(q12), der(19)t(19;19)(pter;q12), del(19)(q12)

Table 1: clinic and pathological features of GBM derived cell lines..

Cells were grown in RPMI[23] supplemented with 5% fetal bovine serum (FBS), 100 U/ml penicillin (Pen) and 100 U/ml streptomycin (Strep) at 37°C and 5% CO_2. They were split during the exponential growth phase using trypsin-EDTA[24]. Cells were tested by Immunofluorescence with DAPI[25] to verify the absence of mycoplasma contamination.

MI60 GBM cell line, initially used for RNAi optimization, because showing heterogeneous populations, has been replaced with G32 GBM cell line, used in siRNA experiments

1.2 Human normal fibroblasts

Adult fibroblasts, used as control, were grown at 37°C in a 5% CO_2 atmosphere in RPMI supplemented with 10% FBS and 100 U/ml Pen-Strept. Fibroblasts, derived from skin biopsy, were obtained from "Cell Line and DNA Biobank from Patients Affected by Genetic Diseases" (G. Gaslini Institute) - Telethon Genetic Biobank Network – Project N. GTB07001

2. PROTEIN HALF-LIFE ASSAY

In order to better define the duration of RNAi experiments, we performed time-lapse Cycloheximide (CHX) treatment (50μg/μL stock solution in 70% EtOH) on MI-60 GBM cell line, harvesting cells at 48, 96, and 120 hours after CHX addition (final concentration 100μg/μL). Western Blot (WB) (described in paragraph 6 of

[23] Developed by Moore at the Royal Park Memorial Institute.
[24] Ethylenediaminetetraacetic acid.
[25] 4',6-Di Amidino-2-Phenyl Indole.

this section) was performed to assess the presence of MARK4 protein. Cycloheximide (CHX) is an inhibitor of protein biosynthesis in eukaryotic organisms, produced by the bacterium *Streptomyces griseus*. CHX exerts its effect by interfering with the translocation step in protein synthesis (movement of two tRNA molecules and mRNA in relation to the ribosome) thus blocking translational elongation. CHX is widely used in biomedical research to inhibit protein synthesis in eukaryotic cells studied in vitro. It works rapidly and its effects are rapidly reversed by simply removing it from the culture medium.

3. RNAi

MARK4L and MARK4S knockdown was obtained by RNAi, which relevant features are summarized in BOX 1.

BOX 1 – RNAi

RNA interference (RNAi) is one of the most important technological breakthroughs in modern biology, considered essential for studying gene function, allowing to directly observe the effects of the loss of function of specific genes in mammalian systems. It has become a prominent tool for protein knockdown studies, phenotype analysis, function recovery, pathway analysis, in vivo knockdown, and drug target discovery.

The molecules that mediate RNAi are short dsRNA oligonucleotides, 21 nucleotides in length, internally processed by Dicer enzyme: the cleavage products are short interfering RNA (siRNA).

RNAi technology takes advantage of the cell natural machinery to effectively knockdown expression of a gene with transfected siRNA. There are several ways to induce RNAi: synthetic molecules, RNAi vectors, and *in vitro* dicing.

In mammalian cells, siRNAs specifically degrade the target mRNA: the antisense strand of siRNA associates with the multiprotein complex, or RNA-induced silencing complex (RISC), which then identifies and cleaves at a specific site the corresponding mRNA, next targeted for degradation. Ultimately this process results in the loss of protein expression.

We performed RNAi by *Silencer®* Select siRNAs or Stealth RNAi™ siRNA duplexes, obtained by Ambion and Invitrogen, transfected by lipid-mediated transfection with Lipofectamine™ RNAiMAX (Invitrogen). This transfection reagent is a cationic lipid formulation suitable for delivering molecules across a diverse range of commonly used cell lines and specifically developed for highly efficient delivery of Stealth RNAi™ siRNA or *Silencer®* Select siRNA to mammalian cells.

It has been reported that it can cause cytotoxicity, thus determining an apparent off-target effects due to suboptimal or excess in delivery reagent. One cause of off-target effects is the up- or down-regulation of genes due to the siRNA delivery procedure. Off-target effects can also be due to non-specific knockdown mediated by the siRNA duplex itself.

To avoid these problems, different concentrations of siRNA were tested to determine the most favorable conditions, that is the lowest siRNA concentration that gives the desired level of knockdown in RNAi experiments.

3.1 Assessing of transfection efficiency

To verify the effective internalization of dsRNA used in RNAi experiments, GBM cell lines and fibroblasts were tested using Cy3-Luciferase siRNA (Upstate), easily detectable by fluorescence microscopy: internalization was considered optimal when at least 90% of the treated cells showed cytoplasmic fluorescent signal at different observation time (24 and 48 hours after transfection). Transfection of Cy3-Luciferase siRNA has been performed using both reverse and forward transfection protocol, as described further on.

3.2 Negative Control

siRNA negative control, not targeting any specific gene product (because designed to have no similarity to mouse, rat, or human transcript sequences), was tested in both GBM cell lines and fibroblasts under study. Since we found that the Silence Negative control siRNA at 40nM (siRNA#1 Ambion) did not show significant impact on cell proliferation, apoptosis or cell morphology, we used it to distinguish non specific (NS) effects on siRNA treated cells.

3.3 Silencer siRNAs and Stealth siRNAs

To obtain MARK4 knockdown we used different siRNA, selected after testing their efficiency (Table 2): siRNA used in the knockdown experiments are indicated with (*).

siRNA		sense	antisense	target region
(*)	**siRNA anti MARK4S+L # 1089 (Ambion)**	GGUUGCCAUCAAGAUUAUCtt	GAUAAUCUUGAUGGCAACCtc	ex 2-3
	siRNA anti MARK4S+L # 1090 (Ambion)	GGGAAACUGAGGAAAUCUUtt	AAGAUUUCCUCAGUUUCCCtc	ex 18
(*)	**Stealth siRNA MARK4S #10 (Invitrogen)**	CGAUCCCUCUAAACGGCAGAACUCU	AGAGUUCUGCCGUUUAGAGGGAUCG	ex 16
	Stealth siRNA MARK4S #11 (Invitrogen)	GAUCCCUCUAAACGGCAGAACUCUA	UAGAGUUCUGCCGUUUAGAGGGAUC	ex 16
	Stealth siRNA MARK4S #17 (Invitrogen)	UCUAAACGGCAGAACUCUAACCGCU	AGCGGUUAGAGUUCUGCCGUUUAGA	ex 16

Table 2: siRNA used in MARK4 silencing experiments

siRNAs silencing both MARK4S and MARK4L were *Silencer Validated siRNAs™* (Ambion # 1089 and # 1090) which are siRNA duplexes already verified to reduce the expression of their individual target genes. Each one has also been functionally proven and is guaranteed to reduce target gene expression at least 70% after 48 hours post-transfection.

Stealth RNAi™ double-stranded are blunt-ended 25-mers that reduce significantly off-target effects, avoid induction of stress response pathways, and with enhanced nuclease stability without loss in potency. *Stealth siRNA™* used in knockdown experiments are customized siRNA, designed by *BLOCk-iT™ RNAi Designer* (Invitrogen – Free Use on line) to specifically target exon 16, skipped in MARK4L isoform, and thus

able to determine specific MARK4S silencing. The 3 Stealth siRNA molecules obtained with the design software were all tested for efficiency in MARK4S knockdown.

Based on MARK4 half-life assay, we performed experiments with the following time table:

Day 0: Reverse Transfection

Day 2: Forward Transfection

Day 3: 72 hours silencing data collection

Day 5: 120 hours silencing data collection

For cell curve and cell cycle analysis by cytofluorimeter (see section 8 of this paragraph), cells were collected every 24 hours since silencing initiation.

3.4 Reverse transfection

In reverse protocol, transfection mix is prepared and then dispensed in each plate: only after, cells and medium are added, following concentration ranges given by the manufacturer (Table 3).

plate	transfection mix volume	reverse transfection		forward transfection
		cell number	cell suspension	culture medium
Ø 35 mm	500 uL	100.000-150.000	2 mL	2 mL
Ø 60 mm	1 mL	200.000-300.000	4 mL	4 mL
Ø 100 mm	2 mL	400.000-600.000	8 mL	8 mL

Table 3: volume/cells number correspondence for reverse and forward transfection protocol in culture plates

RNAi duplexes–Lipofectamine® RNAiMAX complexes were prepared as follows: RNAi duplexes were added to RPMI Medium without serum and without antibiotics to achieve the optimal final concentration. After gentle mixing, Lipofectamine® RNAiMAX was added to the mix (1uL in 100 µL mix), then incubated for 10-20 min at RT and subsequently dispensed in each plate. Cells, diluted in RPMI with 5-10% FBS without antibiotics were added to each plate, then incubated at 37°C 5%CO_2 until ready to assay for gene knockdown or to prolong transfection by forward transfection protocol.

3.5 Forward transfection

In forward transfection, the mix is generally prepared and added the day after the plating of cells. We used this procedure when we need to repeat the transfection 48h hours after the reverse transfection, in order to maintain the silencing over than 120 hours.

The transfection mix was prepared and incubated as previously described for reverse protocol.

The same plates used for reverse transfection, were treated as follows:

culture medium was removed and the correspondent amount of transfection mix (Table 4) was added to each plate. RPMI with 5-10% FBS without antibiotics was added to each plate, then incubated at 37°C 5%CO_2 until ready to assay for gene knockdown.

3.6 Transfection optimization

Different concentrations and combinations (to verify a possible cooperative interaction in silencing) of each siRNA were tested in order to define the optimal transfection condition (Table 4): knock down efficiency has been evaluated by Real Time RT-PCR.

siRNA combination	siRNA 1	Final Concentration (nM)	siRNA 2	Final Concentration (nM)
1	**anti MARK4S+L # 1089**	24	-	-
2	**anti MARK4S+L # 1089**	40	-	-
3	**anti MARK4S+L # 1089**	60	-	-
4	**anti MARK4S+L # 1089**	70	-	-
5	**anti MARK4S+L # 1089**	80	-	-
6	**anti MARK4S+L # 1090**	24	-	-
7	**anti MARK4S+L # 1090**	40	-	-
8	**anti MARK4S+L # 1090**	60	-	-
9	**anti MARK4S+L # 1089**	40	**anti MARK4S+L # 1090**	40
10	**anti MARK4S+L # 1089**	40	**anti MARK4S+L # 1090**	20
11	**anti MARK4S+L # 1089**	30	**anti MARK4S+L # 1090**	30
12	**Stealth anti MARK4S #10**	60	-	-
13	**Stealth anti MARK4S #10**	80	-	-
14	**Stealth anti MARK4S #11**	60	-	-
15	**Stealth anti MARK4S #11**	80	-	-
16	**Stealth anti MARK4S #17**	60	-	-
17	**Stealth anti MARK4S #17**	80	-	-
18	**Stealth anti MARK4S #10**	30	**Stealth anti MARK4S #17**	30
19	**Stealth anti MARK4S #10**	30	**Stealth anti MARK4S #11**	30
20	**Stealth anti MARK4S #11**	30	**Stealth anti MARK4S #17**	30

Table 4: siRNA combinations tested to optimize MARK4 silencing

4. RNA AND PROTEIN EXTRACTION

4.1 RNA extraction

Adherent cells were treated with 1 mL of TRIreagent (Total RNA Isolation reagent, Sigma), to preserve nucleic acids and dissolve cellular components.

As instructed by the manufacturer, the solution was supplemented with chloroform, and after 15'' vigorous shaking, was centrifuged at 14,000 rpm for 15 min at 4°C, obtaining three distinct phases: an upper-aqueous phase (containing RNA), an interphase (containing DNA), and lower-organic phase (containing proteins). RNA has been subsequently obtained by precipitation: 500 µL of isopropyl alcohol were added to the sample and incubated 15' at RT; after centrifugation at 14,000 rpm 15' at 4°C, RNA has been isolated and resuspended in DEPC water. *DNase I (RNase-free,* New England Bio-Labs, Inc., Ipswich, MA, USA) treatment has been performed on RNA samples to remove residual DNA, following manufacturer's protocol.

RNA quantity and quality were determined by measuring absorbance at 230, 260 and 280 nm with the *ND-1000 Spectrophotometer* (NanoDrop products, Waltham, MA, USA, by Thermo Fisher Scientific, Inc.).

4.2 Protein extraction

After harvesting and washing in PBS, cells were counted, resuspended in ***lysis buffer*** (100 µl /1,000,000), and incubated on ice for 30 min with occasional inversion to ensure complete lysis.

After incubation, the lysates were centrifuged at 16,000 g for 25 min (at 4°C to prevent protein degradation): the supernatant (whole cell lysate) was stored at -20°C/-80°C.

Protein concentration was determined using the *BCA Protein Assay Kit* (Pierce, Rockford, IL, USA), according to the manufacturer's protocol, using *ND-1000 Spectrophotometer*.

Lysis buffer: 150 mM NaCl, 50 mM Tris pH 7.5, 1% NP-40, 0.25% deoxycholic acid, protease inhibitor cocktail (*Complete EDTA-free* - Roche).

5. GENE EXPRESSION ANALYSIS

To verify the effective knockdown of *MARK4* S and L mRNAs, Real-time quantitative PCR was carried on cDNAs derived from transfection experiments.

5.1 Reverse transcription PCR (RT-PCR)

Reverse transcriptase PCR (RT-PCR) allows transcribing mRNA into its complementary DNA (cDNA) by *reverse transcriptase* enzyme.

600 ng of RNA extracted from cells treated with siRNA, were retro-transcribed by *High capacity cDNA reverse transcription kit* (Applied Biosystems), with random examers, according to the manufacturer's instructions. Two independent reactions were carried on and a PCR amplifying the housekeeping gene *GAPDH* was performed in order to verify the efficiency of retrotranscription.

forward primer:	5'-ACAACAGCCTCAAGATCATCAG-3';
reverse primer:	5'-GGTCCACCACTGACACGTTG-3';
annealing temperature:	62°C.

5.2 Real-time quantitative PCR

Real-time PCR is a highly sensitive, specific and reproducible technique which measures the expression of the target gene combining a traditional Polymerase Chain Reaction with a TaqMan probe, complementary to the inner region of the PCR product, emitting fluorescence when the template is amplified: TaqMan probe is an oligonucleotide with a reporter fluorophore on the 5' end and a quencher dye on the 3' end. During PCR elongation the DNA polymerase breaks the probe so that the reporter fluorophore is no longer switched off by the quencher and the emitted fluorescence is recorded. Detected fluorescence is therefore proportional to the accumulation of PCR products.

Amplification data are collected during the PCR exponential phase (when PCR products are directly proportional to the original quantity of the target gene cDNA), and expressed as C_T (Threshold cycle) value, corresponding to the PCR cycle at which PCR products are firstly generated. During data analysis, normalization is necessary for relative quantification, and control genes, which are constitutively expressed endogenous genes (housekeeping genes), have to be analyzed in parallel for this purpose.

5.2.1 TaqMan assays and Real-time PCR

Real-time PCR was performed with Applied Biosystems *TaqMan Fast Universal PCR Master Mix 2x No AmpErase UNG* (consisting of DNA polymerase, buffer and dNTPs) and *TaqMan Gene Expression Assays* (specific for each target or control gene), which features are reported in Table 5. Mix conditions are reported in Table 6.

ASSAY	PRIMER SEQUENCE	PROBE SEQUENCE
MARK4L	**F** 5' CCGAAGGGTCGCAGACGAA 3'	5' CCTGAGGTCACAAGTT 3'
	R 5' CCGTTTGATCCCAAGGTAGATG 3'	
MARK4S	**F** 5' GTTACCCTCGATCCCTCTAAACG 3'	5' CAGAACTCTAACCGCTGTGT 3'
	R 5' GTTCGTCTGCGACCTGATCTT 3'	
ACTIN β	*Inventoried assay reagent;* ID: Hs99999903_m1	
GAPDH	*Pre-developed assay reagent*; ID:4333764F	
RPLP0[26]	*Pre-developed assay reagent*; ID:4333761F	

Table 5: primer and probe sequences for MARK4S and L *Assays on demand*; ID for control gene assays.

H_20	2.5 µL
Master Mix (2x)	5.0 µL
TaqMan Assay (20x)	0.5 µL
cDNA (1.5 fold dilution)	2 µL

Table 6: Real Time RT-PCR mix

[26] Ribosomal Phosphoprotein Large P0.

MARK4 primers and probes were designed on the boundary between exons, to avoid genomic DNA amplification and in order to have assays specific for each isoform: MARK4S forward primer and probe bind exon 16, absent in MARK4L mRNA, and reverse primer is on the boundary between exons 16 and 17; MARK4L forward primer was placed between exon 15 and 17 (joined by alternative splicing in MARK4L mRNA), while the probe and reverse primer bind exon 18.

Reactions were performed on the *StepOne Real-Time PCR System* (Applied BioSystems), under these conditions:

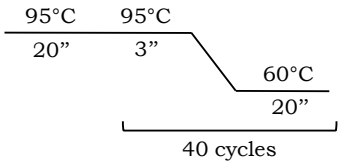

All samples were retro-transcribed in two independent reactions and loaded in triplicate in Real-Time experiments.

5.2.2 Relative quantification analysis

C_T data were analyzed by *StepOne Software* (v1.2; Applied Biosystems) or, alternatively using two different methods: the $2^{-\Delta\Delta C}{}_T$ method (also known as Livak method, [Livak 2001], for which, being more homogeneous, a single control gene was sufficient) and the geNorm method ($E^{-\Delta C}{}_T$) [Vandesompele 2002] (used for assay validation and described further on).

In both cases, *MARK4S* and *L* (target genes) expression levels were normalized by control genes and then referred to a reference sample (Non-Specific - NS), whose expression level was set as 1.

Livak method: for each sample the **target gene expression level = $2^{-\Delta\Delta CT}$**

where: **$\Delta\Delta C_T$** = sample ΔC_T – reference ΔC_T;

sample ΔC_T = [target gene C_T – control gene C_T] in the sample;

reference ΔC_T = [target gene C_T – control gene C_T] in the reference;

(*sample and reference ΔC_T correspond to the mean value between the ΔC_Ts of the two independent RT reactions*).

geNorm method: this method uses multiple control genes and the amplification efficiency (E, set as 2 in the $2^{-\Delta\Delta C}{}_T$ method) is calculated for each assay, taking into account the different efficiency of each assay.

Briefly:

1) For each assay, serial dilutions of a pool of cDNAs are processed by Real-time PCR and C_T values are put in a graph with the respective logarithmic dilution values. The **amplification efficiency E** corresponds to **$10^{-1/S}$**, where S is the slope of the interpolation line.

2) For each assay, the **relative quantity** (Q) is calculated: $\mathbf{Q = E^{-\Delta C_T}}$

   where ΔC_T = sample C_T – reference C_T.

3) For each sample, **normalization factor** (NF) is set on the basis of the geometrical mean (GM) of the relative quantities (Qs) of control genes:

   NF = GM of control gene Qs for each sample / GM of all the GMs.

4) For each sample, the **target gene relative quantity = Q / NF** is calculated.

The target gene mRNA relative quantification corresponds to the mean value between the two independent RT reactions.

Real-time expression data were expressed as mean ± standard error, useful to identify statistically significant data.

5.2.3 TaqMan assay validation

Before performing the relative quantification analysis on the samples under study, we evaluated amplification efficiency and stability of all the assays (MARK4S, MARK4L, *actin β*, *GAPDH*, *HPRT*, *RPLP0*).

Assay amplification efficiency

For each assay, we performed Real-time PCR on serial dilutions of a pool of glioma cDNAs. The obtained C_T values were graphed with the respective logarithmic dilution values. Amplification efficiency (E) was calculated as $E=10^{-1/S}$, where S is the slope of the interpolating line, and was near 2 for all the assays (table 8): E-value equal to 2 correspond to a 100% amplification efficiency, meaning that ideally PCR product quantity should double at every cycle. Therefore all the tested assays proved to have a very good amplification efficiency.

Assay stability

Assay stability is the ability to amplify the target gene with the same efficiency in a broad range of sample dilutions.

To assess this parameter, we first calculated the relative quantity (Q) of each gene in the cDNA serial dilutions, according to the following formula: $Q=E^{-\Delta CT}$ (ΔC_T =sample C_T – reference[27] C_T) and then used the *GeNorm* software (version 3.5; http://medgen.ugent.be/jvdesomp/genorm/) to sort the assays on the basis of their stability (table 7). We therefore decided to use *GAPDH* and *RPLPO* as control genes, since they were the most stable ones in the tested samples: RPLP0 has been used as reference instead of β Actin because the latter demonstrated to be less stable after MARK4 silencing.

[27] In this case the reference was the less diluted sample.

ASSAY	DILUTIONS	C_T	S	E	ΔCt	RELATIVE QUANTITY	STABILITY
GAPDH	1	16.52	-3.30	**2.01**	0.00	1.00	more stable
	1:10	19.73			3.21	0.11	
	1.100	23.05			6.52	0.01	
	1:1000	26.41			9.89	0.00	
ACTB	1	16.78	-3.65	**1.88**	0.00	1.00	
	1:10	20.35			3.57	0.11	
	1.100	24.02			7.25	0.01	
	1:1000	27.71			10.93	0.00	
RPLP0	1	17.74	-3.28	**2.02**	0.00	1.00	
	1:10	20.85			3.10	0.11	
	1.100	24.18			6.44	0.01	
	1:1000	27.56			9.82	0.00	
HPRT	1	21.78	-3.31	**2.00**	0.00	1.00	
	1:10	24.95			3.18	0.11	
	1.100	28.20			6.43	0.01	
	1:1000	31.74			9.96	0.00	less stable
MARK4L	1	23.75	-3.40	**1.97**	0.00	1.00	
	1:10	27.00			3.25	0.11	
	1.100	30.50			6.75	0.01	
	1:1000	33.92			10.17	0.00	
MARK4S	1	28.00	-3.54	**1.92**	0.00	1.00	
	1:10	31.26			3.25	0.11	
	1.100	35.00			6.99	0.01	
	1:1000	N.D.			/	/	

Table 7: assay amplification efficiency (E) and stability. For each assay, C_T values (3rd column), corresponding to serial dilutions of a pool of glioma cDNAs (2nd column), are displayed. S=slope of the interpolating line. N.D.=undetermined.

6. WESTERN BLOTTING

Equal amounts of the whole cell extracts (usually 15-25 µg) were supplemented with reducing SDS[28] loading buffer (*Blue loading buffer pack,* Cell Signaling Technology, Inc., Beverly, MA, USA) and denatured at 99°C for 3 min.

Proteins were separated by 4% (Stacking; 100V for 10') and 10% (resolving; 130V for 115-120') SDS PolyAcrylamide Gel Electrophoresis (SDS-PAGE) and then transferred by electroblotting to a PVDF[29] membrane (Roche). *Mini-PROTEAN Tetra cell* and *Trans-blot semi-dry electrophoretic transfer cell* (both Bio-Rad) were respectively used for electrophoresis and electroblotting (10V, 30 min) as instructed by the manufacturer. *Biotinylated protein ladder* (Cell Signaling Technology) and *ColorBurst electrophoresis marker* (Sigma) were used as MW-standards.

[28] Sodium Dodecyl Sulphate.
[29] Polyvinylidene fluoride.

Membranes were then washed twice (10 min each) in PBS-T (PBS – 0.3% Tween20) and blocked with 5% skimmed milk in PBS-T for 1 or 2 hours (for MARK4S and L respectively) at Room Temperature (RT), in agitation.

For relative quantification studies, the membranes were cut horizontally immediately after the blocking step and incubated with the appropriate antibodies.

The membranes were incubated with primary antibodies (in PBS-T) at 4°C overnight in agitation, washed 4 times in PBS-T and then incubated at RT for 1.5 hours, in agitation, with secondary antibodies (in PBS-T, with 1% skimmed milk for anti-Goat and anti-Mouse antibodies). GAPDH has been used as housekeeping protein.

Primary antibodies *and dilutions:*

Rabbit anti-**MARK4L** (not commercial; GenScript Corporation)	1: 5,000
Goat anti-**MARK4S**[*] (Abcam)	1: 1,250
Mouse anti-**GAPDH**[*] (ab8245; Abcam, Cambridge, UK)	1: 10,000

Secondary antibodies *and dilutions:*

Goat anti-Rabbit IgG-HRP (Santa Cruz Biotechnology)	1: 25,000
Goat anti-Mouse IgG-HRP (Santa Cruz Biotechnology)	1: 25,000
Donkey anti-Goat IgG-HRP (Santa Cruz Biotechnology)	1: 25,000
Anti-biotin, HRP-linked antibody (Cell Signaling)	1: 6,250

The secondary antibodies are HRP[30]-conjugated.

The anti-biotin antibody allows detecting the biotinylated protein ladder.

After 4 washes in PBS-T and 2 washes in PBS, protein detection was performed: the membranes were covered with a peroxide/enhancer solution (*Protein detection system* from GeneSpin, Milano, Italy) for 5 min, and exposed to an *Amersham Hyperfilm ECL* plate (GE Healthcare, Waukesha, WI, USA), then developed by *Dental X-Ray developer* and *Dental X-Ray fixer* (Kodak; Bagnolet Cedex, France).

6.1 Semi-quantitative analysis

To compare MARK4L and S proteins expression in different samples, we carried out a relative quantification analysis, based on densitometry using GAPDH as normalizer (to correct differences in lysate loading, protein transfer and antibody binding).

For quantification, a low exposure time was chosen, so that the signal intensity on the plate was directly proportional (in the linear range) to the emitted signal intensity.

[30] Horse Radish Peroxidase

TIF images were acquired from plates using a scanner and analyzed with the *Image J* software, a public domain JAVA image processing program (http://rsbweb.nih.gov/ij) allowing the analysis of one-dimensional electrophoretic gel or membrane using a simple graphical method (http://rsbweb.nih.gov/ij/docs/menus/analyze.html). Briefly, each lane (including both MARK4L and GAPDH bands) was selected and lane profile plots were generated, displaying a two-dimensional graph reporting peaks corresponding to gel bands (on the X-axis) and their relative pixel intensities (on the Y-axis). After manually subtracting the background (necessary step to compare different plates), the area of each peak of interest (in square pixels) was measured.

For each sample MARK4L/GAPDH or MARK4S/GAPDH ratio was calculated to normalize data (Figure 1).

MARK4L and S expression levels shown in this thesis are referred to the NS sample, chosen as reference, whose value was set as 1.

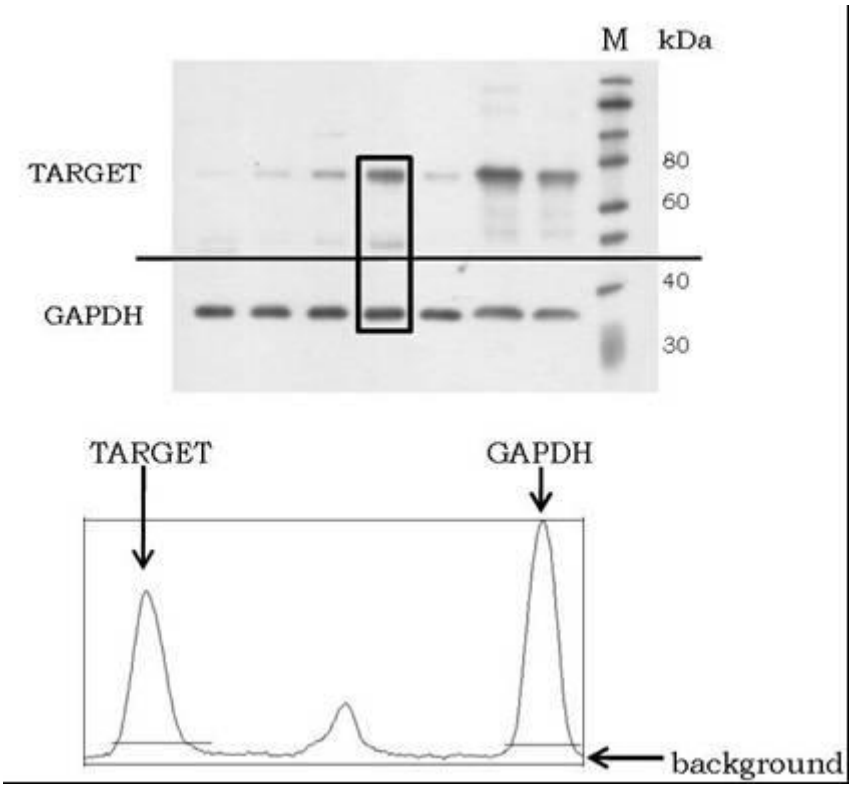

Figure 1: [upper] Example of WB membrane semi-quantitative analysis with Image J software. The box indicates one of the lanes, selected to generate its profile plot in Image J **[lower]** In the profile plot the TARGET (MARK4L or S) and GAPDH peaks are indicated and background subtracted by manually defining the peak boundaries with a line. M=molecular weight standards.

7. IMMUNOFLUORESCENCE

ImmunoFluorescence (IF) has been performed to visualize the subcellular localization of MARK4 both in non treated and transfected cells. IF was carried out in all samples in parallel.

Cells were seeded on glass chamber slides and processed at the end of transfection period (72-120 hours).

To optimize centrosomes visualization, cells were washed in PEM buffer to stabilize microtubules (0.1% Triton X-100, 80 mM PIPES[31], pH 6.9, 5 mM EGTA[32], 1 mM $MgCl_2$), and fixed with methanol for 12 min at -20°C for 12 min at RT . Permeabilization was performed by 0.1% Triton X-100 in PBS for 3 min.

Alternatively, cells were washed in PBS, fixed with methanol for 12 min at -20°C or with 4% paraformaldehyde (PFA) in PBS for 12 min at RT; permeabilization was obtained with PBS 0.1% or 0.5% Triton X-100 for 3 min.

In all samples, blocking was performed by incubation with 5% bovine serum albumin (BSA) in PBS-Tween20 for 30 min, before incubation with primary antibodies.

Primary antibodies *and dilutions:*

Rabbit anti-**MARK4L** (not commercial; GenScript)	1:200
Rabbit anti-**MARK4S** (M4947, Sigma)	1:200
Mouse anti-**γ tubulin** (clone GTU-88; Sigma)	1:200
Mouse anti-**nucleolin** (C23 D-6, Santa Cruz Biotechnology)	1:200
Mouse anti-**nucleophosmin** (B23, clone FC82291, Sigma)	1:200

Antibodies were diluted in PBS with 0.1% Tween20, and 1% goat serum[33] (Sigma) and incubated overnight at 4°C in a humidified chamber. Nucleolin and nucleophosmin were alternatively incubated for 1 hour at RT.

After three 10' washes in PBS, slides were incubated with secondary antibodies diluted in PBS, 0.1% Tween20, 2% BSA and 1% goat serum, for 1 hour at RT in a dark humidified chamber.

Secondary antibodies *and dilutions:*

Goat anti-rabbit IgG-FITC[34] (Sigma)	1:250
Goat anti-mouse IgG-TRITC[35] (Sigma)	1:200

After 3 PBS washes of 10' each, slides were mounted with DAPI /antifade (Vector Labs, Burlingame, CA, USA) and examined using an Olympus IX51 inverted fluorescence microscope, equipped with an Olympus DP71 super high-resolution colour digital camera and U-MNIBA2 excitation 460/490 (FITC), U-MWIG3 excitation 530/550 (TRITC) and U-MNU2 (DAPI) filters.

Images were acquired and processed using the F-View II-Bund-cell F software (Olympus, Tokyo, Japan).

[31] 1,4-piperazinediethanesulfonic acid.
[32] Ethylene Glycol Tetraacetic Acid.
[33] To reduce non-specific binding, the serum of the animal where the secondary antibodies are raised (goat) is added.
[34] Fluorescein IsoThioCyanate.
[35] TetramethylRhodamine IsoThioCyanate.

8. CELL CYCLE ANALYSIS BY FLUORESCENCE-ACTIVATED CELL SORTING

Cell cycle analysis has been performed by flow cytometry. Flow cytometry relevant features are summarized in BOX 2.

Sample preparation

Harvested cells (by Trypsin/EDTA 0.05% in PBS) were counted, centrifuged 7' at 1200 rpm and washed with 1 mL of PBS. The pellet has been accurately resuspended on ice in Saline GM solution (1 mL) by an insulin syringe with 22G needle. 3 mL of 96% EtOH have been added drop by drop, while vortexing, to fix cells preventing aggregation and to obtain a final concentration of 70% EtOH. Fixed samples were preserved at 4°C before staining.

Saline GME solution

Glucose	1.1 g/L
NaCl	8 g/L
KCl	0.4 g/L
Na2HPO4.2H2O	0.2 g/L (0.39 g/L *12 H2O)
KH2PO4	0.15 g/L
EDTA	0.2 g/L (0.5 mM)

Propidium Iodide Staining

Fixed samples were centrifuged at 1200 rpm 10', washed with PBS, then resuspended in 2 mL of 25 µg/mL IP solution and PBS (1:1) and incubated O.N. at 4°C before the analysis with cytofluorimeter. 25uL of RNAse A (1mg/mL) were also added.

Fluorescence intensity of cells stained with Propidium Iodide (PI) correlates with the amount of DNA: since DNA content (and fluorescence intensity) duplicates during S phase, it is possible to discriminate G_0, G_1 and G_2/M.

During cytofluorimetric analysis, doublet discrimination has been performed to avoid artifacts due to aggregation (doublets) of G_0/G_1 cells: as doublets have the same amount of DNA of a single cell in the G_2/M phase, they have to be necessarily excluded. We acquired 10000 events for each sample.

Cell cycle distribution has been evaluated by FACS-Calibur flow cytometer (Becton Dickinson), characterized by an argon laser, with 488 nm wavelength and constant 15mV power.

DNA – Phospho Histone H3 staining

In eukaryotes,phosphorylation of histone H3 is tightly correlated with chromosome condensation during both mitosis and meiosis, so that immunostaining with phospho-specific antibodies in mammalian cells, counterstained with Propidium Iodide, can reveal the fraction of G_2/M phases correspondent to mitosis.

After fixation, cells were centrifuged at 1200 rpm for 10 minutes in PBS 5% FBS to favor pelletting, then washed with PBS 1% BSA (optional). Pellets were incubated in 0.25% Triton X 100 for 5 minutes on ice. 2 mL of cold PBS 1% BSA were added and cells were centrifuged at 1200 rpm 10'. Samples were incubated O.N. at 4°C in agitation with 200 µL of Anti Phospo H3 (1 µg /200 µL of PBS 1% BSA - Upstate code #06-570, 200 µg/µL). After incubation, cells were washed with PBS 1% BSA and centrifuged at 1200 rpm 10'.
Cells were incubated with FITC goat anti-rabbit antibody (Jackson Lab cat 111-096-003) 0.5/0.7 µg in 200 µL 1% BSA at RT for 1 hour in agitation. After washing with PBS 1% BSA, cells were resuspended in 2 mL of Propidium Iodide solution (2.5 µg/mL in PBS) and 25 uL of RNAse (1mg/mL) for at least 60' at RT.
Samples were analyzed at cytofluorimeter (Excitation 488-635 nM; emission 530-620-661716 nm).

9. APOPTOSIS TEST

Apoptosis Test was performed by *Membrane Permeability/Dead Cell Apoptosis Kit with YO-PRO®-1 and PI for flow cytometry* (Invitrogen).
Apoptosis is a regulated process of cell death, distinguished from necrosis by characteristic morphological and biochemical changes. During apoptosis cells undergo compaction and fragmentation of the nuclear chromatin, shrinkage of the cytoplasm and loss of membrane asymmetry.
During apoptosis the cytoplasmic membrane becomes slightly permeant to some dyes, such as the green fluorescent YO-PRO®-1 dye that, combined with PI, provide a sensitive indicator for apoptosis, similarly to what happened by Annexin V/ IP staining.

Transfected cells have been harvested at the end of RNAi treatment and washed in cold PBS; cell density has been adjusted to ~1×10^6 cells/mL in PBS. For each assay, 1 mL has been used.
After adding 1 µL of YO-PRO®-1 solution and 1 µL PI solution (as instructed by manufacturer), cell suspensions were incubated on ice for 20–30 minutes.
After staining with YOPRO®-1 dye and PI, apoptotic cells show green fluorescence, dead cells show red and green fluorescence, and live cells show little or no fluorescence. These populations can easily be distinguished by a flow cytometer that uses the 488 nm line of an argon-ion laser for excitation.
Within 1–2 hours after incubation period, stained cells were analyzed by flow cytometry, using 488 nm excitation with green fluorescence emission for YO-PRO®-1 (i.e., 530/30 bandpass) and red fluorescence emission for propidium iodide (i.e.,610/20 bandpass), gating on cells to exclude debris. Standard compensation was performed using single-color stained cells.

BOX 2 – FLOW CYTOMETRY

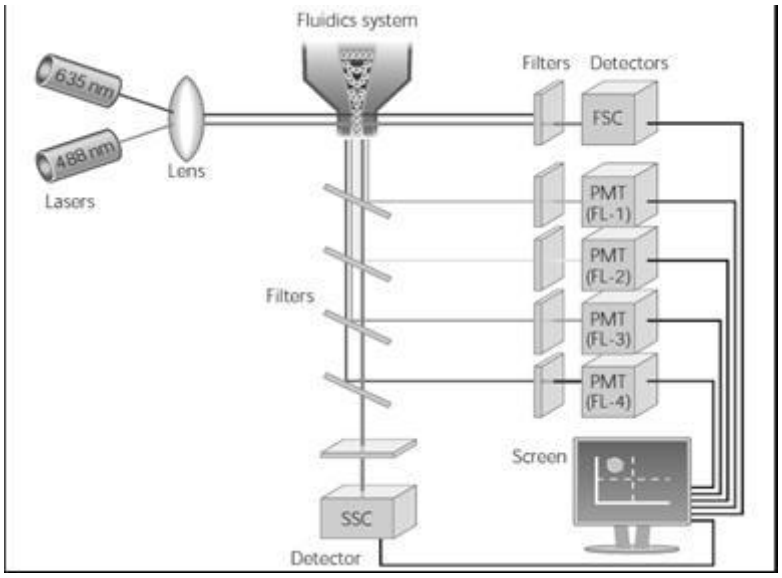

Figure 2: Schematic overview of a typical flow cytometer setup

One of the fundamentals of flow cytometry is the ability to measure the properties of individual particles. When a sample in solution is injected into a flow cytometer, the particles are randomly distributed in three-dimensional space. To be correctly interrogated by the detection system, the sample must therefore be ordered into a stream of single particles by the fluidics system: a central channel/core, through which the sample is injected, is enclosed by an outer sheath that contains faster flowing fluid and creates a massive drag effect on the narrowing central chamber. This process, known as "hydrodynamic focusing", creates a single file of particles. Under optimal conditions (laminar flow) the fluid in the central chamber will not mix with the sheath fluid. After hydrodynamic focusing, each particle passes through one or more beams of light. Light scattering or fluorescence emission (if the particle is labeled with a fluorochrome) provides information about the particle's properties.

Two different types of light source can be used in flow citometry: xenon/mercury arc lamps or lasers.

Principal emission wave lengths (λ) of a mercury arc lamp are 313, 334, 365, 405, 435, 546 and 578 nm, while xenon lamps are characterized by a uniform emission all over the light spectrum: using specific filters it is possible to select the desired λ.

Otherwise, argon lasers show a consistent stability in emission and a very high monochromaticity, optimizing signal-noise ratio. Moreover, differently from mercury lamp, this lasers have a very intense emission at 488 nm, Fluorescein Isothiocyanate excitation band, the most used fluorochrome in IF.

The light scattered in the forward direction, typically up to 20^{o} offset from the laser beam's axis, is collected by a lens known as the forward scatter channel (FSC): its intensity roughly equates to the particle's size and can also be used to distinguish between cellular debris and living cells.

Light measured approximately at a 90° angle to the excitation line is called side scatter. The side scatter channel (SSC) provides information about the granular content within a particle. Both FSC and SSC are unique for every particle, and a combination of the two may be used to differentiate different cell types in a heterogeneous sample.

Fluorescence measurements taken at different wavelengths can provide quantitative and qualitative data about fluorochrome-labeled cell surface receptors or intracellular molecules such as DNA and cytokines.

Flow cytometers use separate fluorescence channels (FL-) to detect light emitted. The number of detectors will vary according to the machine and its manufacturer. Detectors are either silicon photodiodes (commonly used to measure forward scatter when the signal is strong) or photomultiplier tubes (PMTs), more sensitive instruments and ideal for scatter and fluorescence readings.

The specificity of detection is controlled by optical filters, which block certain wavelengths while transmitting (passing) others. There are three major filter types: 'Long pass' filters allow through light above a cut-off wavelength; 'short pass' permit light below a cut-off wavelength and 'band pass' transmit light within a specified narrow range of wavelengths. All these filters block light by absorption.

Dichroic filters/mirrors are filters placed at a 45° angle to the oncoming light, with two functions: to pass specified wavelengths in the forward direction and to deflect blocked light at a 90° angle. To detect multiple signals simultaneously, the precise choice and order of optical filters will be an important consideration.

When light hits a photodetector, the voltage of the small current generated has an amplitude proportional to the total number of light photons received by the detector. This voltage is then amplified by a series of linear or logarithmic amplifiers, and by analog to digital convertors (ADCs), into electrical signals large enough (5–10 volts) to be plotted graphically: Log amplification is normally used for fluorescence studies because it expands weak signals and compresses strong signals, resulting in a distribution that is easy to display on a histogram. Linear scaling is preferable where there is not such a broad range of signals e.g. in DNA analysis.

The measurement from each detector is referred to as a 'parameter' (e.g. forward scatter, side scatter or fluorescence). The data acquired in each parameter are known as 'events' and refer to the number of cells displaying the physical feature or marker of interest.

Flow cytometers are necessarily paired with a computer for data acquisition and analysis, with the possibility to measure different parameters simultaneously and a graphical output known as "cytogram". The operator can fix a threshold value and define an "electronic gate", to exclude irrelevant events (debris, spurious events) or to select the cell population of interest, without recurring to physical cell sorting. It is also possible to acquire and memorize a list of parameters simultaneously and to recall the data afterwards, making the opportune correlations. [Rahman M – Introduction to Flow Cytometry]

Results

1. MARK4 dsRNA INTERNALIZATION

Before investigating MARK4 function by RNAi, we verified the internalization of dsRNAs by Cy3-Luciferase siRNA with Lipofectamine RNAiMax, by using the two cell systems under study, GBM cell lines and fibroblasts. Samples visualization demonstrated a good capture of Cy3 siRNA with both reverse and forward transfection (Figure 1).

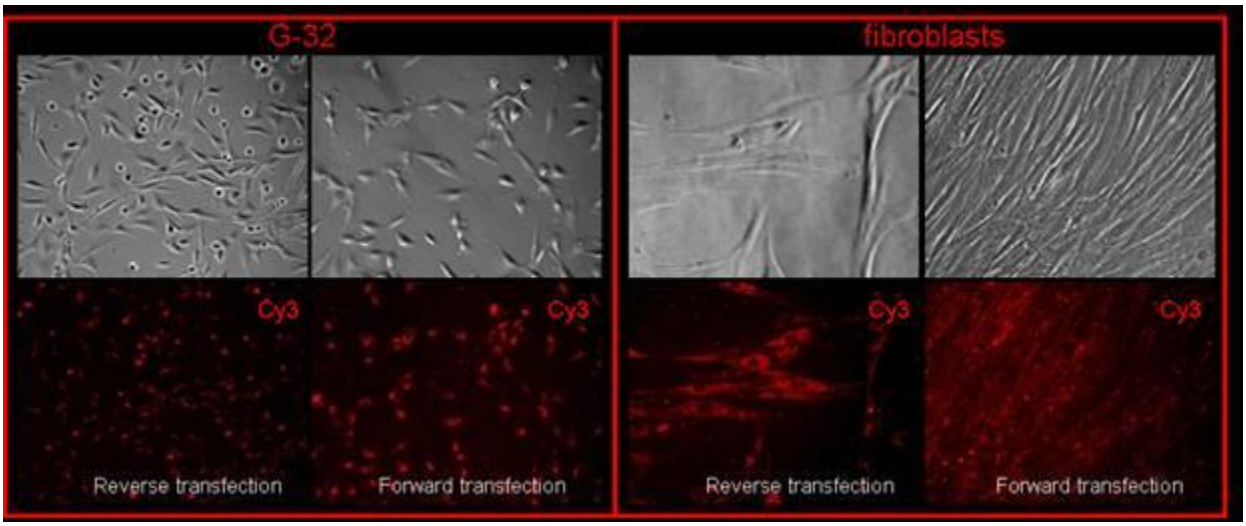

Figure 1 Cy3 siRNA homogeneously localizes in the cytoplasm of G-32 and fibroblasts cells 24 hours after transfection, while the culture medium does not show the presence of free fluorescent marker.

2. ESTIMATION OF MARK4L HALF-LIFE

We estimated MARK4L half-life, in the attempt to define the length of silencing. Experiments were performed by CHX method on the GBM MI-60 cell line. As shown in the WB, MARK4L protein starts to decrease 120 hours after CHX treatment (Figure 2). Thus we decided to prolong silencing experiments at least until 120 hours.

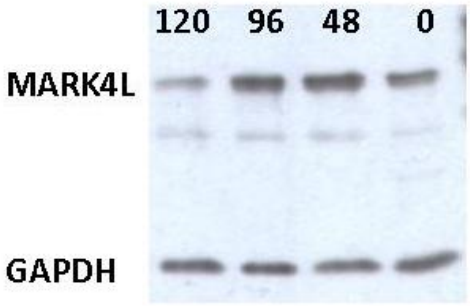

Figure 2 MARK4L protein levels after CHX treatment (final concentration 100ug/uL)

3. OPTIMIZATION OF MARK4 SILENCING

To optimize the knockdown by anti-MARK4S+L and anti-MARK4S, we tested different concentrations of both dsRNAs on GBM cell lines and fibroblasts under study. Real Time PCR, with NS as reference sample, has been used to check the knockdown.

A final concentration of 60 nM of anti-MARK4S+L siRNA #1089 showed the most efficient knockdown of both MARK4 transcripts. Differently, siRNA #1090, targeting exon 18, was less efficient for MARK4L silencing, while the combination of different concentrations of siRNAs #1089

and #1090 showed a very good silencing of MARK4S but worked sub-optimally for MARK4L (Figure 3a,b).

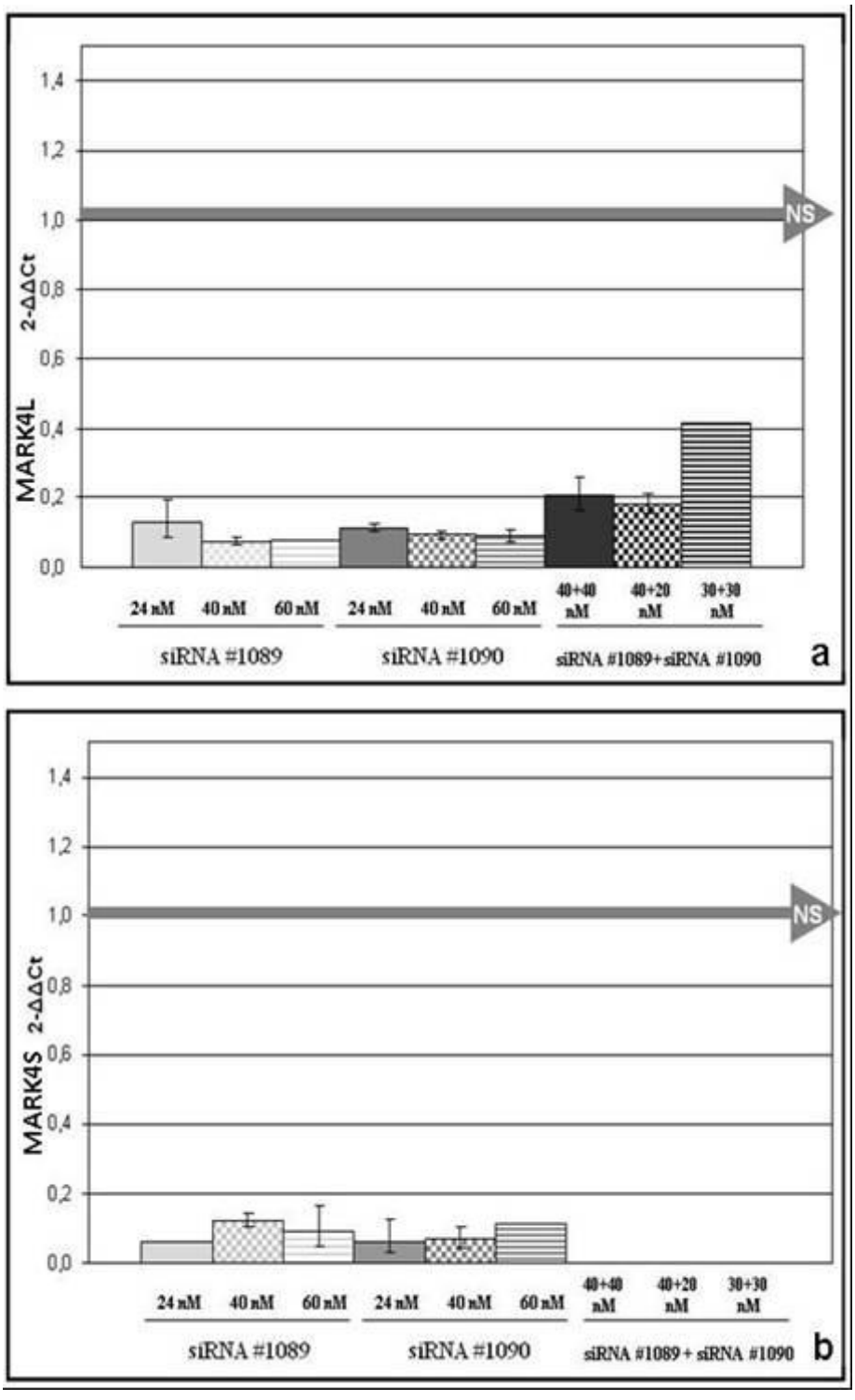

Figure 3 Transcript levels of MARK4L (a) and MARK4S (b) in the MI60 GBM cell line after anti - MARK4S+L siRNAs, at different concentrations and combinations. (Histograms: Light grey = siRNA #1089; Medium grey = siRNA #1090; Dark grey = #1089 and #1090 combinations). Silencing efficiency was estimated by comparing expression levels of silenced samples with NS (control), which expression is, by convention, equal to 1 (horizontal grey arrow).

Optimization experiments with anti-MARK4S siRNA demonstrated that a final concentration of 60nM of siRNA #10 was the most efficient to MARK4S silencing, without significantly influence MARK4L expression levels. In contrast, anti-MARK4S #11 and anti-MARK4S #17 (alone or combined with other siRNAs) despite having a good efficiency for MARK4S silencing, altered MARK4L expression levels (Figure 4a,b).

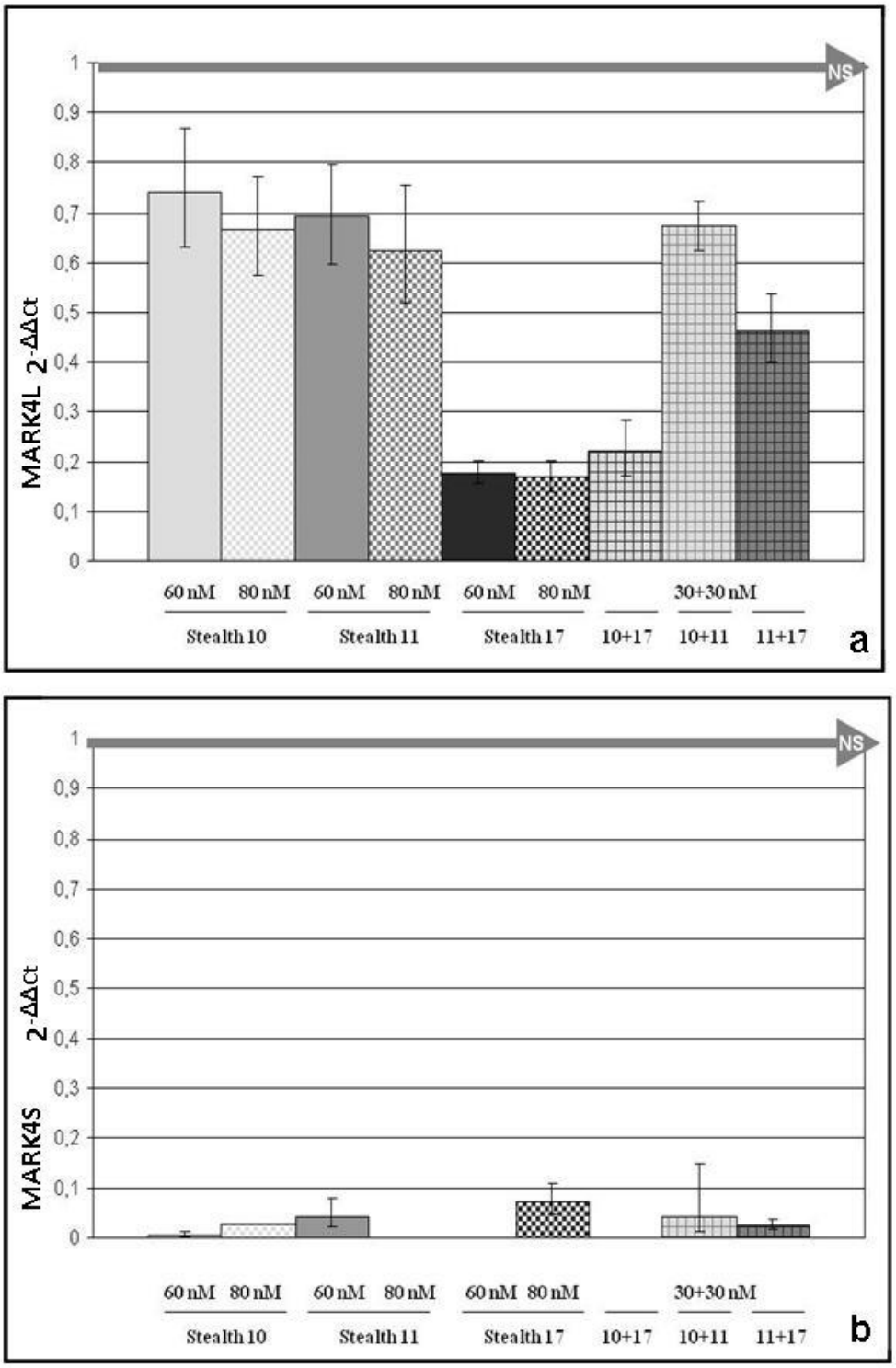

Figure 4 Transcript levels of MARK4L (a) and MARK4S (b) after anti-MARK4S siRNAs with different dsRNAs concentrations and combinations, tested on fibroblasts (Histograms: Light grey = Stealth siRNA #10; Medium grey = Stealth siRNA #1090; Black = Stealth siRNA #17; squared pattern = combinations of stealth siRNAs). Silencing efficiency was estimated by comparing expression levels of silenced samples with NS (control), which expression is, by convention, equal to 1 (horizontal grey arrow).

4. EVALUATION OF MARK4 KNOCKDOWN

Once the optimal concentrations of MARK4 dsRNAs were fixed, we evaluated MARK4L and S expression levels by Real Time PCR 48 and 120 hours after silencing.

We found that anti-MARK4S+L siRNA on G-32 and fibroblasts was very efficient: >85% of MARK4S and >75% of MARK4L transcripts were silenced in both cellular samples. Conversely, anti-MARK4S siRNA showed that >95% of MARK4S transcript was silenced, although a decrease of MARK4L (45%) was also detected in G-32 GBM cell line (figure 5).

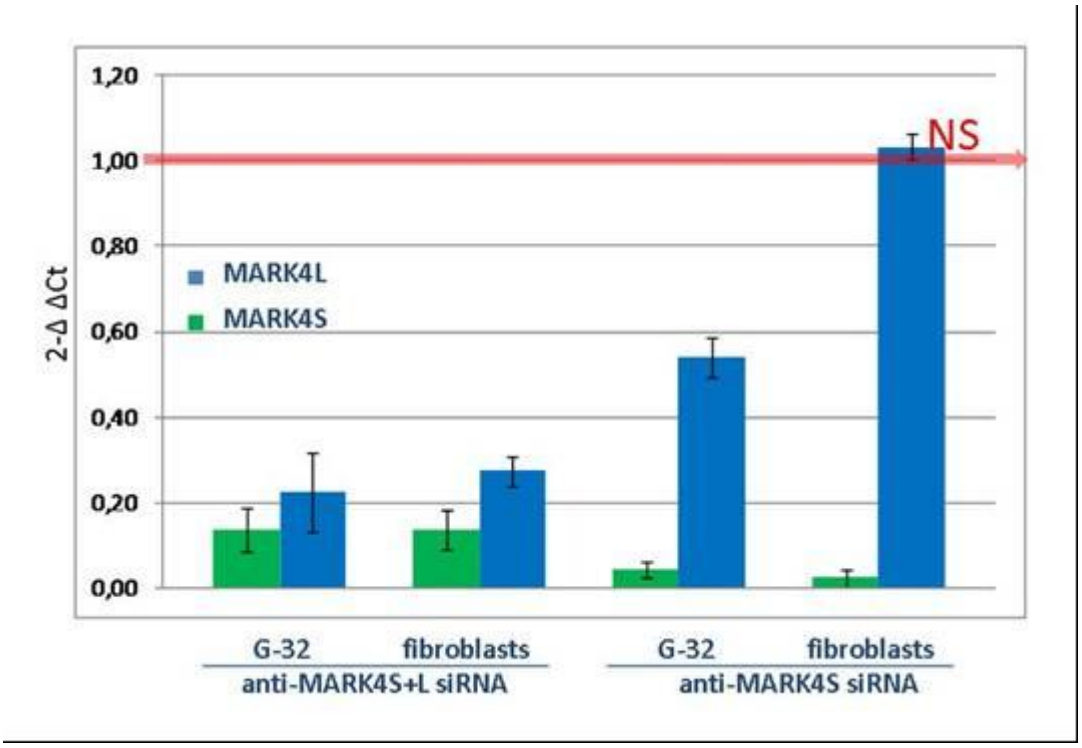

Figure 5 Graphical representation of MARK4L (blue) and MARK4S (green) transcripts after anti-MARK4S+L and anti-MARK4S siRNAs, evaluated by Real Time PCR (Mean expression levels observed in at least three independent silencing experiments, with standard deviations). Silencing efficiency was estimated by comparing expression levels of silenced samples with NS (control), which expression is, by convention, equal to 1 (red arrow).

MARK4S and L silencing has also been verified by WB, and the specific bands have been quantified by semi-quantitative densitometric analysis (Figure 6a, b). It is worth noticing that MARK4S protein decreases after both anti-MARK4S+L and anti-MARK4S siRNAs, in G-32 as well as in fibroblasts, according to Real Time RT-PCR results, while MARK4L protein levels are comparable to the control (NS) values, in contrast with Real Time data.

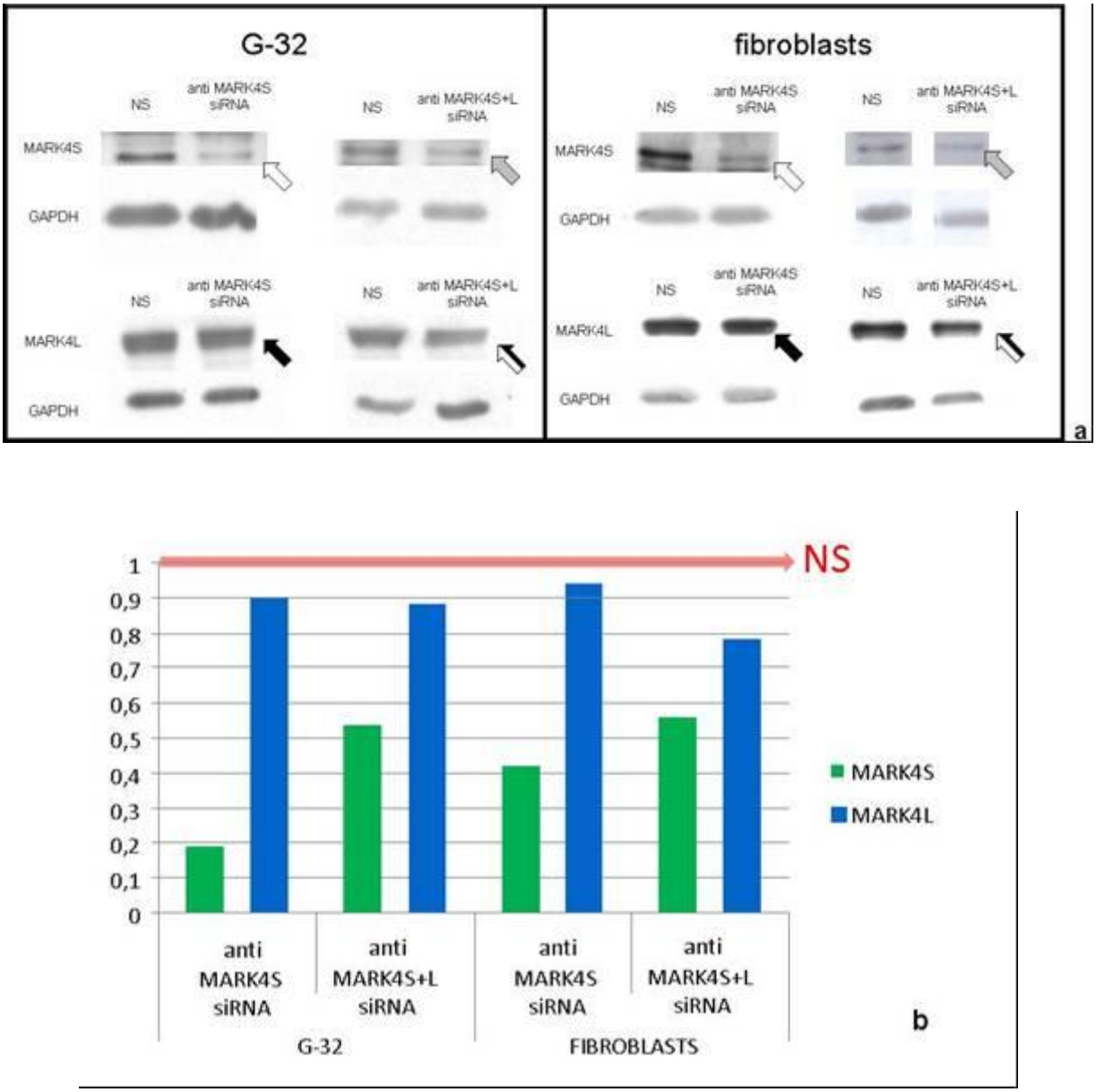

Figure 6 (a) WB of MARK4S and MARK4L 120 hours after anti-MARK4S and anti-MARK4S+L siRNA; b) densitometric quantification of MARK4L (blue) and MARK4S (green) proteins.
After MARK4S silencing, the S isoform is reduced of 80% in G-32 and 60% in fibroblasts (white arrows), while after anti-MARK4S+L siRNA (grey arrows) the decrease of MARK4S isoform is less evident. In contrast, G-32 and fibroblasts don't show a decrease of the L isoform after both anti-MARK4S (black arrows), and anti-MARK4S+L (black and white arrows) siRNAs.

5. EFFECTS OF MARK4 KNOCKDOWN ON CELLULAR MORPHOLOGY

MARK4 depleted cells (G-32 and fibroblasts) showed aberrant cellular morphology already 72 hours post-transfection. G-32 cells appeared polygonal or rounded and fibroblasts lost their typical spindle-shaped morphology, appearing shorter and polygonal (figure 7). The effects of MARK4 depletion on G-32 and fibroblasts morphology were more evident after anti-MARK4S+L siRNA,

which also caused a significant reduction of mitotic cells. Images were acquired by Olympus IX51 inverted microscope, equipped with Olympus DP71 super high-resolution colour digital camera.

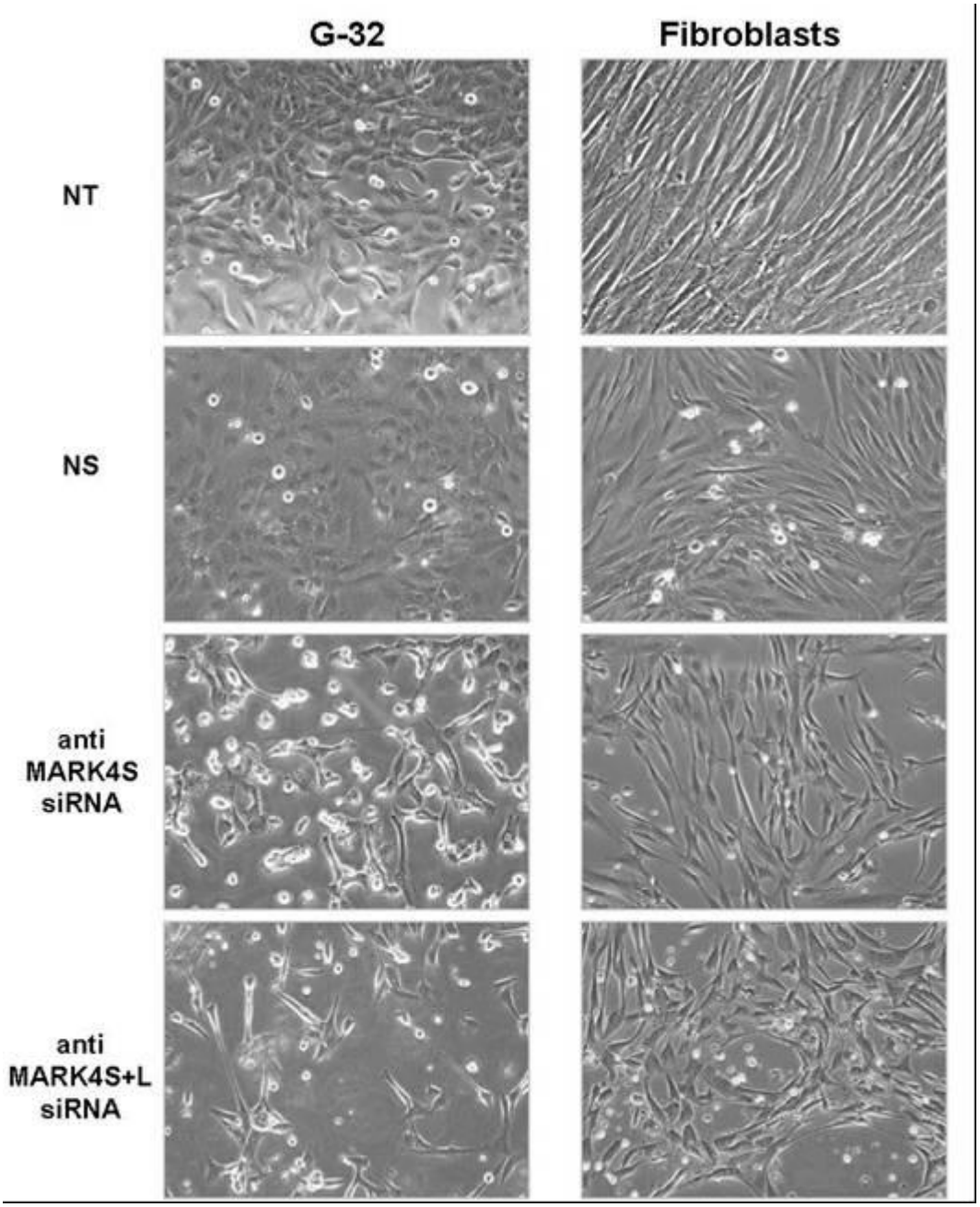

Figure 7 Comparison between non-treated (NT), Non Specific (NS) and silenced cells morphology: after knockdown of both MARK4 isoforms, cellular shape of G-32 GBM cell line and fibroblasts appear strikingly altered.

6. EFFECTS OF MARK4 KNOCKDOWN ON APOPTOSIS

Apoptosis has been investigated after anti-MARK4S+L siRNA by cytometric analysis. Results showed an increase of necrotic, but not of apoptotic cells, in both the G-32 cell line and in fibroblasts (Figure 8).

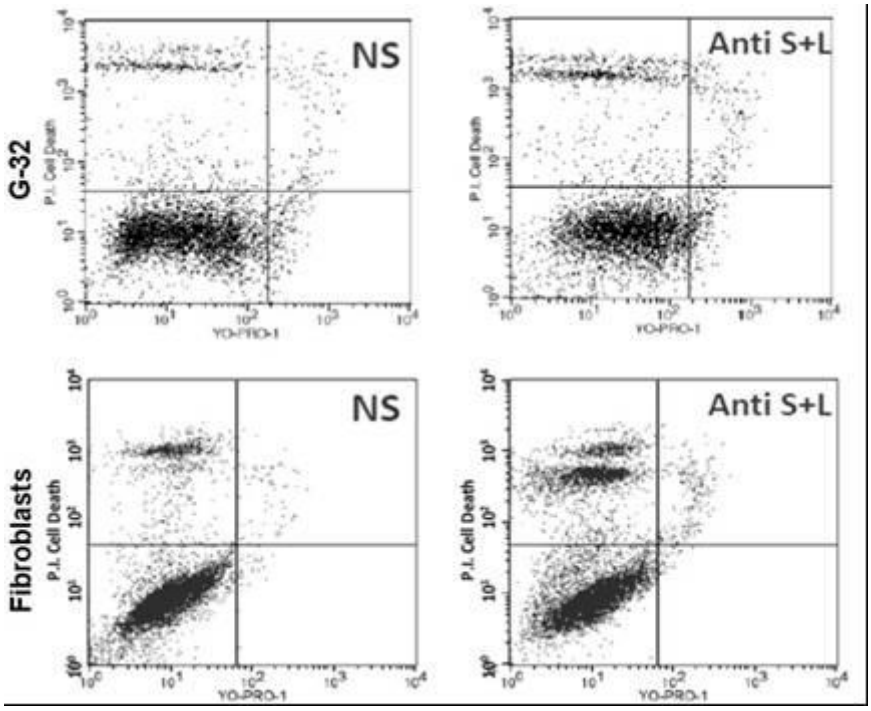

Figure 8 Cytofluorimetric analysis on apoptosis: MARK4 silencing does not induce apoptosis (no variations are shown in the lower-right panel of the diagrams), even though an increase in necrotic cells is present (upper left panel) most likely due to the cytotoxic effect of silencing as reported in M&M. NS=non specific

7. EFFECTS OF MARK4 KNOCKDOWN ON CENTROSOMES AND NUCLEOLI

To evaluate the effects of MARK4 silencing on centrosomes structure and number, we performed IF using MARK4S and γ-tubulin antibodies. G-32 and fibroblasts treated with anti-MARK4S or anti-MARKS+L siRNA showed similar IF results. As a general trend, we observed that most of cells showed the centrosome duplicated, positioned apically to the nucleus (the centrosome duplicates during the G_1/S phase). Conversely, control samples showed centrosomes in all centrosome-cycle phases (Figure 9). Furthermore MARK4 depleted cells showed a strong reduction in mitoses number, and the few ones observable displayed multipolar spindles, spindles without microtubules (MTs) nucleation and spindles misalignment (Figure 10).

Even though MARK4S silencing was verified by Real Time RT-PCR and WB, after IF, a residual signal of the protein was still visible at centrosomes.

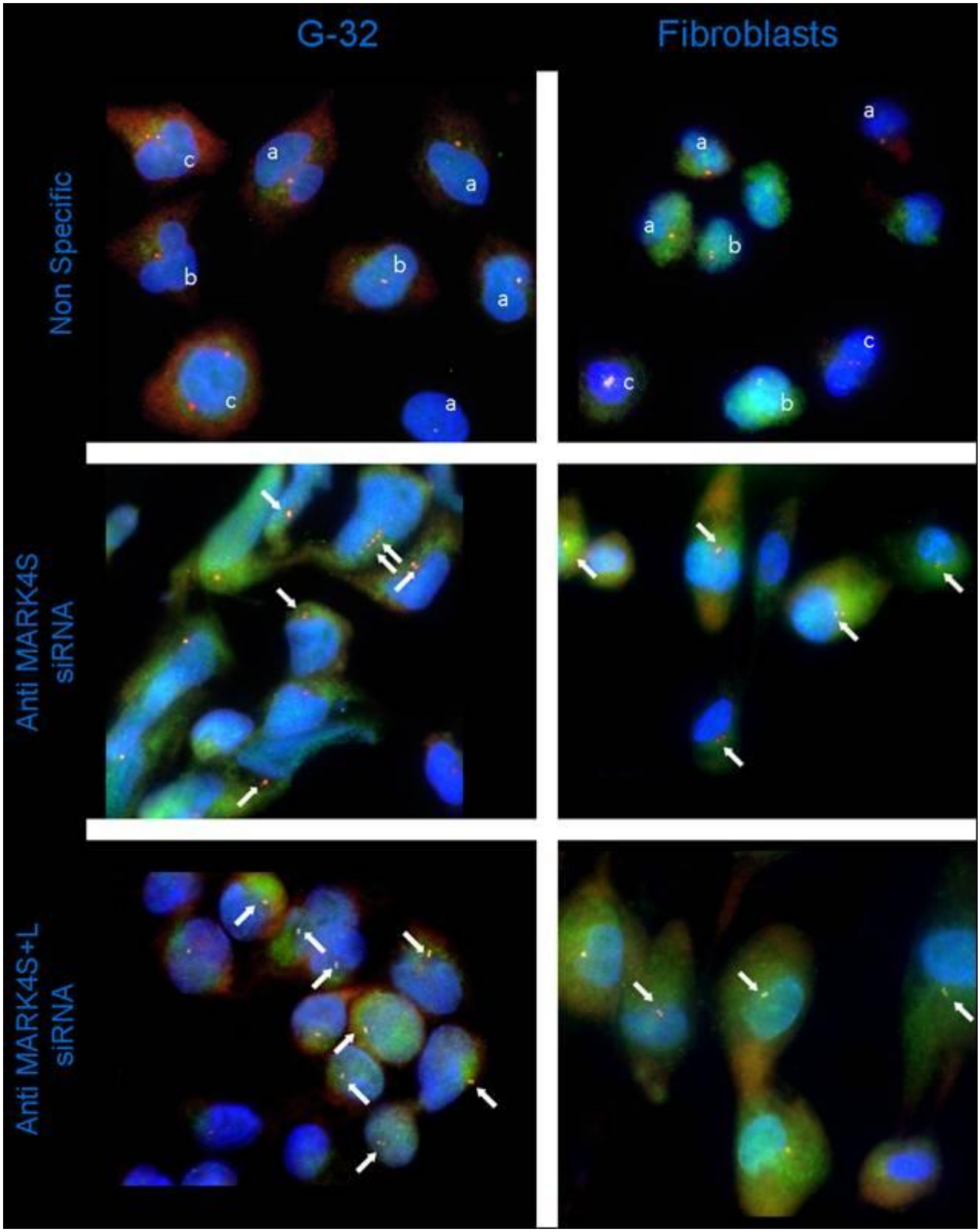

Figure 9 IF on centrosomes of G-32 cell line and fibroblasts. After MARK4 silencing, both samples show most of cells with the duplicated centrosome apical to the nucleus (arrows), as expected in G_1-S phase. NS samples show centrosomes either in G_0 -G_1 phase (a), G_1-S (b) or G_2 -M (c). Nuclei are DAPI counterstained. MARK4S (green) and γ-Tubuline (red)

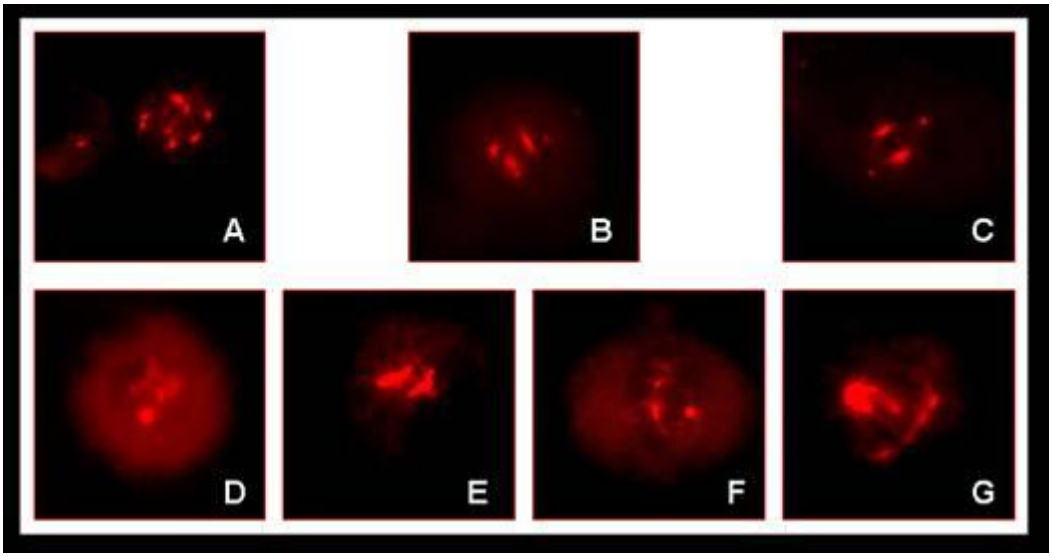

Figure 10 G-32 aberrant mitoses after MARK4 knockdown. Multipolar spindles (A and B); Quadripolar spindle with only two nucleating centrosomes (C); Mis-aligned and/or multipolar spindles (D, E, F and G.)

We evaluated MARK4 silencing on nucleoli at 72, 96 and 120 hours, obtaining homogeneous results. IF was carried out with MARK4L, nucleolin or nuclephosmin antibodies. After anti-MARK4S+L and anti-MARK4S siRNA, MARK4L signals were stronger than in control samples, but not detectable in some nucleoli which were, on the contrary, marked with nucleolin or nuclephosmin (Figure 11). Counterstaining with nucleolin or nuclephosmin gave concordant results.

Figure 11 IF on nucleoli of G-32 GBM cell line 96 hours after silencing. After both anti-MARK4S and anti-MARK4S+L siRNA, MARK4L signal is more intense than control samples (arrows), despite few nucleoli are negative after both isoforms knockdown (asterisks). Otherwise NS samples show MARK4L overlapping nucleolin signals. MARK4L (green) nucleolin (red).

IF on fibroblasts, after MARK4 depletion, showed an unexpected signal of MARK4L around nucleoli (not shown). Given that in our previous study [Magnani, *In press*] we did not observe a MARK4L nucleolar/perinucleolar association in normal cells, we wondered whether this result reflected

MARK4 silencing or might be an artifact due to IF treatments. To verify this hypothesis, we applied IF on fibroblasts after MARK4 RNAi, using different combinations of fixation and permeabilization, as shown in table 1.

Permeabilization	Fixation	MARK4L signal
0,1% Triton X-100	MetOH	- -
0,1% Triton X-100	Paraformaldehyde 4% in PBS	- -
0,5% Triton X-100	MetOH	+ -
0,5% Triton X-100	Paraformaldehyde 4% in PBS	+ +

Table 1 Different combinations of IF conditions tested: intensity of MARK4L signals inside nucleoli is indicated in the third column: "- -" = absent; "+ -" = weak; "+ +" = high signal

We observed that the combination of 0,5% Triton X-100 and cold paraformaldehyde abolished the perinucleolar MARK4L signals in fibroblasts deprived of MARK4; however, signals of MARK4L, counterstained with nucleolin or nucleophosmin, were present inside nucleoli 96 hours after silencing and showed a higher intensity than those in control samples (Figure 12a). Interestingly, after 120 hours of MARK4S silencing, MARK4L, nucleolin and nucleophosmin were no more visible in a small fraction of nucleoli. After MARK4S+L silencing, much more nucleoli were unlabeled by MARK4L, nucleolin and nucleophosmin, compared to NS controls. Concordant IF results have been obtained in at least three independent silencing experiments.

Figure 12a IF on nucleoli of fibroblasts. After 96h of both MARK4 silencing, MARK4L overlaps nucleolin signals that appear more intense than in NS. MARK4L (green) and nucleolin (red).

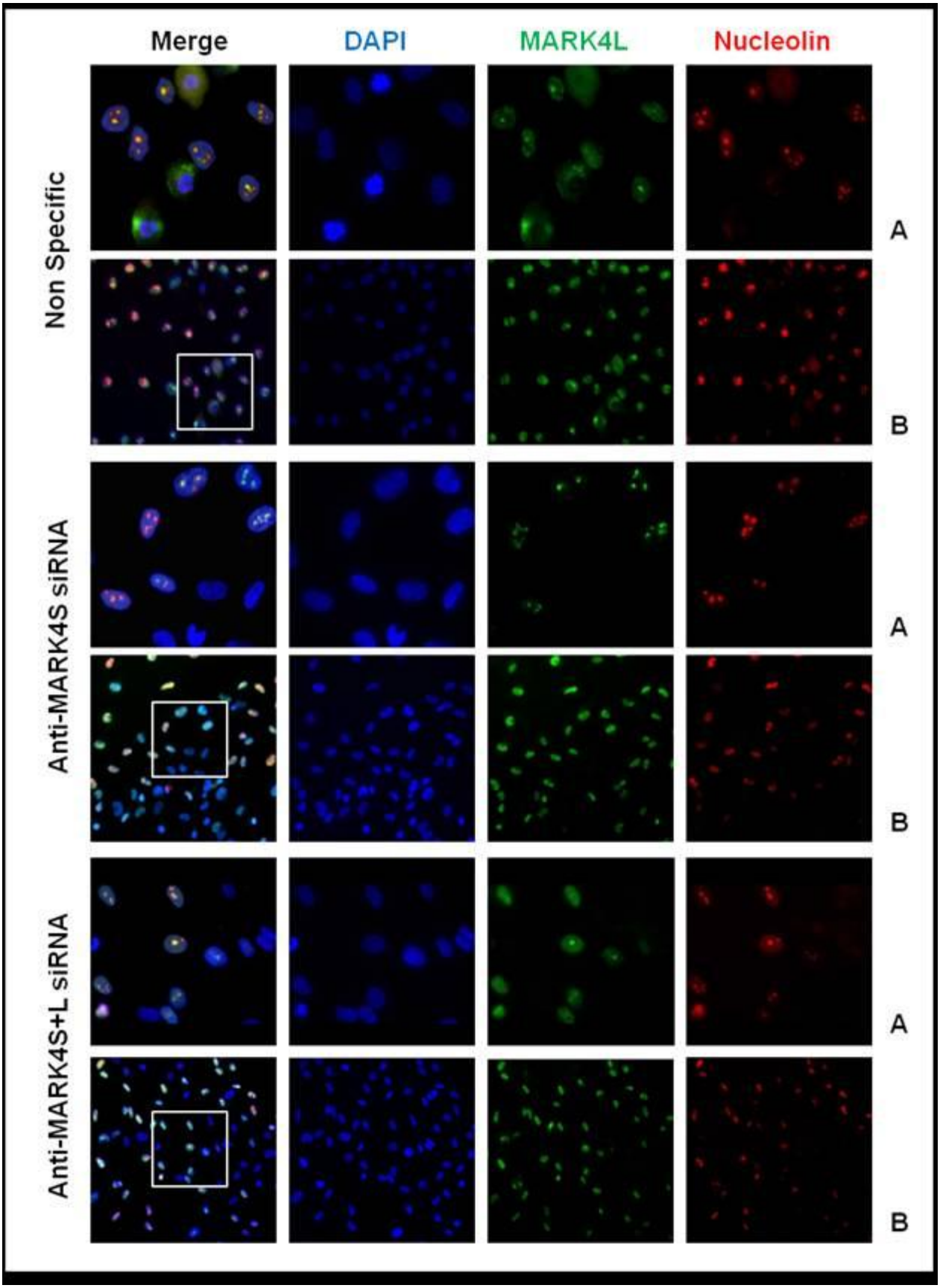

Figure 12b IF images on nucleoli of fibroblasts after 120 hours of silencing. Anti-MARK4S siRNA shows some nucleoli negative for MARK4L and nucleolin, while much more nucleoli are unlabeled after siRNA anti-MARK4S+L. MARK4L (green) and Nucleolin (red). (A) 60X objective, (B) 20X objective

8. EFFECTS OF MARK4 SILENCING ON CELL CYCLE PROGRESSION

Since we observed that MARK4 silencing affected the mitosis, apparently along with the centrosome cycle, in both G-32 and fibroblasts, we investigated, by flow cytometry, the cell cycle progression after MARK4 knockdown.

We performed a bi-parametric cytometric analysis by Propidium Iodide and Phospho histone H3 (a mitotic marker) assay. G-32 and fibroblasts were plated and treated during their exponential growth phase.

After 72 hours of silencing, an inhibitory effect on G-32 growth was already evident, when cells looked almost steady if compared with NS control (Figure 13a).

To determine if G-32 cell growth was blocked at a specific phase of the cell cycle and if MARK4S rather than MARK4S+L depletion affected mitotic progression, we performed histone H3/DNA flow cytometry analysis. Since 48 hours after transfection with anti-MARK4S+L siRNA (but not with anti-MARK4S siRNA), G-32 undergoes a significant decrease in mitotic cells: from 1.90% of NS to 0.17% in silenced cells (figure 13b – panels D and F) that was maintained up to 72 hours. G-32 DNA histograms reveal that 72 hours of MARK4S depletion determined a slight increase in G_1 fraction, with a concomitant decrease of G_2/M and S phase cells (figure 13c – panels G,H). A different effect on cell cycle was detected with MARK4S+L siRNA: after 48 hours an increase of S fraction (33% vs. 21% of NS sample) and a decrease of G_2/M were observed, due to a delay in entering from G_1 to S phase (figure 13c – panels D,F,G,I). Overall, these data support the hypothesis that MARK4 silencing, may induce G_1 arrest by blocking the G_1/S transition.

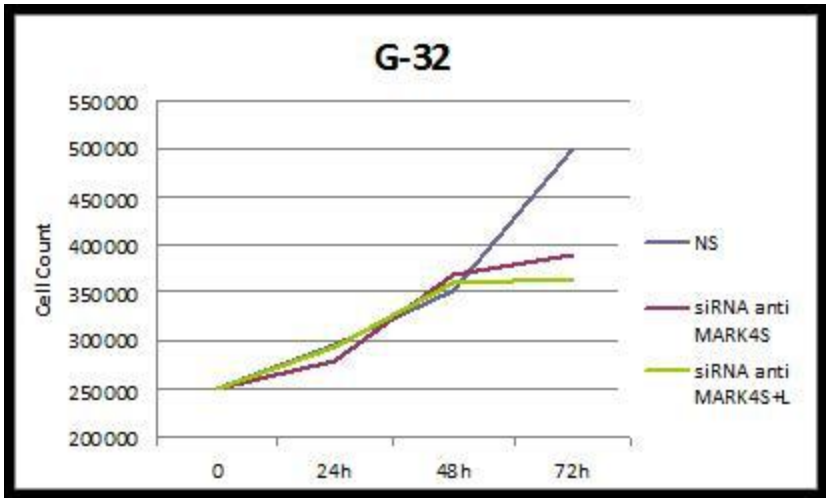

Figure 13a Growth Curve of G-32 GBM cell line. After both anti-MARK4S (red) and anti-MARK4S+L (green) siRNA, proliferation rate is reduced if compared to NS sample (blue).

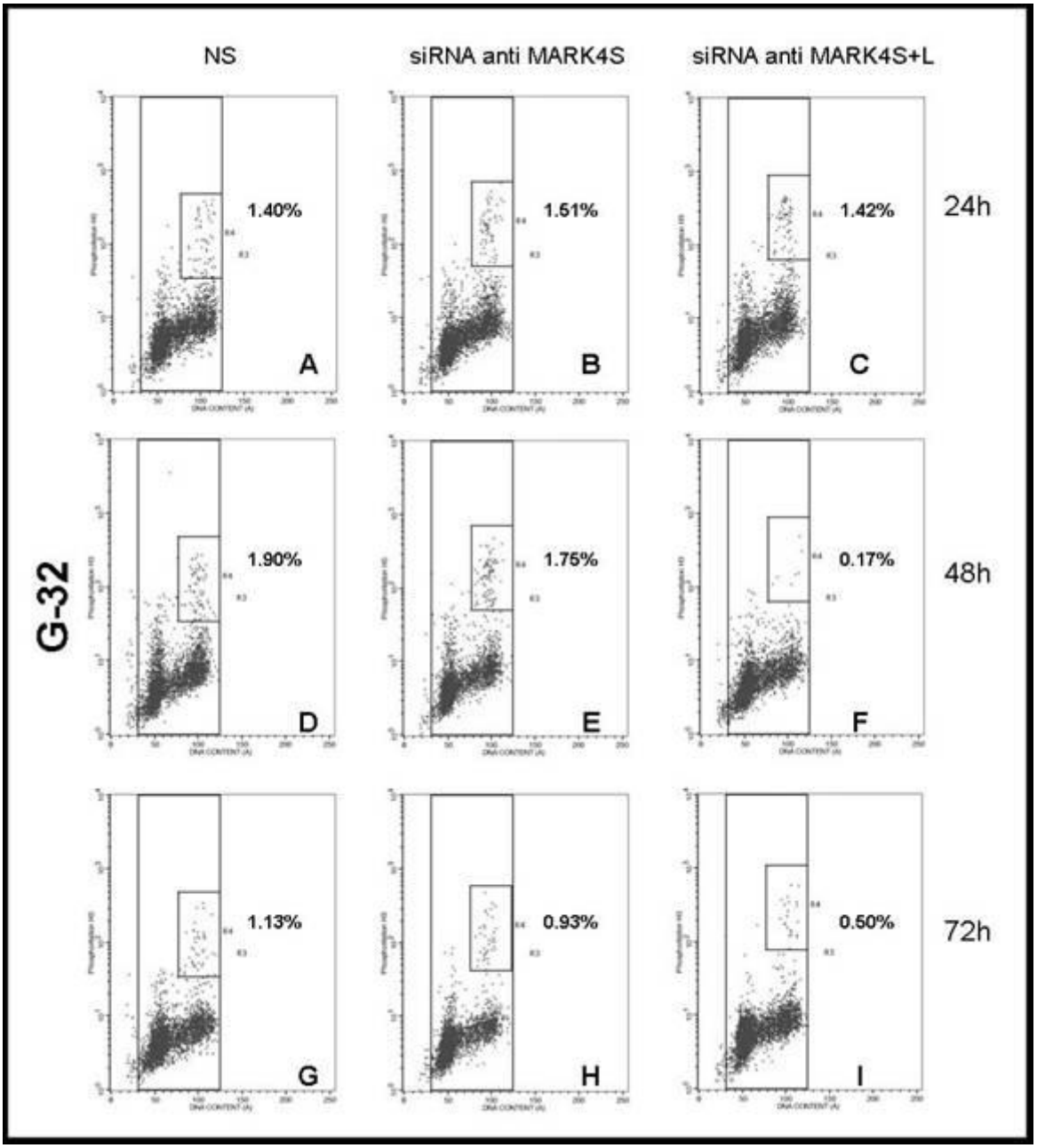

Figure 13b Evaluation of G-32 GBM cell line mitotic fractions by double staining with propidium iodide and anti-phospho histone H3. Mitotic events are double-positive and gated by a rectangle. 24 hours after plating, no differences in mitotic events are observable between NS and silenced samples. After 48 and 72 hours, antiMARK4S+L siRNA induces a significant decrease in the mitotic fraction.

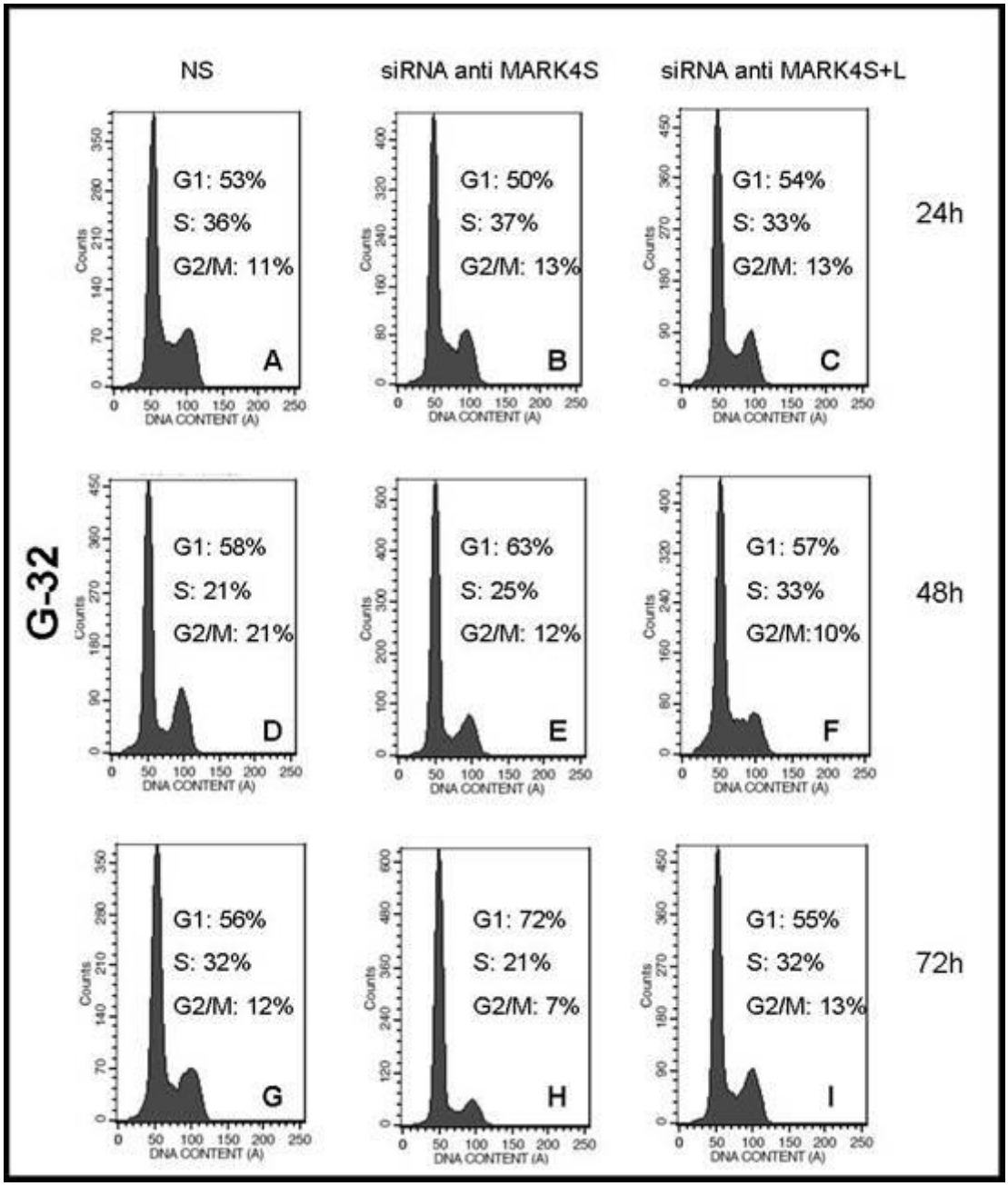

Figure 13c DNA content analysis of G-32 cell line. Both MARK4 silencing determines a reduction of G_2/M cell cycle phase already after 48 hours (panels E and F). anti-MARK4S si-RNA reduces S phase cells 72 hours after transfection (panel H), while silencing of both isoforms determines a delay in moving from G_1 to S phases (panel F and I).

Fibroblasts growth kinetics showed after 72 and 120 hours of antiMARK4S and MARK4S+L siRNA a reduction of proliferation rate (figure 14a). MARK4 deprived fibroblasts showed after 72 hours a significant reduction of the mitotic fraction (Figure 14b, panels E, F, H, I) and of the S phase (Figure 14 c, panels E, F, H, I), that became more pronounced after 120 hours of silencing. In particular, after 72h of MARK4S+L siRNA, we observed in silenced fibroblasts an increase of G_1 (90% vs. 76% of NS - Figure 14c, panels D,F) and a decrease of S phase (2% vs. 16% - Figure 14c panels D,F). After 120 hours, a G_2/M reduction was observed (2% vs. 12% of NS), while the S phase of silenced and NS samples was comparable (Figure 14c, panels G,I). Concordantly, anti-MARK4S siRNA showed similar cell cycle profiles (Figure 14c, panels E, H). In addition, since mitotic events are significantly reduced after MARK4 silencing, it is interesting to point out that G_2/M component of silencing cells is mainly imputable to G_2 cells and not to mitotic events, which frequence is higher in NS sample (figure 14 b and c).

The slight progressive decrease in the S phase-fraction in NS cells (Figure 14c, panels A,D,G), is probably due to cell contact inhibition, also inferred by optical microscopy (Figure 7) and by the cell curve, with a growth arrest 72 hours after plating (figure 14a).

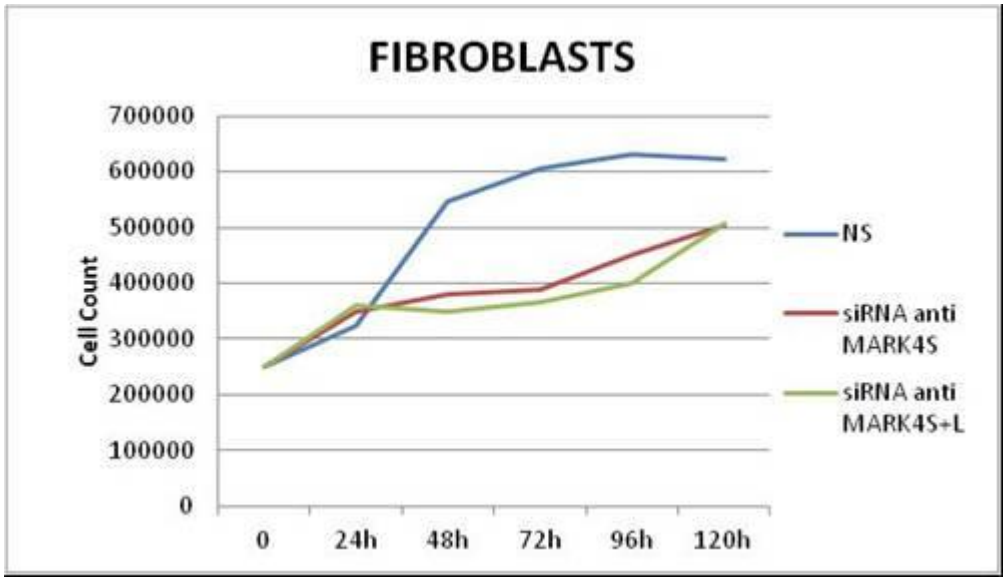

Figure 14a Growth Curve of fibroblasts. After antiMARK4S (red) and anti-MARK4S+L (green) siRNA, proliferation is slower than in NS sample (blue)

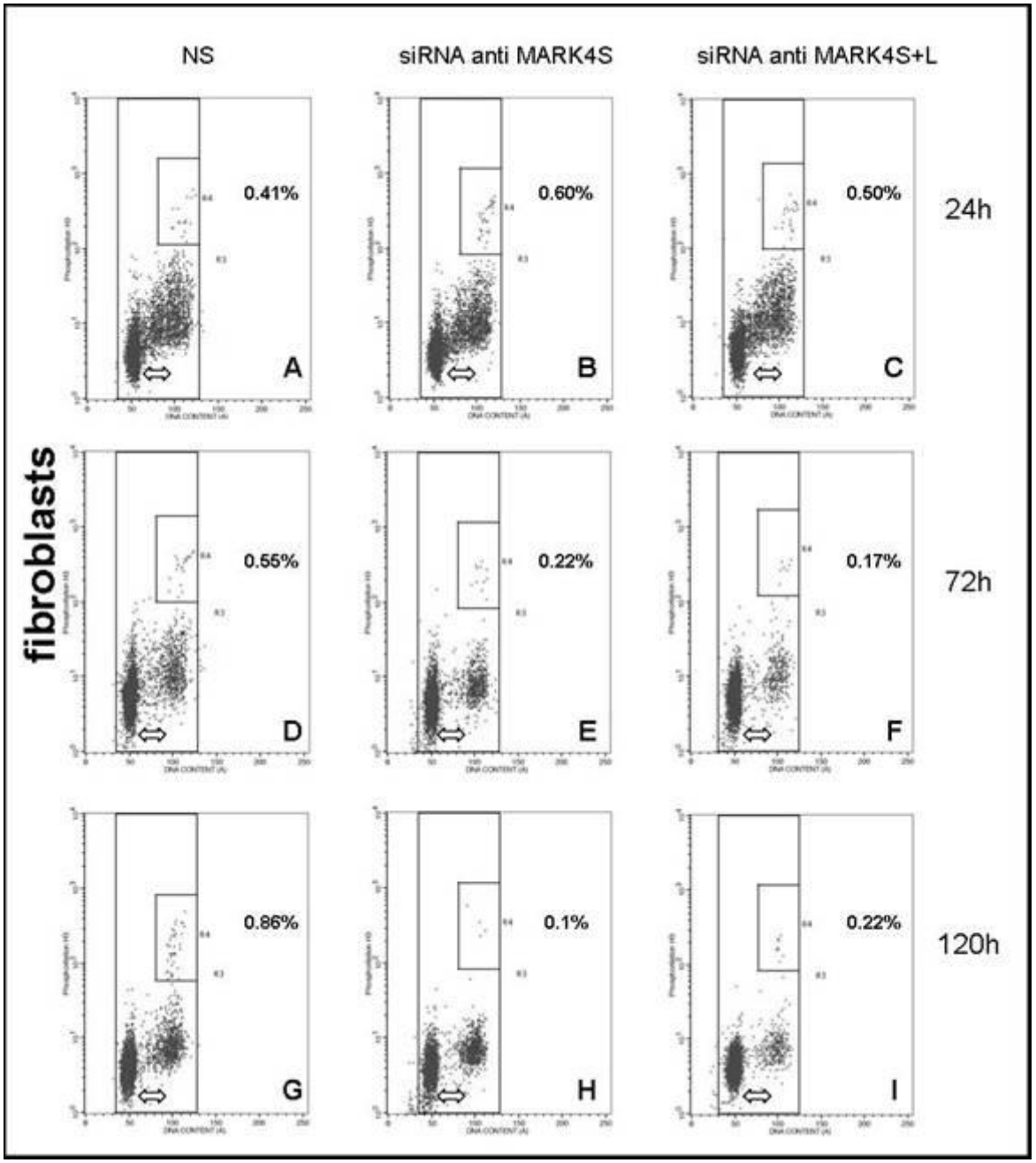

Figure 14b Evaluation of fibroblasts mitotic fraction by double staining with propidium iodide and anti-phospho histone H3. Mitotic events are double-positive and gated by a rectangle. 24hours after plating, no differences in mitotic events are observed between NS and silenced samples. After 72 and 120 hours, of antiMARK4S and antiMARK4S+L siRNA a significant decrease in mitotic fraction is observed. Moreover, silenced fibroblasts show a reduction of cells in the S phase, arrowed by ⇔ (see also Figure 14c).

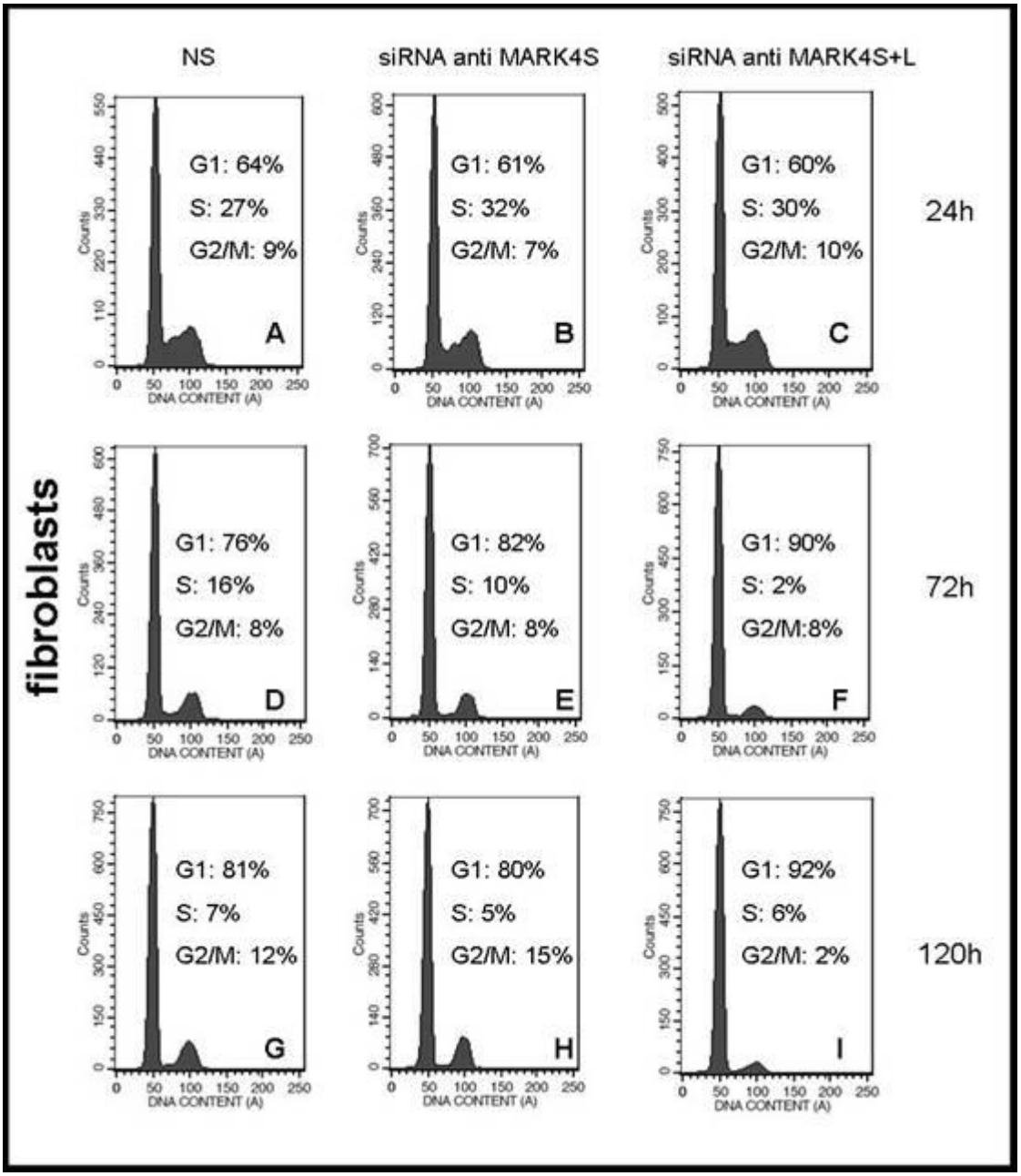

Figure 14c DNA content analysis of fibroblasts. Both MARK4 silencing determines a significant reduction of S-phase cell count already after 72 hours, that is maintained at 120 hours. The G_2/M phase is instead reduced only after anti-MARK4S+L siRNA.

Discussion

We undertook this study to highlight the functional impact of MARK4 gene in glioma and in normal cells and to assess if there is a distinct role for its L and S isoforms, with respect to their subcellular localization.

Given that both isoforms of MARK4 have been found associated to centrosomes and midbody, in glioma as well as in normal cells, we previously suggested that the kinase might exert its function throughout all phases of the cell cycle. Moreover, the additional nucleolar localization of MARK4L in tumor cells, suggested that the L variant has isoform-specific functions and interactions (with nucleolar components) in tumors [Magnani, *In press*]. The dual nature of MARK4 has also been pinpointed by the S and L expression profiling in glioma, GBM-derived cell lines and neural stem cells, and the balance of the two isoforms has been foreseen as a potential target of dysregulation in glial tumors. We wondered whether the predominant expression in glioma of MARK4L, variant of a protein involved in microtubule dynamics, may concur to mitotic errors during gliomagenesis.

To investigate MARK4 function, we set up RNAi experiments on the G-32 glioblastoma cell line and on fibroblasts. Due to the lack of information on MARK4 half-life, to plan a proper silencing time-lapse, we performed cycloheximide (CHX) treatment on the selected cell systems and obtained evidence of a long (>96 hours) MARK4L half-life. On the basis of the observation of a decreased protein level after 120 hours of CHX, we monitored MARK4 silencing at 72, 96 and 120 hours.

The only commercially available and validated dsRNAs contemporaneously silence both isoforms of MARK4. Hence, to obtain the specific silencing of S isoform, we designed a custom panel of 3 dsRNAs, taking advantage of the retention of exon 16, skipped in MARK4L transcript, and which is the target of the anti-MARK4S siRNAs. Unfortunately, it was not possible to design a dsRNA specific for MARK4L, since the sequence of this transcript is partially shared with MARK4S, thus not ensuring a specific target effect.

Real Time RT-PCR demonstrated a good silencing efficiency of both MARK4S and L mRNAs (>70%). However, while silencing of the S isoform was confirmed by WB, the L protein still persisted after 120 hours of silencing, (in contrast to the CHX experiments). This let us hypothesize that the protein detected in WB could be the fraction pre-existing to the RNAi treatment, hard to be depleted because of its long half-life. In addition, since RNAi acts by inducing degradation of the target mRNA, preventing its translation, a residual pre-existing protein cannot be abolished.

An overview summarizing the effects of MARK4 knockdown on cell morphology, centrosomes, nucleoli and cell cycle is depicted in Figure 1.

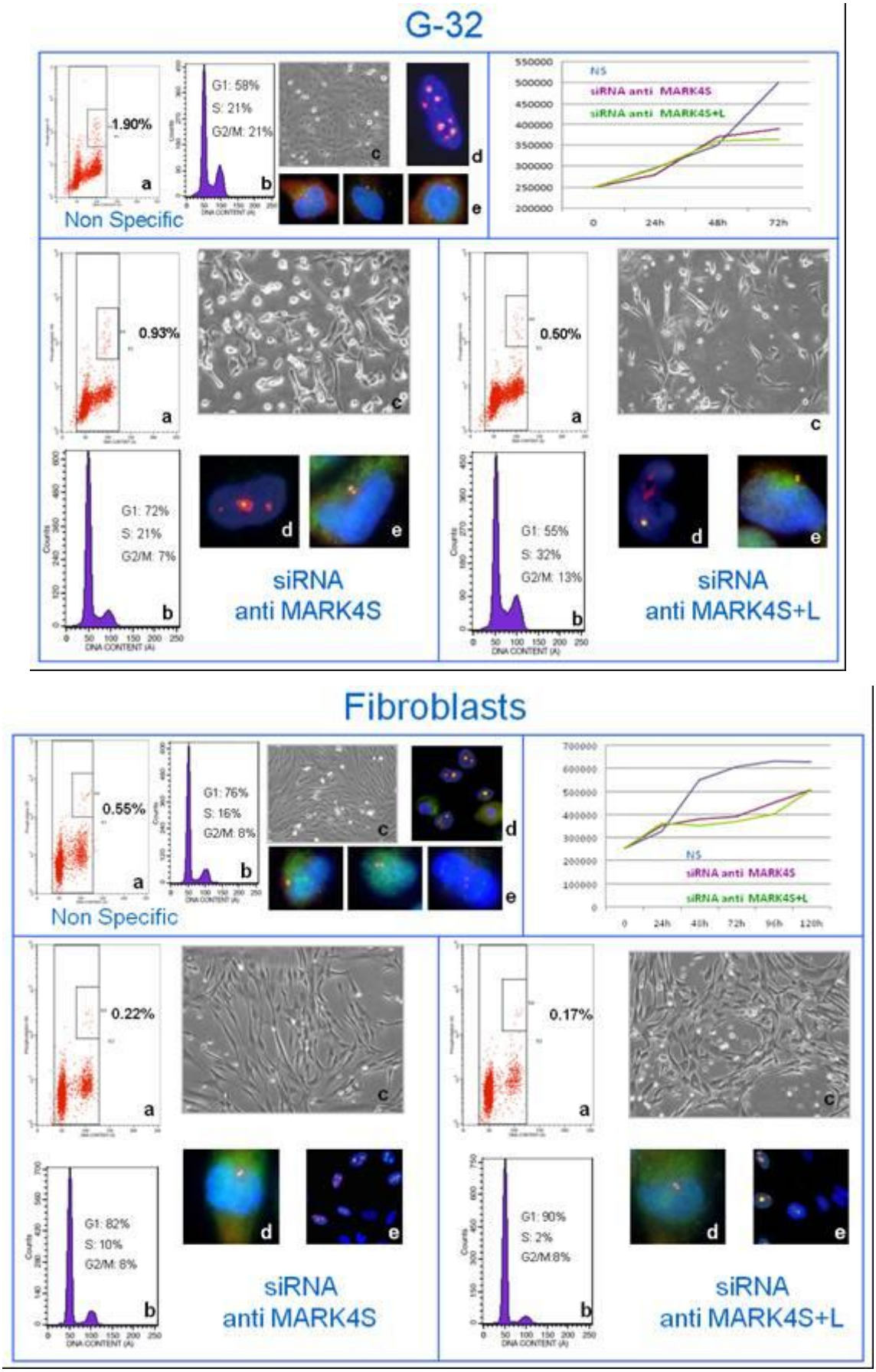

Figure 1 Overview of MARK4 silencing effects on mitosis (a); cell cycle (b); cell morphology (c), nucleoli (d) and centrosome (e). Growth curves of the treated cells are reported too.

We showed that MARK4 depletion determines alterations in both G-32 and fibroblasts cell shape, supporting MARK4 role in cytoskeleton organization. Morphologic aberrations are usually a consequence of cytoskeleton defects, compatible with the known role of MARK proteins in influencing MTs dynamics. In accordance, PAR proteins, orthologs of MARKs in lower eukaryotes, are involved in establishing cell polarity and embryonic segmentation: Par-1 has been described in *C. Elegans* as a regulator of stability, density, and/or organization of the microtubule cytoskeleton [Kemphues 1988].

MARK4 silencing particularly affected the centrosome cycle. Silenced G-32 glioblastoma cells and fibroblasts displayed most of the cells with duplicated centrosomes, apical to the nucleus as hallmark of G_1/S transition. Differently, control cells showed centrosomes in all phases of the centrosome cycle. Accordingly, cell cycle analysis showed an increase of G_1 cells fraction and a strong reduction of mitoses in both treated tumor cells and fibroblasts: the few observable mitoses showed huge aberrations, supporting a role for MARK4 in regulating MTs and MAPs, during the mitotic process.

In particular, silencing of both isoforms of MARK4 heavily reduced mitotic cells in G-32 GBM cell line, while MARK4S knockdown effects were weaker. On the contrary, in fibroblasts, both anti-MARK4S and anti-MARK4S+L siRNA determined a significant decrease of mitotic fraction and S-phase, with a concomitant increase of G_1, compatible with G_1 arrest. Thus, cells are unable to overcome the G_1/S checkpoint and to proceed through the S phase, in agreement with the observed arrest at G_1/S of centrosome cycle after silencing. (Centrosome initiates the duplication at the transition from G_1 to S phase, and subsequently migrates to cell poles to prepare the mitotic process - Nigg 2002).

The inability of the duplicated centrosome to separate and migrate to the cell poles raises the hypothesis of the involvement of motor proteins, such as myosin II, which inhibition has been reported to block the separation and positioning of duplicated centrosomes [Rosenblatt 2004]. Interestingly, MARK4 is known to co-immunoprecipitate with a complex containing α, β, and γ tubulin, and non-muscle myosin and actin [Trinczek 2004; Brajenovic 2004].

14-3-3 proteins are other putative interactors of MARK4, acting as pivot in various cellular processes, including mitotic exit and cytokinesis, and G_1/S transition, and are regulated, as MARK4, by PKC, MAPK and GSK3 [Brajenovic 2004; Timm 2008]. The overall observations let us to hypothesize that MARK4 depletion may perturb phosphorylation pathways mostly implicated at G_1/S checkpoint (Figure 2).

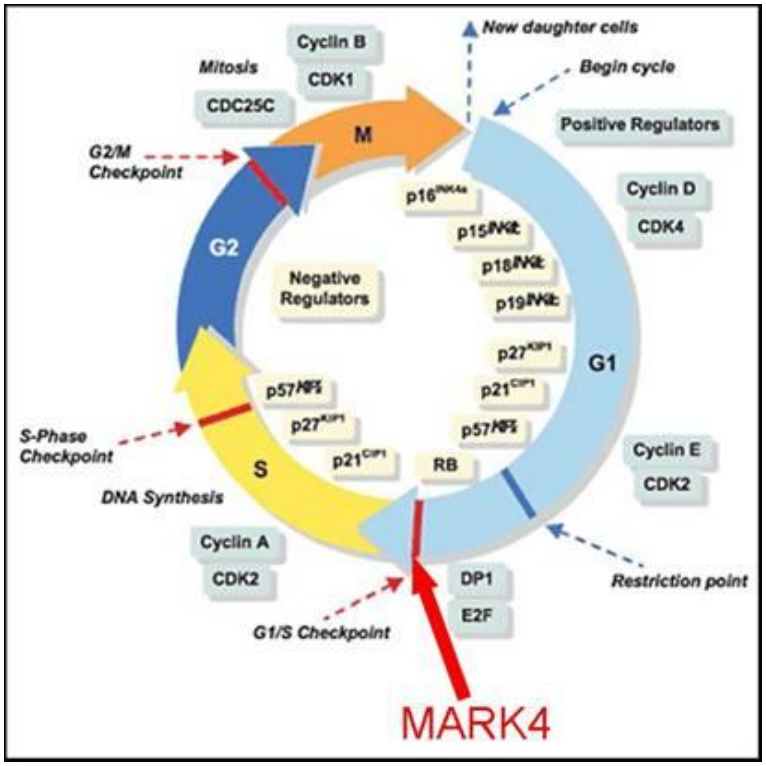

Figure 2 Diagram of the main actors of cell cycle checkpoints regulation. MARK4 may act, likely as positive regulator, at the G_1/S checkpoint.

Even though MARK4S silencing has been verified by Real Time PCR and WB, a residual signal, compatible with a pre-existing MARK4S protein that cannot be abolished by RNAi, was still visible in G_1/S arrested, likely non functional centrosomes

Examining MARK4 silencing effects on nucleolus, we observed that MARK4L is also detectable in fibroblasts nucleoli, apparently in contrast with previous data that depicted MARK4L as a nucleolar tumor marker [Magnani 2011, *In press*]. The presence of the protein in nucleoli of normal cells has been investigated after modifications of IF protocols with a stronger fixation/permeabilization procedure. Thus the differential localization previously observed between normal and tumor cells can be explained by the intrinsic difficulty to unmask the L isoform of MARK4 in the nucleolus of normal cells using standard protocols.

MARK4 silencing on G-32 did not point out differences between anti-MARK4S and MARK4S+L siRNAs, as both showed an increase of MARK4L signal intensity, even though some nucleoli appeared silenced. This finding agrees with the detection of MARK4L in WB after silencing.

In contrast, MARK4-silenced fibroblasts showed several nucleoli unlabeled with MARK4L, in particular when both isoforms were targeted. Interestingly, MARK4L+S-depleted nucleoli were also deprived of nucleolin or nucleophosmin, suggesting that MARK4L silencing in fibroblasts could

affect the most relevant structural components of the nucleolus. In keeping with this view, we have previously observed that RNAse treatment abolishes both MARK4L and nucleophosmin, suggesting MARK4L interaction with a ribonucleoproteic complex in the nucleolus.

It has been reported that nucleolin depletion, even not affecting centrosome duplication, leads to alterations of cell cycle, with increase of G_2/M population, and a significant decrease of mitotic index, compatible with a G_2 arrest [Ugrinova 2007]; nuclephosmin downregulation is instead thought to be responsible of a delays in mitotic entry [Amin 2008].

A suggestive hypothesis is that the observed differences between G-32 and fibroblasts nucleoli after MARK4 silencing might be imputable to diverse MARK4L conformations, post-translational modifications or interactions in the two cell systems.

The nucleolar fraction of MARK4L could represent the end point of nucleolar sequestration, as already known for other proteins that, at different phases of the cell cycle, can be internalized into the nucleolus, and usually show a distinctive state of phosphorylation/dephosporylation, suggesting a role for this compartment and its proteins in checkpoint signaling. Significant examples include: i) Cdc14, a phosphatase critical for promoting mitosis exit, which is kept inactive in the nucleolus until the onset of anaphase, thus preventing the premature onset of mitotic exit; ii) the p53 inhibitor Mdm2, which is sequestered in response to the activation of the Myc oncoprotein or replicative senescence, allowing p53 to become active and iii) Pch2, required for halting meiotic cell-cycle progression in response to recombination and chromosome synapsis defects [Sirri 2008, Visintin 2000, Pederson 2011].

Furthermore, the concomitant alterations in both centrosomal and nucleolar compartments after MARK4 silencing suggest a putative role of the protein in the regulation of the Nucleus - (Nucleolus) - Centrosome (NC) axis [Gant Luxton 2011]. The NC - axis is oriented and paired with polarization and migration axis of many cell types, including fibroblasts. Microtubules are the major players in organizing a dynamic structure along NC - axis, regulating nuclear movement during cell migration and polarization. Since MARK4 cooperates with microtubules network, its depletion likely interferes with the correct activity of the NC-axis orientation. It is worth pointing out that like MARK4, its orthologous Par6α localizes at the centrosome and is essential for its positioning during neuronal migration [Solecki 2004]. Cdc42, already identified as a MARK4 potential interactor [Brajenovic 2004; Angrand 2006] is implied in controlling NC - axis formation during fibroblasts migration, thanks to its effect on Par6. Par3, another member of PAR family,

associates with dynein light intermediate chains (LIC2), also required for centrosome centration [Schmoranzer 2009]. Other known interactors of MARK4, such as actin and myosin II, are implied in defining the NC - axis, together with cell-cell junctions mediated by cadherin. These effectors have been found crucial during cell division [Gant Luxton 2011].

In addition, knockdown of nucelophosmin has been demonstrated to determine dramatic changes in nuclear morphology and defects of cytoskeleton structure, particularly of microtubule polymerization, leading to hypothesize a functional interaction between the nucleolus and the microtubule network. Such functional connection may also apply to MARK4, as it associates with both centrosome and nucleolus.

All together, MARK4 RNAi experiments showed that alterations of cell morphology, centrosome and cell cycle progression and mitosis are more evident when both isoforms of MARK4 are silenced.

These findings suggest that the functions of the two isoforms are strictly intermingled, as inferable by their common subcellular localization. The reciprocal influence between MARK4S and L isoforms has also been highlighted by the reduction of MARK4L mRNA levels following MARK4S specific silencing in G-32 cell line (Results - Figure 5)

In conclusion, we addressed MARK4 function by silencing S isoform or both S+L in two cellular systems, one prototypical of normal cells (i.e fibroblasts) and a GBM cell line (G-32), derived from a stage IV glioma, which exemplifies a tumor pathology at its most advanced stage. Glioma cell lines and tumor biopsies have been intensively investigated and characterized in our laboratory in the last few years and have been instrumental in the characterization of the MARK4 gene.

Both interference approaches showed that the two isoforms synergistically cooperate in the main MARK4 function of guarding the G_1/S checkpoint: a subtle unbalance of the S/L ratio may direct the switch to terminal differentiation or contribute to tumor development and progression. The driving causes of disequilibrium between S and L are currently unknown: one promising research line is currently under way in our lab, and addresses the fine-tuned regulation of alternative splicing [Luco & Misteli 2011] and its disruption in tumors [Venables 2006; Grosso 2008]. Interestingly a role for alternative splicing in chromosome instability has been recently envisaged [Lopez-Saavedra & Herrera 2010] linking a feature typical of glial tumours to dysregulation of MARK4S/MARK4L ratio.

1. CONCLUSIONS

After MARK4 depletion we observed:

- Arrest of the cell cycle at the G_1 phase with significant reduction of the mitotic index
- Arrest of centrosome cycle at G_1/S checkpoint
- A more evident effect on cell proliferation, mitosis and centrosomal anomalies when silencing both isoforms, suggestive of merging functions for the two isoforms
- Perturbation of nucleolus structure , also abolishing nucleolin or nucleophosmin when MARK4L is depleted
- MARK4L nucleolar localization also in normal cells, i.e. fibroblasts.

2. PERSPECTIVES

- Definitely confirm that the G_2-M proportion of cells observed after silencing is mainly imputable to G_2 events by performing a cytometry assay using CycB1 staining, as complementary to phospho H3 assay (G_2 cells are CycB1 positive, while mitotic cells are CycB1 negative).
- Complete MARK4 functional study with overexpression assays by constructs already generated in our laboratory, inducing specific overexpression of the two isoforms.
- Deepen splicing regulation of MARK4 mRNA, identifying the putative regulators and the implied signaling pathways.
- Investigate other MARK4 interactors by co-immunoprecipitation.
- Verify the phosphorylation status of the two isoforms in both tumor and normal cells, more specifically looking for differences in post-translational modifications and/or interactions in the two cell systems.

References

Al-Hakim AK, Zagorska A, Chapman L, *et al.*
Control of AMPK-related kinases by USP9X and atypical Lys^{29}/Lys^{33}-linked polyubiquitin chains.
The Biochemical journal 2008; 411: 249-60.

Amin Ma, Matsunaga S, Uchiyama S, Fukui K.
Depletion of nucleophosmin leads to distortion of nucleolar and nuclear structures in HeLa cells.
Biochem. Journal 2008 415, 345-351

Angrand PO, Segura I, Völkel P, *et al.*
Transgenic mouse proteomics identifies new 14-3-3-associated proteins involved in cytoskeletal rearrangements and cell signaling
Molecular and cellular proteomics 2006; 5(12): 2211-27.

Bachmann M, Hennemann H, Xing PX, *et al.*
The oncogenic serine/threonine kinase Pim-1 phosphorylates and inhibits the activity of Cdc25C-associated kinase 1 (C-TAK1): a novel role for Pim-1 at the G2/M cell cycle checkpoint.
Journal of biological chemistry 2004; 279: 48319-28.

Bantounas I, Phylactou LA and Uney JB
RNA interference and the use of small interfering RNA to study gene function in mammalian systems
Journal of Molecular Endocrinology 2004; 33, 545-557

Bass BL
RNA interference, the short answer
Nature 2001 411, 428-429

Beghini A, Magnani I, Roversi G, *et al.*
The neural progenitor-restricted isoform of the MARK4 gene in 19q13.2 is upregulated in human gliomas and overexpressed in a subset of glioblastoma cell lines.
Oncogene 2003; 22: 2581-91.

Benton R, Palacios IM and St Johnston D.
Drosophila 14-3-3/PAR-5 is an essential mediator of PAR-1 function in axis formation.
Developmental Cell 2002; 3: 659-71.

Bernstein E, Denli AM and Hannon GJ
The rest is silence
RNA 7, 1509-1521 (2001)

Bessone S, Vidal F, le Bouc Y, *et al.*
EMK protein kinase-null mice: dwarfism and hypofertility associated with alterations in the somatotrope and prolactin pathways.
Developmental biology 1999; 214: 87-101.

Biernat, J. et al. (2002) Protein kinase MARK/par-1 is required for
neurite outgrowth and establishment of neuronal polarity.
Mol. Biol. Cell 13, 4013–4028

Bohm H, Brinkmann V, Drab M, *et al.*
Mammalian homologues of *C. Elegans* PAR-1 are asymmetrically localized in epithelial cells and may influence their polarity.
Current biology 1997; 7: R603-6.

Brajenovic M, Joberty G, Küster B, *et al.*
Comprehensive proteomic analysis of human Par protein complexes reveals an interconnected protein network.
The journal of biological chemistry 2004; 279(13): 12804-11.

Bright NJ, Carling D and Thornton C.
The regulation and function of mammalian AMPK-related kinases.
Acta Physiologica 2009; 196: 15-6.

Bringmann H
Cytokinesis and the spindle midzone.
Cell cycle 2005; 4(12): 1709-12.

Canoll P and Goldman JE.
The interface between glial progenitors and gliomas.
Acta neuropathologica 2008; 116: 465-77.

Carmo-Fonseca M, Mendes-Soares L and Campos I.
To be or not to be in the nucleolus.
Nature cell biology 2000; 2: E107-12.

Chatterjee S, Sang TK, Lawless GM, *et al.*
Dissociation of tau toxicity and phosphorylation: role of GSK-3β, MARK and Cdk5 in a *Drosophila* model.
Human molecular genetics 2009; 18(1): 164-77.

Chen YM, Wang QJ, Hu HS, *et al.*
Microtubule affinity-regulating kinase 2 functions downstream of the PAR-3/PAR-6/atypical PKC complex in regulating hippocampal neuronal polarity.
PNAS 2006; 103: 8534-9.

Chen L, Jiao ZH, Zheng LS, *et al.*
Structural insight into the autoinhibition mechanism of AMP-activated protein kinase.
Nature 2009; 459: 1146-50.

Chi AS and Wen PY.
Inhibiting kinases in malignant gliomas.
Expert opinion on therapeutic targets 2007; 11(4): 473-96.

Chin J, Knowles RB, Schneider A, *et al.*
Microtubule-Affinity Regulating Kinase (MARK) is tightly associated with neurofibrillary tangles in Alzheimer brain: a fluorescence energy transfer study.
Journal of neuropathology and experimental neurology 2000; 59(11): 966-71.

Cohen D, Brennwald PJ, *et al.*
Mammalian PAR-1 determines epithelial lumen polarity by organizing the microtubule cytoskeleton.
Journal of cell biology 2004; 164: 717-27.

Collins VP.
Brain tumors: classification and genes.
Journal of neurology, neurosurgery and psychiatry 2004; 75(Suppl II): ii2-ii11.

D'Assoro AB, Lingle WL, Salisbury JL.
Centrosome amplification and the development of cancer.
Oncogene 2002 Sep 9;21(40):6146-53. Review.

de Leng WWJ, Jansen M, Carvalho R, *et al.*
Genetic defects underlying Peutz-Jeghers syndrome (PJS) and exclusion of the polarity-associated *MARK/Par1* gene family as potential PJS candidates.
Clinical genetics 2007; 72: 568-73.

Dequiedt F, Martin M, Von Blume J, *et al.*
New role for hPar-1 kinases EMK and C-TAK1 in regulating localization and activity of class IIa histone deacetylases.
Molecular cell biology 2006; 26(19): 7086-102.

Doxsey S.
Re-evaluating centrosome function.
Nature 2001; 2(9): 688-98.

Doxsey S, McCollum and Theurkauf W.
Centrosomes in cellular regulation.
Annual review of cell and developmental biology 2005; 21: 411-34.

Drewes G, Ebneth A, Preuss U, *et al.*
MARK, a novel family of protein kinases that phosphorylate microtubule-associated proteins and trigger microtubule disruption.
Cell 1997; 89: 297-308.

Drewes G and Nurse P.
The protein kinase kin1, the fission yeast hortologue of mammalian MARK/PAR-1, localizes to new cell ends after mitosis and is important for bipolar growth.
FEBS letters 2003; 554: 45-9.

Drewes G.
MARKing tau for tangles and toxicity.
TRENDS in biochemical science 2004; 29(10): 548-55.

Duesberg P, Li R, Fabarius A, Hehlmann R.
Aneuploidy and cancer: from correlation to causation.
Contrib Microbiol. 2006;13:16-44. Review.

Dykxhoorn DM,Novina CD and Sharp PA.
Killing the messenger: short RNAs that silence gene expression
Nature reviews, Mol Cell Biol 2003 4, 457-467

Elbashir SM , Lendeckel W and Tuschl T
RNA interference is mediated by 21- and 22-nucleotide RNAs
Genes and development 2001; 15, 188-200

Elbert M, Rossi G and Brennwald P.
The yeast Par-1 homologs Kin1 and Kin2 show genetic and physical interactions with components of the exocytic machinery.
Molecular biology of the cell 2005; 16: 532-49.

Espinosa L and Navarro E.
Human serine/threonine protein kinase EMK1: genomic structure and cDNA cloning of isoforms produced by alternative splicing.
Cytogenetics and cell genetics 1998; 81: 278-82.

Fabbro M, Zhou BB, Takahashi M, Sarcevic B, Lal P, Graham ME, Gabrielli BG, Robinson PJ, Nigg EA, Ono Y, Khanna KK.
Cdk1/Erk2- and Plk1-dependent phosphorylation of a centrosome protein, Cep55, is required for its recruitment to midbody and cytokinesis.
Dev Cell 2005 Oct;9(4):477-88

Fire A et al
Potent and specific genetic interference by double-stranded RNA in Caenorhabditis Elegans
Nature 1998 391, 806-811

Fischer JL, Schwartzbaum JA, Wrensch M, *et al*.
Epidemiology of brain tumors.
Neurologic clinics 2007; 25(4): 867-90.

Fukasawa K.
Introduction.
Oncogene 2002; 21: 6140-5.

Galli R, Gritti A, Bonfanti L, *et al.*
Neural stem cells. An overview.
Circulating research 2003; 92; 598-608.

Gamblin TC, Chen F, Zambrano A, *et al*.
Caspase cleavage of tau: linking amyloid and neurofibrillary tangles in Alzheimer's disease.
PNAS 2003; 100(17): 10032-7.

Gant Luxton GW and Gundersen GG
Orientation and function of the nucelolar-centrsomal axis during cel migration
Curr Opin in Cell Biology 2011, 23: 579-588

Germano I, Swiss V and Casaccia P.
Primary brain tumors, neural stem cell and brain tumor cancer cells: where is the link?
Neuropharmacology 2010; 58: 903-10.

Gladson CL, Prayson RA and Liu WM.
The pathobiology of glioma tumors.
Annual review of pathology 2010; 5: 33-50.

Greenman C, Stephens P, Smith R, *et al.*
Patterns of somatic mutation in human cancer genomes.
Nature 2007; 446: 153-8.

Gritti A and Bonfanti L.
Neuronal-glial interactions in central nervous system neurogenesis: the neural stem cell perspective.
Neuron glia biology 2007; 3(4): 309-23.

Gromley A, Jurczyk A, Sillibourne J, Halilovic E, Mogensen M, Groisman I, Blomberg M, Doxsey S.
A novel human protein of the maternal centriole is required for the final stages of cytokinesis and entry into S phase.
J Cell Biol. 2003 May 12;161(3):535-45

Grosso AR, Martins S, Carmo-Fonseca M.
The emerging role of splicing factors in cancer.
EMBO Rep. 2008 Nov;9(11):1087-93.

Hammond SM, Bernstein E, Beach D and Hannon GJ
An RNA-directed nuclease mediates post-transcriptional gene silencing in Drosophila cells
Nature 2000 404, 293-296

Hartmann C, Johnk L, Litange G, *et al.*
Transcript map of the 3.7 Mb D19S112-D19S246 candidate tumor suppressor region on the long arm of chromosome 19.
Cancer Research 2002; 62: 4100-8.

Holen T, Amarzguioui M, Wiiger MT, Babaie E, and Prydz H
Positional effects of short interfering RNAs targeting the human coagulation trigger tissue factor.
Nucleic Acids Res. 2002 30, 1757-1766

Hurov JB, Stappenbeck TS, Zmasek CM, *et al.*
Immune system dysfunction and autoimmune disease in mice lacking Emk (Par-1) protein kinase.
Molecular cell biology 2001; 21: 3206-19.

Hurov JB, Watkins JL and Piwnica-Worms H.
Atypical PKC phosporylates PAR-1 kinases to regulate localization and activity.
Current Biology 2004; 14: 736-41.

Hurov J and Piwnica-Worms H.
The Par-1/MARK family of protein kinases: from polarity to metabolism.
Cell cycle 2007; 6: 1966-9.

Huse JT and Holland EC.
Targeting brain cancer: advances in the molecular pathology of malignant glioma and medulloblastoma.
Nature reviews 2010; 10: 319-30.

Ignatova TN, Kukekov VG, Laywell ED, *et al.*
Human cortical glial tumors contain neural stem-like cells expressing astroglial and neuronal markers in vitro.
Glia 2002; 39(3): 193-206.

Jain RK, di Tomaso E, Duda DG, *et al.*
Angiogenesis in brain tumours.
Nature reviews. Neuroscience 2007; 8(8): 610-22.

Jeon S, Kim YS, Park J, *et al.*
Microtubule Affinity-Regulating Kinase 1 (MARK1) is activated by electroconvulsive shock in the rat hippocampus.
Journal of neurochemistry 2005; 95: 1608-18.

Kato T, Satoh S, Okabe H, *et al.*
Isolation of a novel human gene, MARKL1, homologous to MARK3 and its involvement in hepatocellular carcinogenesis.
Neoplasia 2001; 3(1): 4-9.

Katsetos CD, Reddy G, Dráberová E, *et al.*
Altered cellular distribution and subcellular sorting of *γ*-tubulin in diffuse astrocytic gliomas and human glioblastoma cell lines.
Journal of neuropathology and experimental neurology 2006; 65(5): 465-77.

Kemphues KJ, Priess JR, Morton DG, Cheng NS.
Identification of genes required for cytoplasmic localization in early C. elegans embryos.
Cell 1988 Feb 12;52(3):311-20.

Kramer A, Neben K and Ho AD.
Centrosome replication, genomic instability and cancer.
Leukemia 2002; 16: 767-75.

Krauss SW, Spence JR, Bahmanyar S, Barth AI, Go MM, Czerwinski D, Meyer AJ.
Downregulation of protein 4.1R, a mature centriole protein, disrupts centrosomes, alters cell cycle progression, and perturbs mitotic spindles and anaphase.
Mol Cell Biol. 2008 Apr;28(7):2283-94

Lim DA, Cha S, Mayo MC, *et al.*
Relationship of glioblastoma multiforme to neural stem cell regions predicts invasive and multifocal tumor phenotype.
Neuro-oncology 2007; 9(4): 424-9.

Linos E, Raine T, Alonso A, *et al.*
Atopy and risk of brain tumors: a meta-analysis.
Journal of the National Cancer Institute 2007; 99(20): 1544-50.

Livak KJ and Schmittgen TD.
Analysis of relative gene expression data using real-time quantitative PCR and the $2^{-\Delta\Delta CT}$ method.
Methods 2001; 25:402-8.

Lizcano JM, Göransson O, Toth R, *et al.*
LKB1 is a master kinase that activates 13 kinases of the AMPK subfamily, including MARK/par-1.
The EMBO Journal 2004; 23(4): 833-43.

López-Saavedra A, Herrera LA.
The role of alternative mRNA splicing in chromosome instability.
Mutation Research 2010 Dec;705(3):246-51. Epub 2010 Oct 20. Review.

Luco RF, Misteli T.
More than a splicing code: integrating the role of RNA, chromatin and non-coding RNA in alternative splicing regulation.
Curr Opin Genet Dev. 2011 Aug;21(4):366-72.

Magnani I, Guerneri S, Pollo B, *et al.*
Increasing complexity of the karyotype in 50 human gliomas.
Cancer genetics and cytogenetics 1994; 75: 77-89.

Magnani I, Novielli C, Bellini M, *et al.*
Multiple localization of endogenous MARK4L protein in human glioma.
Cellular oncology 2009; 31: 357-70.

Magnani I, Novielli C, Fontana L, Tabano S, Rovina D, Moroni RF, Bauer D, Mazzoleni S, Colombo EA, Tedeschi G, Monti L, Porta G, Frassoni C, Galli R, Bello L, Larizza L
Differential signature of the centrosomal MARK4 isoforms in glioma.
Analytical Cellular Pathology, 2011 In press

Mandelkow EM, Thies E, Trinczek B, *et al.*
MARK/PAR1 kinase is a regulator of microtubule-dependent transport in axons.
The journal of cell biology 2004; 167(1): 99-110.

Martinez J, Patkaniowska A, Urlaub H, Luhrmann R and Tuschl T
Single-stranded antisense siRNAs guide target RNA cleavage in RNAi
Cell 2002; 110, 563-574

Martinez-Garay I, Rustom A, Gerdes HH, *et al.*
The novel centrosomal associated protein CEP55 is present in the spindle midzone and the midbody.
Genomics 2006; 87: 243–53.

Marx A, Nugoor C, Panneerselvam S, *et al.*
Structure and function of polarity-inducing kinase family MARK/Par-1 within the branch of AMPK/Snf1-related kinases.
The FASEB journal 2010; 24: 1637-48.

Matenia D, Griesshaber B, Li XY, *et al.*
PAK5 kinase is an inhibitor of MARK/Par-1, which leads to stable microtubules and dynamic actin.
Molecular biology of the cell 2005; 16: 4410-22.

Matenia D and Mandelkow EM.
The tau of MARK: a polarized view of the cytoskeleton.
Trends in biochemical sciences 2009; 34(7): 332-42.

Maussion G, Carayol J, Lepagno-bestel AM, *et al.*
Convergent evidence indentifying MAP/Microtubule Affinity-Regulating Kinase 1 (MARK1) as a susceptibility gene for autism.
Human molecular genetics 2008; 17(16): 2541-51.

Mitchell DA, Xie W, Schmittling R, *et al.*
Sensitive detection of human cytomegalovirus in tumors and peripheral blood of patients diagnosed with glioblastoma.
Neuro-oncology 2008; 10(1): 10-8.

Moroni RF, De Biasi S, Colapietro P, *et al.*
Distinct expression pattern of microtubule-associated protein/microtubule affinity-regulating kinase 4 in differentiated neurons.
Neuroscience 2006; 143: 83-94.

Müller J, Ory S, Copeland T, *et al.*
C-TAK1 regulates Ras signalling by phophorylating the MAPK scaffolds, KSR1.
Molecular cell 2001; 8: 983-93.

Müller J, Ritt DA, Copeland T, *et al.*
Functional analysis of C-TAK1 substrate binding and identification of PKP2 as a new C-TAK1 substrate.
EMBO journal 2003; 22: 4431-42.

Mullins JM and Biesele JJ.
Terminal phase of cytokinesis in D-98S cells.
The journal of cell biology 1977; 73: 672-684.

Mullins JM and McIntosh JR.
Isolation and initial characterization of the mammalian midbody.
The journal of cell biology 1982; 94: 654-61.

Munro EM.
PAR proteins and the cytoskeleton: a marriage of equals.
Curr Opin Cell Biol. 2006 Feb;18(1):86-94. Epub 2005 Dec 20. Review.

Murphy JM, Korzhnev DM, Ceccarelli DF, *et al.*
Conformational instability of the MARK3 UBA domain compromises ubiquitin recognition and promotes interaction with the adjacent kinase domain.
PNAS 2007; 104: 14336-41.

Nesic D, Miller MC, Quinkert ZT, *et al.*
Helicobacter pylori CagA inhibits PAR1-MARK family kinases by mimicking host substrates.
Nature structural & molecular biology 2010; 17(1): 130-2.

Ney DE and Lassman AB.
Molecular profiling of oligodendrogliomas: impact on prognosis, treatment, and future directions.
Current oncology reports 2009; 11(1): 62-7.

Nigg EA.
Centrosome aberrations: cause or consequence of cancer progression?
Nat Rev Cancer 2002 Nov;2(11):815-25. Review

Ohgaki H.
Epidemiology of brain tumors.
Methods in molecular biology 2009; 472: 323-42.

Olsen MK, Reszka AA, Abraham I.
KT5720 and U-98017 inhibit MAPK and alter the cytoskeleton and cell morphology.
J Cell Physiol 1998 Sep;176(3):525-36.

Paddison PJ, Caudy AA and Hannon GJ
Stable suppression of gene expression by RNAi in mammalian cells
PNAS 2002 99, 1443-1448

Panneerselvam S, Marx A, Mandelkow EM, *et al.*
Structure of the catalytic and ubiquitin-associated domains of the protein kinase MARK/Par-1.
Structure 2006; 14: 173-83.

Park DM and Rich JN.
Biology of glioma cancer stem cells.
Molecules and cells 2009; 28: 7-12.

Pederson T
The Nucleolus
CSH Perspectives in Biology 2011 Mar 1;3(3).

Pellettieri J, Seydoux G.
Anterior-posterior polarity in C. elegans and Drosophila-PARallels and differences.
Science 2002 Dec 6;298(5600):1946-50. Review.

Pelliccia F, Curatolo A, Limongi ZM, *et al.*
Transcriptional profiling of genes at the human common fragile site FRA1H in tumor-derived cell lines.
Cancer genetics and cytogenetics 2007; 178(2): 144-50.

Peng CY, Graves PR, Ogg S, *et al.*
C-TAK1 protein kinase phosphorylates human Cdc25C on serine 216 and promotes 14-3-3 protein binding.
Cell growth and differentiation 1998; 9:197-208.

Perego P, Boiardi A, Carenini N, *et al.*
Characterization o fan established human, malignant, glioblastoma cell line (GBM) and its response to conventional drugs.
Journal of cancer research and clinical oncology 1994; 120(10): 585-92.

Pollock C, Huang S.
The perinucleolar compartment.
J Cell Biochem. 2009 May 15;107(2):189-93. Review.

Purow BW, Haque RM, Noel MW, *et al.*
Expression of Notch-1 and its ligands, Delta-like-1 and Jagged-1, is critical for glioma cell survival and proliferation.
Cancer research 2005; 65(6): 2353-63.

Quigley MR, Post C and Ehrlich G.
Some speculation on the origin of glioblastoma.
Neurosurgery reviews 2007; 30: 16-21.

Rahman M
Introduction to Flow Cytometry Principles, Data analysis, Protocols, Troubleshooting
Abd serotec - Manual

Reifenberger J, Ring GU, Gies U, *et al.*
Analysis of p53 mutation and epidermal growth factor receptor amplification in recurrent gliomas with malignant progression.
Journal of neuropathology and experimental neurology 1996; 55(7): 822-31.

Reya T, Morrison SJ, Clarke MF, *et al.*
Stem cells, cancer, and cancer stem cells.
Nature 2001; 414(6859): 105-11.

Rosenblatt J, Cramer LP, Baum B, McGee KM.
Myosin II-dependent cortical movement is required for centrosome separation and positioning during mitotic spindle assembly.
Cell 2004 Apr 30;117(3):361-72.

Roversi G, Pfundt R, Moroni RF, *et al.*
Identification of novel genomic markers related to progression to glioblastoma through genomic profiling of 25 primary glioma cell lines.
Oncogene 2006; 25: 1571-83.

Rousseau A, Mokhtari K and Duyckaerts C.
The 2007 WHO classification of tumors of the central nervous system – what has changed?
Current opinions in neurology 2008; 21(6): 720-7.

Saadat I, Higashi H, Obuse C, *et al.*
Helicobacter pylori CagA targets PAR1/MARK kinase to disrupt epithelial cell polarity.
Nature 2007; 447: 330-3.

Sapir T, Sapoznik S, Levy T, *et al.*
Accurate balance of the polarity kinase MARK2/Par-1 is required for proper cortical neuronal migration.
Journal of neuroscience 2008; 28: 5710-20.

Sathornsumetee S, Reardon DA, Desjardins A, *et al.*
Molecularly targeted therapy for malignant glioma.
Cancer 2007; 110(1): 13-24.

Shapiro JR.
Genetic alterations associated with adult diffuse astrocytic tumors.
American journal of medical genetics 2002; 115: 194-201.

Schaar BT, Kinoshita K, McConnell SK.
Doublecortin microtubule affinity is regulated by a balance of kinase and phosphatase activity at the leading edge of migrating neurons.
Neuron 2004; 41: 203-13.

Schmitt-Ulms G, Matenia D, Drewes G, *et al.*
Interactions of MAP/Microtubule Affinity Regulating Kinases with the Adaptor Complex AP-2 of clathrin-coated vesicles.
Cell motility and the cytoskeleton 2009; 66: 661-72.

Schmoranzer J, Fawcett JP, Segura M, Tan S, Vallee RB, Pawson T, Gundersen GG
Par3 and dynein associate to regulate local microtubule dynamics and centrosome orientation during migration.
Curr Biol 2009.

Schneider A, Laage R, von Ahsen O, *et al.*
Identification of regulated genes during permanent focal cerebral ischemia: characterization of the protein kinase 9b5/MARKL1/MARK4.
Journal of Neurochemistry 2004; 88: 1114-26.

Schwarzacher HG and Wachtler F.
Nucleolus organizer regions and nucleoli.
Human genetics 1983; 63: 89-99.

Segu L, Pascaud A, Costet P, *et al.*
Impairment of spatial learning and memory in ELKL Motif Kinase 1 (EMK1/MARK2) knockout mice.
Neurobiology of aging 2008; 29: 231-40.

Shete S, Hosking FJ, Robertson LB, *et al.*
Genome-wide association study identifies five susceptibility loci for glioma.
Nature genetics 2009; 41: 899-904.

Sirri V, Urcuqui-Inchima S, Roussel P, Hernandez-Verdun D
Nucleolus: the fascinating nuclear body
Histochemic Cell Biology, 2008; 129:13-31

Smith JS, Tachibana I, Lee HK, *et al.*
Mapping of the chromosome 19 q-arm glioma tumor suppressor gene using fluorescence in situ hybridization and novel microsatellite markers.
Genes, chromosomes and cancer 2000; 29(1): 16-25.

Solecki DJ, Model L, Gaetz J, Kapoor TM, Hatten ME
Par6alpha signaling controls glial-guided neuronal migration.
Nat Neurosci 2004, 7:1195-1203.

Stiles CD and Rowitch DH.
Glioma Stem Cells: a midterm exam.
Neuron 2008; 58: 832-46.

Sun W, Zhang K, Zhang X, *et al.*
Identification of differentially expressed genes in human lung squamous cell carcinoma using suppression subtractive hybridization.
Cancer letters 2004; 212(1): 83-93.

Suzuki, A. et al.
aPKC acts upstream of PAR-1b in both the establishment and maintenance of mammalian epithelial polarity.
Curr. Biol. 14, 2004 1425–1435

Terabayashim T, Itoh TJ, Yamaguchi H, *et al.*
Polarity-regulating kinase partitioning-defective 1/microtubule affinity-regulating kinase 2 negatively regulates development of dendrites on hippocampal neurons.
Journal of neuroscience 2007; 27: 2896-907.

The Cancer Genome Atlas (TGCA) Research Network
Comprehensive genomic characterization defines human glioblastoma genes and core pathways.
Nature 2008; 455(7216): 1061-8.

Thies E and Mandelkow EM.
Missorting of tau in neurons causes degeneration of synapses that can be rescued by the kinase MARK2/Par-1.
The journal of neuroscience 2007; 27(11): 2896-907.

Timm T, Marx A, Panneerselvam S, *et al.*
Structure and regulation of MARK, a kinase involved in abnormal phosphorylation of Tau protein.
BMC Neuroscience 2008; 9(Suppl 2): S9.

Timm T, von Kries JP, Li X, Zempel H, Mandelkow E, Mandelkow EM.
Microtubule Affinity Regulating Kinase Activity in Living Neurons Was Examined by a Genetically Encoded Fluorescence Resonance Energy Transfer/Fluorescence Lifetime Imaging-based Biosensor: INHIBITORS WITH THERAPEUTIC POTENTIAL.
J Biol Chem. 2011 Dec 2;286(48):41711-22. Epub 2011 Oct 7.

Tochio N, Koshiba S, Kobayashi N, *et al.*
Solution structure of the kinase-associated domain 1 of mouse microtubule-associated protein/microtubule affinity-regulating kinase 3.
Protein science 2006; 15: 2534-43.

Tomankak P, Piano F, Riechmann V, *et al.*
A *Drosophila melanogaster* homologue of *Caenorhabditis elegans* par-1 acts at an early step in embryonic-axis formation.
Nature Cell biology 2000; 2: 458-60.

Trinczek B, Brajenovic M, Ebneth A, *et al.*
MARK4 is a novel Microtubule-associated Proteins/Microtubule Affinity-regulating Kinase that binds to the cellular microtubule network and to centrosomes.
The journal of biological chemistry 2004; 279(7): 5915-23.

Umeda M, Murata-Kamiya N, Saito Y, *et al.*
Helicobacter pylori CagA causes mitotic impairment and induces chromosomal instability.
Journal of biological chemistry 2009; 284(33): 22166-72.

Ugrinova I, Monier K, Ivaldi C, Thiry M, Stork S, Mongelhard F, Bouvet P.
Inactivation of nucelolin leads to nucelolar disruption, cell cycle arrest and defects in centrosome duplication.
BMC Molecular Biology 2007 8:66

Vandesompele J, De Preter K, Pattyn P, *et al.*
Accurate normalization of real-time quantitative RT-PCR data by geometric averaging of multiple internal control genes.
Genome biology 2002; 3(7):research0034.1-11.

Venables JP.
Unbalanced alternative splicing and its significance in cancer.
Bioessays. 2006 Apr;28(4):378-86. Review.

Vescovi AL, Galli R, Reynolds BA.
Brain tumour stem cells.
Nature reviews. Cancer 2006; 6(6): 425-36.

Visintin R. and Amon A.
The nucleolus: the magician's hat for cell cycle tricks.
Current opinion in cell biology 2000; 12(3): 372-7.

Wakida NM, Botvinick EL, Lin J, Berns MW.
An intact centrosome is required for the maintenance of polarization during directional cell migration.
PLoS ONE 2010, 5: e15462

Weaver BA, Silk AD, Montagna C, Verdier-Pinard P, Cleveland DW.
Aneuploidy acts both oncogenically and as a tumor suppressor.
Cancer Cell. 2007 Jan;11(1):25-36. Epub 2006 Dec 28.

Wrensch M, Jenkins RB, Chang JS, *et al.*
Variants in the CDKN2B and RTEL1 regions are associated with high-grade glioma susceptibility.
Nature genetics 2009; 41: 905-8.

Yamashita S, Tsujino Y, Moriguchi K, *et al.*
Chemical genomic screening for methylation-silenced genes in gastric cancer cell lines using 5-aza-2'deoxycytidine treatment and oligonucleotide microarray.
Cancer science 2006; 97(1): 64-71.

Yang S, Liu X, Yin Y, Fukuda MN, Zhou J.
Tastin is required for bipolar spindle assembly and centrosome integrity during mitosis
The FASEB journal 2008 June, Vol. 22

Zempel H, Thies E, Mandelkow E, *et al.*
Aβ oligomers cause localized Ca^{2+} elevation, missorting of endogenous tau into dendrites, tau phosphorylation and destruction of microtubules and spines.
The journal of neuroscience 2010; 30(36): 11938-50.

Zhang H, Ma X, Shi T, *et al*.
NSA2, a novel nucleolus protein regulates cell proliferation and cell cycle.
Biochemical and biophysical research communications 2010; 391(1): 651-8.

Zhu Y and Parada LF.
The molecular and genetic basis of neurological tumours.
Nature reviews. Cancer 2002; 2(8): 616-2

Acknowledgments

Foremost, I would like to express my gratitude to Prof. Lidia Larizza for giving me the opportunity to run my PhD study in her Medical Genetics laboratory, together with Dr. Ivana Magnani who supported and flanked me in this research project, for her motivation, enthusiasm, and knowledge: her guidance helped me in all the time of research and writing of this thesis.

My gratitude goes also to Eugenio Erba and his unit of Mario Negri Insitute (Department of Oncology) who supported us in our cytometry experiments, with great expertise and helpfulness.

I would like also to thank my MARK-fellow labmates: Chiara Novielli, Davide Rovina and Laura Fontana, who always offered precious help and funny amusement when necessary. Many thanks also to the other lab-goers, who participated in the enjoying atmosphere in our laboratory: Patrizia, Cristina, Gloria, Ilaria, Jacopo, Elisa, but also Silvia&Silvia and Monica, always available for stimulating conversations, suggestions or laughable breaks.

Last but not the least, I would like to thank my family: my husband, my parents and my sister, who always support me unconditionally in every step of my life.